LBL-28104

Lawrence Berkeley Laboratory
UNIVERSITY OF CALIFORNIA

Materials & Chemical Sciences Division

Polyatomic Reaction Dynamics

B.A. Ruf
(Ph.D. Thesis)

November 1989

LOAN COPY
Circulates
for 2 weeks
LBL-28104
Copy 2
Bldg. 50 Library.

Prepared for the U.S. Department of Energy under Contract Number DE-AC03-76SF00098.

DISCLAIMER

This document was prepared as an account of work sponsored by the United States Government. While this document is believed to contain correct information, neither the United States Government nor any agency thereof, nor the Regents of the University of California, nor any of their employees, makes any warranty, express or implied, or assumes any legal responsibility for the accuracy, completeness, or usefulness of any information, apparatus, product, or process disclosed, or represents that its use would not infringe privately owned rights. Reference herein to any specific commercial product, process, or service by its trade name, trademark, manufacturer, or otherwise, does not necessarily constitute or imply its endorsement, recommendation, or favoring by the United States Government or any agency thereof, or the Regents of the University of California. The views and opinions of authors expressed herein do not necessarily state or reflect those of the United States Government or any agency thereof or the Regents of the University of California.

LBL-28104

Polyatomic Reaction Dynamics

Beverly Ann Ruf

(Ph.D. Thesis)

Department of Chemistry

University of California

and

Materials and Molecular Research Division

Lawrence Berkeley Laboratory

Berkeley, California 94720

November 1989

POLYATOMIC REACTION DYNAMICS

Beverly A. Ruf

ABSTRACT

This work presents five theoretical methods of describing chemical reactions such as hydrogen transfer in polyatomic systems, where it is necessary to describe how energy is transferred between vibrational modes. These methods combine a minimal amount of *ab initio* computation with other theoretical tools.

The first technique is accurately describing two important degrees of freedom by generating a 2-dimensional potential surface that is a function of these coordinates and coupling the latter to vibrational modes. The second technique is the formation of a simple cartesian Hamiltonian without any kinetic coupling. Another method for generating an expression without kinetic coupling is presented. This third method rigorously transforms the kinetic energy coupling terms of the linear reference Hamiltonian into potential energy coupling terms. As an alternative to using only *ab initio* data as input into the potential, a fourth method is described which uses empirical information as well as *ab initio* data. Finally, the last approach presented uses Monte Carlo path integral techniques with density matrices to abstract tunneling splittings of a hydrogen transfer process.

ACKNOWLEDGMENT

This research has been supported by the Director, Office of Energy Research, Office of Basic Energy Sciences, Chemical Sciences Division of the U.S. Department of Energy under Contract No. DE-AC03-76SF00098.

TABLE OF CONTENTS

Page

Chapter 1: Introduction 1

Chapter 2: Vinylidene-Acetylene

2.1 Introduction 6

2.2 Potential Energy 8

2.3 Kinetic Energy 18

2.4 Hamiltonian 22

2.5 Results 25

2.6 Multiple Pathways 32

2.7 Concluding Remarks 42

2.8 Appendix 2.1: Energy Diagram 43

2.9 Appendix 2.2: Basis set 45

2-d Contour

1-d Contour

2.10 Appendix 2.3: Intensity Spectrum 48

Chapter 3: Cartesian Reaction Path

3.1 Introduction 53

3.2 Cartesian Model 55

3.3 System/Bath Dynamics 63

3.4 Application to Three-atom Model 66

3.5 Concluding Remarks 70

3.6 Appendix 3.1: Reaction coordinate as lowest mode 72

Chapter 4: Diabatic Hamiltonian

4.1 Introduction 74

4.2 Linear Reference Path 77

4.3 Straight Line Reference Path 81

4.4 Elimination of Kinetic Coupling 85

4.5 Application 92

4.6 Concluding Remarks 94

4.7 Appendix 4.1: Diabatic Potential for Malonaldehyde 96

Chapter 5: Empirical Valence Bond Model

5.1 Introduction 104

5.2 Theory 105

5.3 Applications 109

5.4 Summary 114

5.5 Appendix 5.1: LEPS Potential for Malonaldehyde 115

MM2 Empirical Potential

Chapter 6: Density Matrix Tunneling Splittings

6.1 Introduction 122

6.2 Density Matrices 122

6.3 Multidimensional Integrals 125

6.4 Applications 131

6.5 Concluding Remarks 136

References 137

Chapter 1

INTRODUCTION

One of the challenges of theoretical chemistry is to understand dynamical features of chemical systems. A fundamental approach to this is to calculate a Born-Oppenheimer potential surface using computational *ab initio* quantum chemistry techniques. In order to accurately describe dynamical properties, one needs to calculate on the order of 10 points on the surface along each dimension. Because the Born-Oppenheimer potential surface has 3N-6 dimensions (for an N-atom system), one needs 10^{3N-6} points. This becomes a enormous amount of work for systems with many atoms. Because polyatomic systems allow one to probe the effects of energy fluctuations on reaction rates, mechanisms, lifetimes, and product formation which is fundamental to understanding chemical reactions, it would be advantageous to be able to investigate large systems. This thesis presents new theoretical techniques for analyzing polyatomic systems as well as applications to systems ranging from triatomic test models to a 21-degree-of-freedom problem.

Historically, polyatomic systems have been modelled by isolating one degree of freedom of the system which is the most important [e.g., the reaction coordinate] and describing that exactly along a "reaction path". Unfortunately, if there is more than one coordinate that is important or if other modes are strongly coupled to this first coordinate so as to affect chemical properties, it is not sufficient to describe only one degree of freedom. The effects of the other degrees of freedom can be included with statistical approximations if they exhibit rapid energy flow amongst themselves at an equal rate. If, however, some modes are more strongly coupled than others or restrict energy transfer, these techniques will not work. One would like a way to include all

of the degrees of freedom in a more detailed way in describing polyatomic systems .

One method for doing this is to include them by a local approximation about a one-dimensional reaction path[1]. A specific example of this type of approximation is the use of the *minimum energy reaction path* by Miller, Handy, and Adams[2]. This method takes advantage of the progress that has been made in computational quantum chemistry while offering a tractable use of it. In their model, one follows the negative gradient of the potential from the transition state backwards to reactants and forwards to products (in mass-weighted coordinates) and then calculates *ab initio* quantum chemistry energies along this path. The resulting minimum energy path describes the one-dimensional motion of the reaction coordinate, $\{s\}$. For an N-atom system, the remaining 3N-7 internal modes $\{Q_k\}$ needed to describe the entire system are approximated by a quadratic expansion about this "path of steepest descent". (These remaining orthogonal modes shall be referred to as the "bath" because they are the many degrees of freedom to which the reaction coordinate is coupled, similar to the way a solvent may form a bath with respect to the solute.) This is accomplished by calculating *ab initio* second derivatives along the path. (The first derivatives are zero by the unique definition of the minimum energy path.) The result is the *Reaction Path Hamiltonian* which is one-dimensional motion along the "intrinsic reaction path" coupled to harmonic vibration orthogonal to it (plus three Euler angles for overall rotation). This process is much easier to implement than trying to generate the full *ab initio* surface because one only needs to perform *ab initio* calculations at points along a one-dimensional path. The potential can be written:

$$V(s,Q) = V_o(s) + \frac{1}{2}\sum_k \omega_k^2(s)\, Q_k^2 \quad . \tag{1.1}$$

While the contribution of this Reaction Path Hamiltonian to theoretical calcula-

tions has been appreciable[3], there are situations for which it is not appropriate. Local expansion about the mass-weighted minimum energy path cannot adequately describe systems with large curvature in the path. One of the most important examples of this type of system is hydrogen atom transfer reactions, an example of which is the simple atom-diatom reaction

$$Cl + HCl \rightarrow ClH + Cl\,. \tag{1.2}$$

For this atom-diatom system it is well known[4] that the minimum energy path is very sharply curved, so that the relevant dynamical motion deviates far from it. It is also well known that the Reaction Path Hamiltonian (which reduces to Marcus' natural collision coordinates[1a] for an A + BC system) is not useful in this case.

The situation is actually much worse for intramolecular H-atom transfer than for the atom-diatom case. The minimum energy path of the polyatomic version of a heavy + light-heavy mass combination reaction undergoes many sharp turns in 3N-6 dimensional space on its way from the transition state down to reactants and products. In fact one knows in general that the steepest descent path approaches a local minimum on the potential surface [i.e., reactants or products] along the normal mode of lowest frequency. [cf. Appendix 1 of Chapter 3] For example, in the H-atom transfer in malonaldehyde,[5]

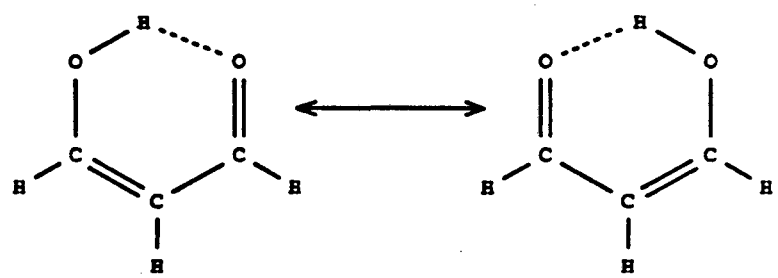

(1.3)

the steepest descent path begins (at the saddle point) being mostly motion of the H-atom that is transferred, but in moving downhill in energy it switches successively to other motions, finally approaching the potential minimum along the vibration which is the lowest frequency in-plane mode. This "kinky" path is not appropriate for defining a reaction coordinate. An alternative description for the potential is needed.

Carrington and Miller[5] proposed the Reaction Surface Hamiltonian as one means of overcoming this problem (although there have been other expansions to the one-dimensional description[6]). The basic strategy of the Reaction Surface Hamiltonian is to describe *two* degrees of freedom exactly (within the Born-Oppenheimer approximation) and then approximate the remaining 3N-8 normal "bath" modes as small amplitude motions. One can, therefore, correctly describe all dynamical phenomena in a reaction involving only two degrees of freedom [e.g., collinear atom-diatom reactions] or approximate the dynamics of a polyatomic system with two strongly coupled anharmonic degrees of freedom. The procedure for obtaining this Hamiltonian is similar to that for the Reaction Path Hamiltonian: one minimizes the *ab initio* energies at points defined in a two-dimensional mass-weighted coordinate space [i.e., on a "surface"] and uses the second derivatives of the potential with respect to the remaining degrees of freedom to define the global potential energy surface. The two-dimensional surface acts as a reference from which the remaining orthogonal degrees of freedom are expanded to quadratic terms in order to form a "bath" of normal modes. The expression for the potential is similar to that for the Reaction Path Hamiltonian in Equation 1.1 but the reaction coordinate {s} is now a two dimensional vector. The full derivation is given in reference 6.

The purpose of this thesis is to try to understand what takes place during chemical reactions, such as hydrogen transfer, in polyatomic systems and to present methods for their theoretical treatment. An application of the Reaction Surface Hamiltonian as well

as four other methods for describing polyatomic systems are presented. Chapter 2 describes the application of the Reaction Surface Hamiltonian to examine the isomerization of vinylidene to acetylene as hydrogen is transferred from one carbon atom to the other. Chapter 3 discusses a new cartesian Hamiltonian to use for hydrogen transfer reactions. A cartesian coordinate system is chosen in order to guarantee that there is no kinetic energy coupling. The advantages of its simple form are presented as well as the disadvantage of only approximately conserving angular momentum. This cartesian method is tested on a model system resembling the H-transfer process in malonaldehyde [Equation 3]. In Chapter 4 we present yet another way to include many degrees of freedom via a Linear Reference Path and apply it to a polyatomic system. In this model, the kinetic energy coupling terms that arise from using an internal coordinate system are rigorously transformed into potential couplings. The result is an easily generated Hamiltonian which has the correct coupling terms but a simple kinetic energy expression. Chapter 5 uses empirical information with a minimal amount of *ab initio* information to generate potential energy surfaces. Chapter 6 explores the use of Monte Carlo path integration techniques for evaluating intramolecular dynamics. The aim is to use density matrices and typically thermodynamic techniques to allow for the inclusion of many degrees of freedom.

Chapter 2

VINYLIDENE-ACETYLENE

2.1 Introduction

This chapter applies the Reaction Surface Hamiltonian of Carrington and Miller [5] to the intramolecular dynamics of the vinylidene-acetylene isomerization

(2.1)

There exists a dispute over whether or not an activation barrier to isomerizaton exists. Until 1981 theoretical calculations[7] reported barrier heights of isomerization ranging from 3.0 to 8.6 kcal/mol. However, in 1981 Krishnan, Frisch, and Pople[8] reported a barrier of 2.2 kcal/mol (which reduces to 0.9 kcal/mol with the inclusion of zero point energies) using an MP2 basis set. They concluded that further refinements of their calculation could easily result in the barrier height of zero and that, therefore, previous experimental conclusions that vinylidene played an important role as an intermediate in carbene chemistry[9] needed reconsideration and spectroscopic detection of vinylidene was unlikely. Then, in 1983 photodetachment experiments of the anion H_2CC^- were performed in Lineberger's lab

$$H_2CC^- + h\nu \rightarrow H_2CC: + e^- \tag{2.2}$$

Burnett, Stevens, Feigrle and Lineberger[10] reported a spectrum for vinylidene and in-

ferred that the presence of structure in their spectrum indicated a lifetime for vinylidene of at least one vibrational period (~.01 psec) and that the widths of the peaks indicate a lower limit of a lifetime of 0.14 psec. They were able to support their claim by assigning the C-C stretch and the CH_2 scissors modes of vinylidene with frequencies in close agreement with TZ+P CI *ab initio* theoretical calculations done by Carrington et al[11]. in 1984. Carrington et al. report a classical barrier height of 6.4 kcal/mol for the gorund state, which reduces to a best estimate of 2-4 kcal/mol. Together with Burnett's spectrum, Carrington's large *ab initio* calculation challenged Krishnan's claim of a barrier height of zero.

In addition to determining the barrier height, Carrington et al. calculated what the barrier height would have to be in order to remain consistent with Lineberger's lower estimate of the lifetime, and proceeded to examine the effects of two vibrational modes on the lifetime of vinylidene. They performed a polynomial fit to three stationary points on the potential and included the coupling of two vibrational modes via Feshbach projection[11]. They did not calculate the entire reaction path of Handy and Miller. However, because various modes may significantly affect the lifetime of vinylidene, a better description would include these more directly. We decided to make a closer examination of the theoretical calculations by generating a 2-dimensional Reaction Surface Hamiltonian to describe two degrees of freedom exactly and include all of the bath modes harmonically. In this way one can study the effects that the internal modes have on the lifetime of vinylidene.

We calculate only the ground electronic state of vinylidene and acetylene because we believe that higher electronic states will not greatly interfere with isomerization. The reason for this is that previous *ab initio* calculations have determined the excited electronic states of vinylidene to be over 30-50 kcal/mol above its ground state and those of acetylene to be ~70 kcal/mol above its ground state. [see Appendix 2.1 for a

more detailed information on the energy diagram for various states of vinylidene and acetylene.]

The potential energy surface, the kinetic energy, and the final Hamiltonian are presented in Sections 2-4 and the results are given in Section 5. Section 6 is a digression from lifetimes and rates to deal explicitly with the multiple pathways that arise from the high periodicity of the potential surface and Section 7 concludes this chapter.

2.2 Potential

In order to generate the Reaction Surface Hamiltonian (RSH) one needs to perform *ab initio* calculations as a function of two degrees of freedom. One advantage to the RSH formalism is that, unlike the Reaction Path Hamiltonian, the choice of these two large amplitude coordinates is not unique. Because the isomerization from vinylidene to acetylene requires a 1,2-hydrogen shift, we chose to describe this process with two angular coordinates that reflect hydrogen motion about the two carbons.

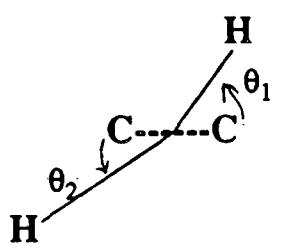

Define:

$$\theta = \theta_1 + \theta_2$$
$$\Delta\theta = \theta_1 - \theta_2$$

Angular coordinates for vinylidene.

Figure #2.1

θ_1 and θ_2 are defined as the angles between a hydrogen, the center of mass of the two carbons, and one carbon atom. We form a two dimensional potential surface as a function of linear combinations of these angles, θ and $\Delta\theta$ by *ab initio* SCF quantum chemistry techniques using a 3-21G basis set. (A more detailed description of this basis set is given in Appendix 2.1.) At each of the corresponding values for θ_1 and θ_2, the remaining four degrees of freedom were varied to optimize the energy, and the second derivatives were calculated at this optimum geometry. The energies were fitted via least squares to a fourier expansion to give the zeroth order potential V_o. (The explicit form is given in Appendix 2.1.)

$$V_o = V_o(\theta,\Delta\theta) = \sum_{m,n} a_{m,n} \cos(m\theta) \cos(n\Delta\theta) \tag{2.5}$$

Due to the symmetry of the vinylidene-acetyene problem, the full potential surface construction was from a grid of 42 points ranging for θ from 0 to π and $\Delta\theta$ from 0 to π. It can be seen in Figure 2.2 that the geometry for acetylene corresponds to $(\theta,\Delta\theta) = (0,0)$, vinylidene at $(1.56,\pi)$, and the transition state at (1.2,1.6). The 3-dimensional plot of V_o in Figure 2.3 shows the lowest well corresponding to acetylene and the two higher local wells corresponding to vinylidene.

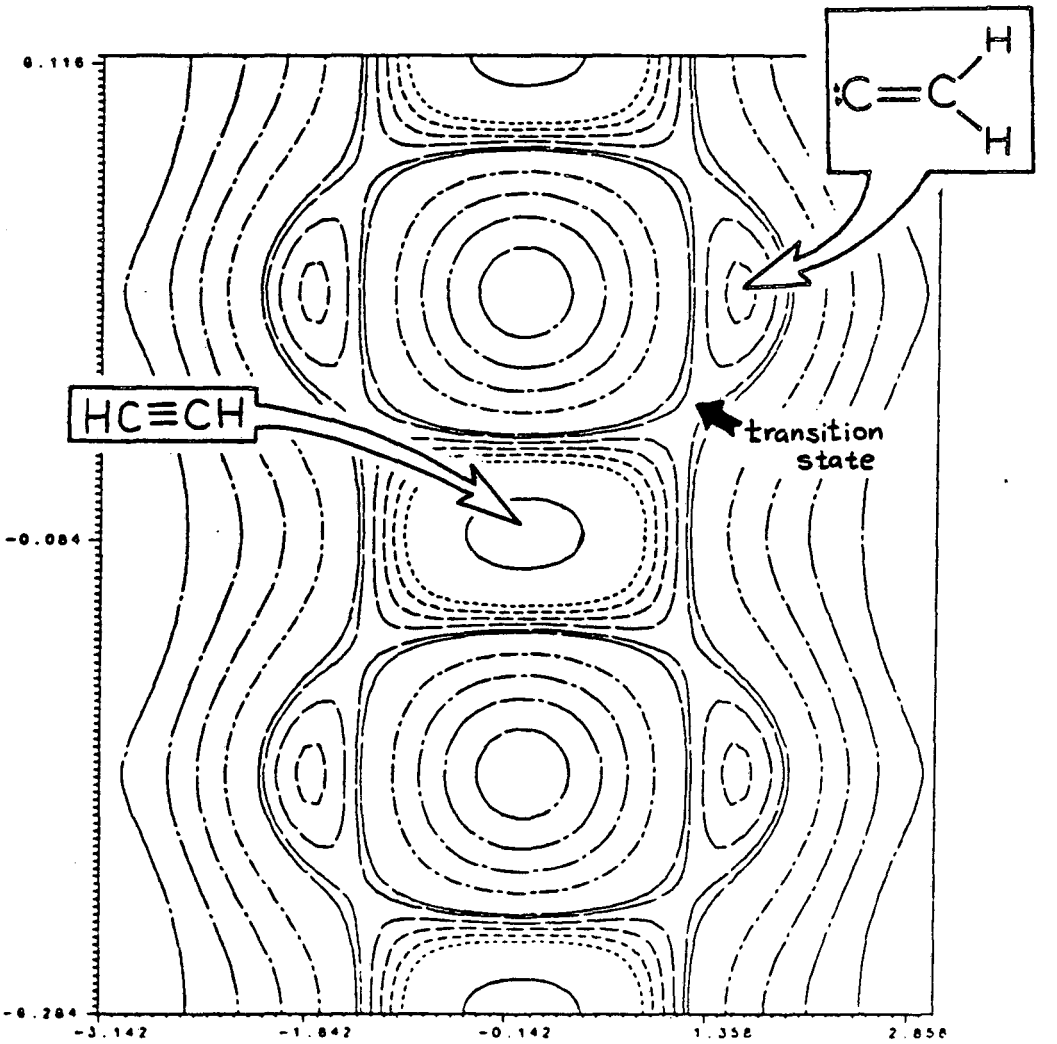

Contour plot for 2-dimensional vinylidene/acetylene isomerization as a function of (Δtheta,θ).

Figure 2.2

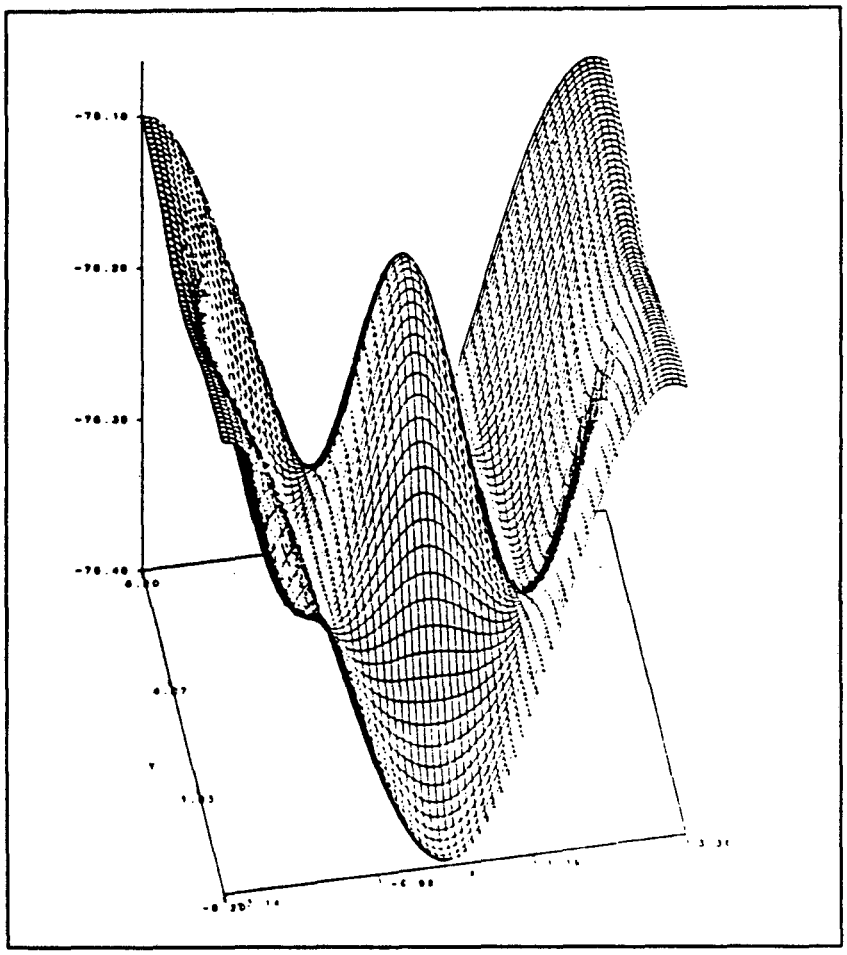

3-dimensional potential surface for vinylidene/acetylene isomerization.

Figure #2.3

The solid curves in Figure 2.4 depict three possible isomerization paths in the 2-dimensional surface. These paths are equivalent representations of H rotation about the carbons. Each of these paths are equally accessible but correspond to different physical motions.

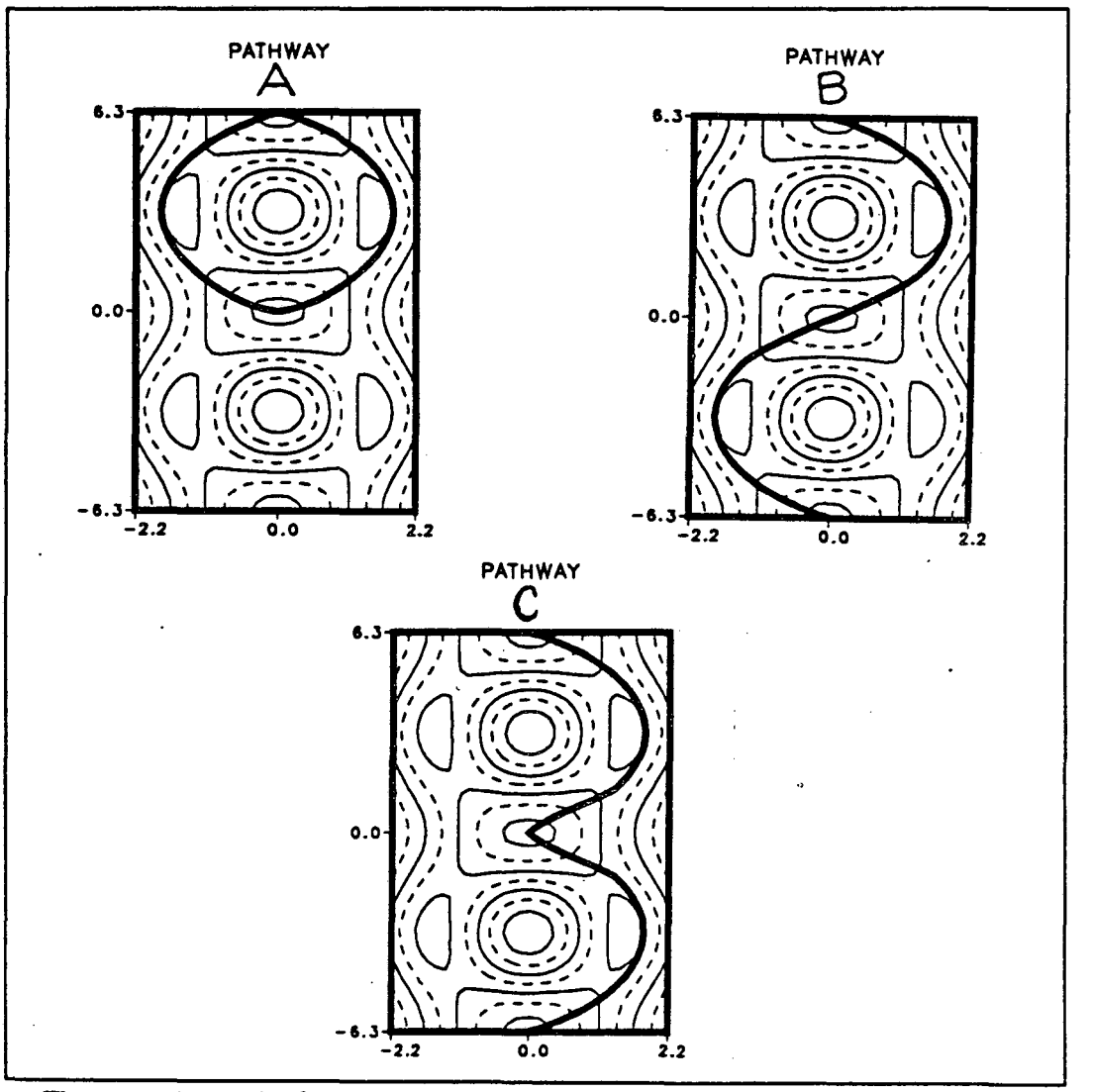

Three reaction paths for isomerization to occur. (A) Closed loop. (B) Independently around. (C) One hydrogen chases the other.

Figure 2.4

The closed loop in Figure 2.4a illustrates the motion of one hydrogen rotating below the C-C skeleton after the other rotates above it and then reversing that process for one complete period. (Recall that the C-C bond length is *not* rigid and the two hydrogens do not rotate at a rigid distance from the C-C frame.) The second path, Figure 2.4b, illustrates the motion of one hydrogen rotating completely around the two carbons before the second one begins to move substantially. The last example depicts an effect where one hydrogen is closely chased by the second as it rotates around the C-C frame. There are many other paths that could be considered, such as a libration motion of one hydrogen rotating to one carbon and then returning to the original carbon. All are equivalent representations of the isomerization process.

A 1-d representation of any of these paths can be constructed as a function of the dimensionless angle = $\gamma = \frac{\pi s}{s_o}$ where s is the reaction coordiante and s_o is the length along this path over one full period from the acetylene geometry to the vinylidene geometry and back to an acetylene geometry. This potential is written as a fourier series similar to what was done for the surface

$$\begin{aligned} \gamma &\equiv \frac{\pi s}{s_o} \\ V_o(\gamma) &= \sum_n a_{2n} \cos(2n\gamma) \end{aligned} \tag{2.6}$$

and is fitted using the three stationary points on the 2-d surface (n ranges from 0 to 2). Figure 2.5 plots the potential $V_o(\gamma)$ for path 2.4c. Similarly to Figure 2.3 the deepest wells correspond to the acetylene geometry and the higher wells correspond to vinylidene. The values for γ that correspond to acetylene and vinylidene are given in Table 2.1.

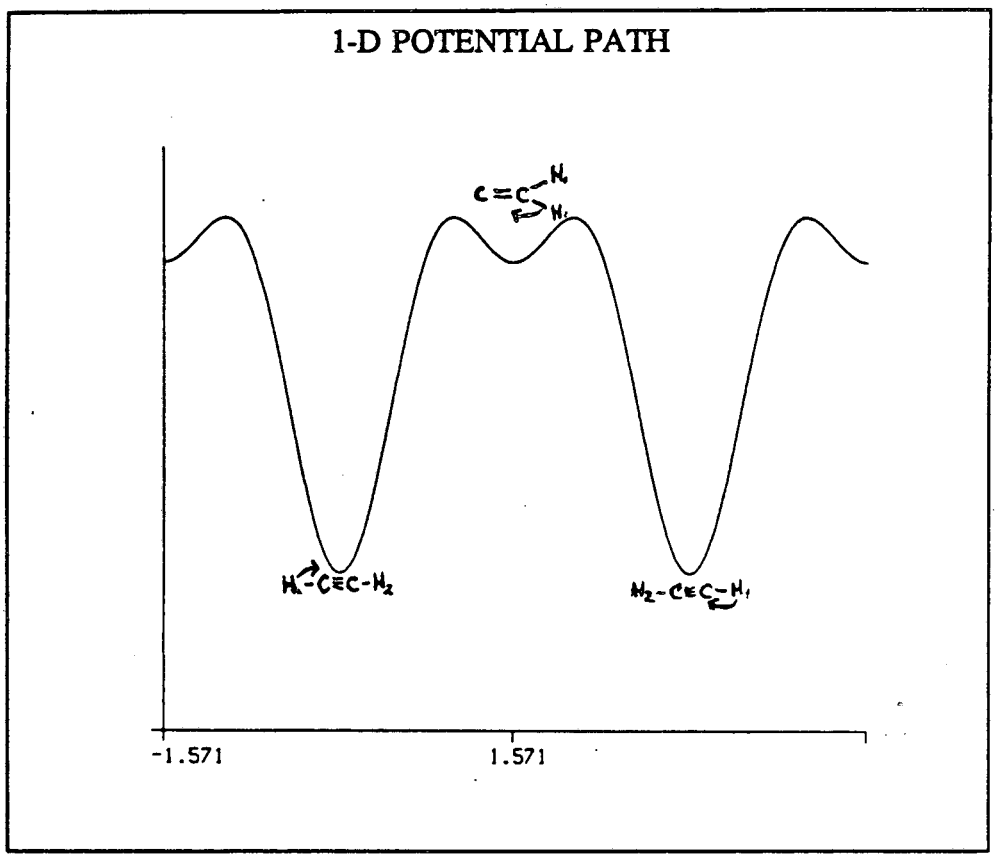

Potential as a function of γ. Hydrogens are labelled 1 and 2 to assist in determining the path taken during isomerization.

Figure #2.5

TABLE 1

Potential Values		
$s=-s_{vin}$	$\gamma=-\frac{\pi}{2}$	Vinylidene
$s=0$	$\gamma=0$	Acetylene
$s=s_{vin}$	$\gamma=\frac{\pi}{2}$	Vinylidene
$s=s_o$	$\gamma=\pi$	Acetylene

We now have two *ab initio* surfaces: one in terms of $\theta,\Delta\theta$ and the other as a function of γ, but the final potential energy surface must include all vibrational degrees of freedom. As was written in Equation 1.1, the remaining orthogonal bath modes of the Hamiltonian are included harmonically, with their frequencies being a function of the reaction coordinates. In order to do this, the *ab initio* second derivatives are diagonalized and then fitted to equations similar to those of the zeroth order potential, V_o.

$$\begin{aligned} V &= V_o + V_{bath} \\ V(\Delta\theta,\theta) &= V_o(\Delta\theta,\theta) + \frac{1}{2}\sum_{k=1}^{4}\omega_k^2(\Delta\theta,\theta)\,Q_k^2 \\ V(\gamma) &= \sum_{n=0}^{2} a_{2n}\cos(2n\gamma) + \frac{1}{2}\sum_{k=1}^{4}\sum_{n=0}^{2} b_{k,2n}\cos(2n\gamma)\,Q_k^2 \end{aligned} \quad . \qquad (2.7)$$

How accurate a potential is this? Our goal is to determine how well a local expansion about a two dimensional surface can approximate the necessary dynamical information for systems with high curvature intrinsic paths where the minimum energy path methods fail. The calculation presented here is intended to test the applicability of the Reaction Surface Hamiltonian as opposed to its quantitative accuracy. This is why a fairly simple basis set was used. Nonetheless, the 3-21G basis set gives the correct qualitative features of the surface.

Table 2.2 compares our *ab initio* energies with calculations done earlier by Carrington et al. using TZ+P CI techniques; experimentally and theoretically determined frequencies are shown in Table 2.3; the geometries from our calculations are shown in Figure 2.6; and Figure 2.7 illustrates the eigenfunctions which shall be referred to in the results Section 4. Because the 3-21G barrier height is 20 kcal/mol whereas the TZ+P CI barrier is 6.3 kcal/mol, the 3-21G barrier height will need to be scaled for quantitative use of the potential surface.

TABLE 2

ENERGY (kcal/mol)		
	TZ+P CI * + Davidson	3-21G
Acetylene	0.000	0.000
Vinylidene	44.044	43.92
Trans. State	49.447	64.38
Barrier	5.403	20.46

*ref 11

TABLE 3

FREQUENCY (cm-1)				
	TZ+P CI	3-21G	Experimental*	Mode
Acetylene	3605	3719	337	CH_s
	3492	3596	3295	CH_a
	2102	2234	1974	C-C
	788	919	729	CCH
	654	903	612	CCH
Transition State	3469	3755		CH_s
	2673	1943		CH_a
	1898	1709		C-C
	951	723		Out of plane
	1012i	442i		Rxn coordinate
Vinylidene	3312	2892		CH_a
	3217	2892		CH_s
	1719	1856	1650	C-C
	1289	1109	1120	Out of plane
	800	458		Rock
	422	73		Scissors

* ref 10, 14

GEOMETRIES

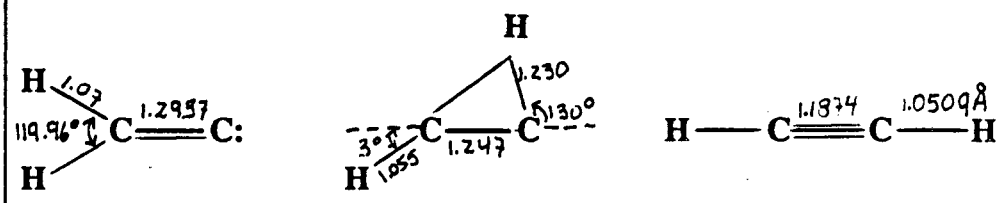

3-21G *ab inito* geometries for vinylidene isomerization to acetylene.

Figure #2.6

NORMAL MODES

	Vinylidene	Acetylene	
CH_a	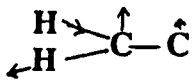		CH_a
CH_s	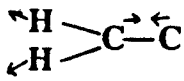	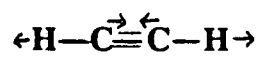	CH_s
CC	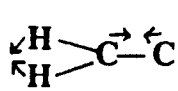	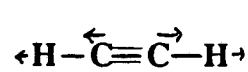	CC
Out	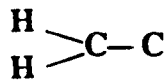	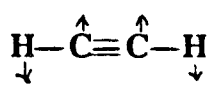	CCH
Sciss	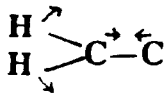	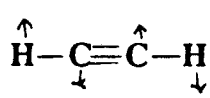	CCH
Rock	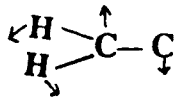		

3-21G Normal mode eigenvectors for vinylidene and acetylene

Figure #2.7

2.3 Kinetic Energy

The kinetic energy expression for both the Reaction Path and Reaction Surface Hamiltonians have been given in earlier papers[5]. This section gives the kinetic energy expression in terms of our parameter γ [cf. Equation 2.6] for the path in Figure 2.5c. In order to do this we begin with the expression for the Reaction Path kinetic energy (with J=0) that is given in Reference 2

$$T_{RPH} = \frac{1}{2}\sum_k P_k^2 + \frac{1}{2}\frac{\left[P_s - \sum_k P_k B_{k,k'} Q_{k'}\right]^2}{\left[1 + \sum_k B_{k,s} Q_k\right]^2} \tag{2.8}$$

where P_k is the momentum conjugate to the Q_k bath modes, P_s is the reaction coordinate momentum, $B_{k,k'}$ couples the Q_k bath mode to the $Q_{k'}$ bath mode [e.g., coupling the C-C stretch to the CH_2 scissors mode], and $B_{k,s}$ couples the kth bath mode to the reaction coordinate s. The $B_{k,s}$ term is a direct result of the curvature of the reaction path whereas $B_{k,k'}$ are coriolis-like couplings that arise from the bath eigenvectors twisting about the path in going from reactant to product.

If one expands the denominator in Equation 2.8 and sets $B_{k,k'}$=0 the result is:

$$T = \frac{1}{2}\sum_k P_k^2 + \frac{1}{2}P_s^2 - P_s^2\left[\sum_k B_{k,s} Q_k + \frac{3}{2}(\sum_k B_{k,s} Q_k)^2 - \cdots\right] \tag{2.9}$$

Note that this expression still retains the coupling between the Q_k bath modes and the reaction coordinate. The kinetic energy can now be rewritten in terms of the 1-d reaction coordinate, $\gamma = \frac{s\pi}{s_o}$, and one obtains the following expression to second order in

Q_k:

$$T = \frac{1}{2}\sum_k P_k^2 + \frac{1}{2\mu_\gamma}P_\gamma^2 - \mu_\gamma^{\frac{3}{2}}P_\gamma^2\left[\sum_k B_{k,\gamma}(\gamma)\, Q_k\right] + \frac{3}{2}\mu_\gamma^2 P_\gamma^2\left[\sum_k B_{k,\gamma}(\gamma)\, Q_k\right]^2 \qquad (2.10)$$

This is the kinetic energy expression as a function of reaction angle γ and bath modes $\{Q_k\}$. The first term in this expression is the kinetic energy for the harmonic bath with a mass of 1. The second term is the kinetic energy of the reaction angle with an effective mass μ_γ. The third and fourth terms give the kinetic coupling between the system and the bath.

The value of the effective reaction coordinate mass can be calculated from the definition that results with the s to γ transformation:

$$\frac{1}{\mu_\gamma} \equiv \left(\frac{\pi}{s_o}\right)^2 \qquad (2.11)$$

Because the value for s_o is the path length over one full period, it can be written in terms of the cartesian coordinates of the molecule

$$s_o = \int_{\text{one period}} \sqrt{\sum_{i=1} m_i\,(dx_i^2 + dy_i^2 + dz_i^2)}\ , \qquad (2.12)$$

and geometry tells us the relation between these cartesian coordinates and the internal coordinates that were used to generate the potential surface. For our potential, we can rewrite Equation 2.12 in terms of the angles θ_1 and θ_2 [cf., Figure 2.1] as

$$s_o = \int_0^{\pi} d\theta_1 \sqrt{m_H} \left[\left(\frac{dr_1}{d\theta_1}\right)^2 + r_1^2 + \left(\frac{dr_2}{d\theta_1}\right)^2 + r_2^2 \left(\frac{d\theta_2}{d\theta_1}\right)^2 + \frac{m_C}{m_H} \frac{dr_{CC}}{d\theta_1{}^2} \right]^{\frac{1}{2}} . \qquad (2.13)$$

Because the reaction surface potential was generated by freezing two degrees of freedom while varying the remaining coordinates in order to optimize the energy, we can fit the internal coordinates as a function of the selected values of the angles θ_1 and θ_2. However, if we don't know the derivatives of r_1, r_2 and θ_2 with respect to θ_1 then a simple approximation can be made based on the following three assumptions.

$$\begin{aligned} \frac{d\theta_2}{d\theta_1} &= 1 \quad ; \quad d\theta_2 = d\theta_1 \\ \frac{dr_{CC}}{d\theta_1} &= 0 \quad ; \quad r_{CC} = \text{constant} \\ \frac{dr_i}{d\theta_1} &= 0 \quad ; \quad r_1 = r_2 = \text{constant} \end{aligned} \qquad (2.14)$$

Given these three approximations,

$$\begin{aligned} s_0 &= \sqrt{m_H} \int_0^{\pi} \sqrt{r_1^2 d\theta_1 + r_2^2 d\theta_1} \\ s_o &= \pi \sqrt{m_H} \sqrt{r_1^2 + r_2^2} \\ \frac{1}{\mu_\gamma} &= \left(\frac{\pi}{s_o}\right)^2 = \frac{1}{m_H [r_1^2 + r_2^2]} = \frac{1}{\sum_{i=1}^{2} m_i r_i^2} \end{aligned} \qquad (2.15)$$

Equation 2.15 expresses the effective reaction coordinate mass in terms of the moment of inertia for two hydrogens rotating about a point with their respective radii being r_1 and r_2. Using this expression with the average value of radii from the poten-

tial surface (r_1=1.552, r_2=1.4073 Angstroms) gives a value of s_o=532.55 and μ_γ=3.542x10^{-5}. For simplicity, we use this value for the mass of γ.

Finally, the kinetic energy coupling terms, $B_{k,\gamma}$ (remember these couple the Q_k bath modes to the γ reaction coordinate) must be fitted to an analytic expression in γ because the coupling between the bath modes and the reaction coordinate changes as isomerization occurs. In order to do this the normal mode eigenvectors [cf. Fig. 2.7] need to be fitted because of the definition of the coupling term:

$$B_{k,\gamma}(\gamma) = \frac{\partial L_k(\gamma)}{\partial \gamma} \cdot L_\gamma(\gamma) \tag{2.16}$$

where L_k is the eigenvector for the kth bath mode. Luckily, because of the symmetry of this problem, one can separate the components of L_k according to their symmetry with respect to reflection about γ=0 and to $\gamma = \frac{\pi}{2}$ by writing them in symmetrized cartesian coordinates:

$$\begin{aligned} L_{k,1} &= (r_{C_1}-r_{C_2})_x \\ L_{k,2} &= (r_{C_1}-r_{C_2})_y \\ L_{k,3} &= (r_{C_1}+r_{C_2})_y + (r_{H_1}-r_{H_2})_x + (r_{H_1}+r_{H_2})_y \\ L_{k,4} &= (r_{C_1}+r_{C_2})_x + (r_{H_1}+r_{H_2})_x + (r_{H_1}-r_{H_2})_y \end{aligned} \tag{2.17}$$

The notation used to describe the classification of each component is as follows: $L_{k,i}^{e,o}$ corresponds to the ith element of the kth normal mode eigenvector that is *even* with respect to reflection about γ=0 and *odd* with respect to reflection about $\gamma=\frac{\pi}{2}$. Now each component can be fitted to a Fourier series according to its symmetry properties. For example, one vector can be written as:

$$L_k = \begin{bmatrix} L_{k,1}^{e,e} \\ L_{k,2}^{o,e} \\ L_{k,3}^{e,o} \\ L_{k,4}^{o,o} \end{bmatrix} = \begin{bmatrix} \sum_n a_n \cos(2n\gamma) \\ \sum_n a_n \sin(2n\gamma) \\ \sum_n a_n \cos((2n-1)\gamma) \\ \sum_n a_n \sin((2n-1)\gamma) \end{bmatrix} \tag{2.18}$$

We now have the eigenvectors in terms of sines and cosines of γ. Again, for our example, we use the *ab initio* information from the three stationary points to perform the fit. The derivatives of the L_k are straightforward, and we write the coupling terms $B_{k,\gamma}$ in terms of sines and cosines.

$$B_{k,\gamma}(\gamma) = \sum_{m,n} a_{mn} \sin(\gamma) \cos(\gamma) \tag{2.19}$$

We now proceed to use this kinetic energy expression in the full vinylidene/acetylene Hamiltonian.

2.4 Hamiltonian

The final vinylidene/acetylene Hamiltonian is given by the kinetic energy expression of Equation 2.10 plus the potential, Equation 2.7. The simplest way to use this Hamiltonian is to reduce it to an effective one-dimensional problem. This can be achieved by averaging over the bath modes. Similar to how one separates the fast electronic coordinates from the slow nuclear ones with the Born-Oppenheimer approximation, we integrate out the fast bath modes from the slow reaction coordinate by transforming to action-angle variables and integrating over q_k in the usual manner[12]:

$$
\begin{aligned}
Q_k &= \sqrt{\frac{n_k+1}{\omega_k(\gamma)}}\,\sin q_k \\
P_k &= -\sqrt{(2n_k+1)\,\omega_k(\gamma)}\,\cos q_k.
\end{aligned}
\tag{2.20}
$$

The two kinetic energy coupling terms in Equation 2.10 become:

$$
\begin{aligned}
-\mu_\gamma^{\frac{3}{2}} P_\gamma^2 \sum_k B_{k,\gamma}(\gamma)\, Q_k &= -\mu_\gamma^{\frac{3}{2}} P_\gamma^2 \sum_k \iint dq_k\, B_{k,\gamma}(\gamma) \sqrt{\frac{2n_k+1}{\omega_k(\gamma)}}\,\sin q_k \\
&= 0
\end{aligned}
$$

and similarly,

$$
\frac{3}{2}\mu_\gamma^2 P_\gamma^2 \Big(\sum_k B_{k,\gamma}(\gamma)\, Q_k\Big)^2 = \frac{3\pi}{2}\mu_\gamma^2 P_\gamma^2 \sum_k \frac{2n_k+1}{\omega_k(\gamma)} B_{k,\gamma}^2(\gamma)\,\pi \ .
$$

Therefore, the Reaction Path Hamiltonian that we use is written:

$$
H_{RPH}(\gamma) = \frac{1}{2\mu_\gamma} P_\gamma^2 + V_o(\gamma) + \sum_k (n_k+1)\,\omega_k^2(\gamma) + \pi\,\mu_\gamma^2 P_\gamma^2 \sum_k \frac{2n_k+1}{\omega_k(\gamma)} B_{k,\gamma}^2(\gamma). \tag{2.21}
$$

If the terms $B_{k,\gamma}$ that couple the Q_k bath modes to the γ reaction coordinate are set to zero, the result would be the standard vibrationally adiabatic Hamiltonian with "good" action quantum numbers. In other words, it would be a one-dimensional Hamiltonian plus the ground state energies of the harmonic baths with n_k being a constant of motion. This is the type of Hamiltonian that was used by Carrington et al[11]. And whereas they added the coupling terms via the Feshbach approach, Equation 2.21 explicitly incorporates the direct coupling between γ and the bath.

Furthermore, because Equation 2.7 expresses $V_o(\gamma)$ and $\omega_k(\gamma)$ with a Fourier series, and Equation 2.19 gives $B_{k,\gamma}(\gamma)$ in a Fourier series as well, the adiabatic Hamil-

tonian can be written as a Fourier series in cos(mγ) and sin(nγ).

$$H(\gamma) = \frac{1}{2\mu_\gamma}P_\gamma^2 + \sum_n A_{2n}\cos(2n\gamma) + \sum_m B_{2m}\sin(2m\gamma)$$

and by choosing a basis set with sines and cosines of γ,

$$\begin{aligned} \phi &= \sum_m A_m\cos(m\gamma) + \sum_n B_n\sin(n\gamma) \\ \phi_{m_a,n_b} &= |A_m\cos(m_a\gamma),\ B_n\sin(n_a\gamma)\rangle \end{aligned} \tag{2.23}$$

we are able to evaluate the Hamiltonian matrix elements analytically. An added benefit is that the Hamiltonian matrix becomes block diagonal under these conditions.

$$\langle m|T|n\rangle = \frac{1}{\mu_\gamma}\delta_{m,n}$$

$$\langle \cos m_a|V|\cos n_a\rangle = \frac{(2n+1)}{2\sqrt{\delta_{m,0}+1}\sqrt{\delta_{n,0}+1}}\left[A_{m-n}(\delta_{m-n,0}+1) + A_{m+n}(\delta_{m+n,0}+1)\right]$$

$$\langle \sin m_b|V|\sin n_b\rangle = \frac{(2n+1)}{2\sqrt{\delta_{m,0}+1}\sqrt{\delta_{n,0}+1}}\left[A_{m-n}(\delta_{n-m,0}+1) - A_{m+n}(\delta_{m+n,0}+1)\right]$$

$$\langle \cos m_a|V|\sin n_b\rangle = 0$$

$$H = \begin{bmatrix} H_{aa} & H_{ab} \\ H_{ba} & H_{bb} \end{bmatrix} = \begin{bmatrix} H_{aa} & 0 \\ 0 & H_{bb} \end{bmatrix}$$

2.5 Results

Diagonalizing the Hamiltonian using the above basis set does not provide direct information on the dynamics of the problem because we obtain eigenvalues and eigenvectors but not rates and lifetimes. Fortunately, one can rely upon the association of the width of the intensity spectrum with the lifetime of a state because a stationary state is defined as having a spectral width of zero (corresponding to a delta function at its given energy) while a state that dissociates with a lifetime τ is regarded as having a nonzero width $\Gamma = \frac{h}{\tau}$. The origin of this width results from the fact that the intensity spectrum for nonradiative decay of state [cf. Appendix 2.2 for the derivation] can be approximated as a Lorentzian:

$$I(E)_{nonrad} = |H_{iE}|^2 \frac{\frac{1}{2}\Gamma(E)}{(\frac{1}{2}\Gamma(E))^2 + (E_i - E)^2} \tag{2.24}$$

The width Γ can, therefore, be determined by examining the full-width-half-maximum of the Lorentzian shape of the spectrum I(E). Once we recognize this relationship, we need only plot the spectrum of vinylidene coupled to the many highly excited acetylene states in order to determine its lifetime. This is done by calculating the Fourier transform of the autocorrelation of the vinylidene wavefunction under the influence of the vinylidene/acetylene Hamiltonian.

$$
\begin{aligned}
I(E) &= \text{FourierTransform} \langle\phi_v(0)|\phi_v(t)\rangle \\
&= \int_{-\infty}^{\infty} dt\, e^{\frac{iEt}{h}} \langle\phi_v|\phi_v(t)\rangle \\
&= \int_{-\infty}^{\infty} dt\, e^{\frac{iEt}{h}} \langle\phi_v|e^{\frac{-iHt}{h}}|\phi_v\rangle \\
&= 2\pi \langle\phi_v|\delta(E-H)|\phi_v\rangle \\
&= 2\pi \sum_i \langle\phi_v|\delta(E-H)|\phi_i\rangle\langle\phi_i|\phi_v\rangle \\
&= 2\pi \sum_i |\langle\phi_v|\phi_i\rangle|^2\, \delta(E-E_i)
\end{aligned}
\tag{2.25}
$$

Therefore, the spectrum is the square of the overlap between the eigenstates ϕ_i of the full Hamiltonian with those of the pure vinylidene states ϕ_v, Because the vinylidene wavefunction is not an eigenfunction of the full Hamiltonian, the intensity spectrum will appear as a series of delta functions with a height that corresponds to the overlap of ϕ_v with the eigenfunction ϕ_i. [In reality, the energy levels that couple to vinylidene have a finite lifetime so these delta functions would have a width corresponding to the respective lifetimes of the levels.] The full-width-half-maximum of the resulting intensity spectrum is interpreted as the lifetime of vinylidene.

One cannot isolate vinylidene apart from the highly excited states of acetylene so we use harmonic oscillator wavefunctions centered at the vinylidene well as the pure vinylidene state. Figure 2.8a plots the overlap of the pure vinylidene state with one eigenstate of the vinylidene/acetylene Hamiltonian that is localized mostly in the vinylidene well. This overlap will be close to one. However, Figure 2.8b plots a wavefunction that is more localized in the acetylene well. The 1-dimensional potential is plotted above it for reference. Overlap with this wavefunction will result in a small value.

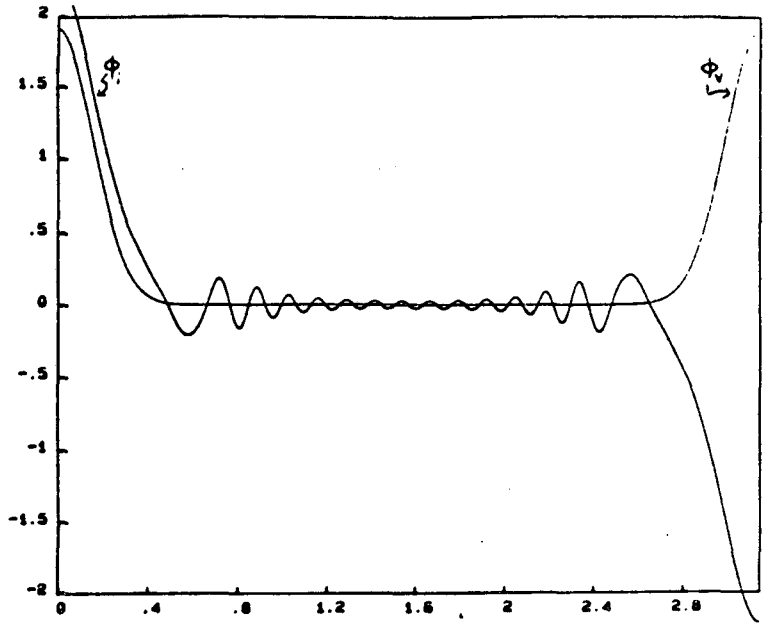

Eigenvector ϕ_i is plotted overlapping vinylidene wavefunction ϕ_v. ϕ_i has energy comparable to vinylidene and is mostly localized in the vinylidene wells.

Figure #2.8a

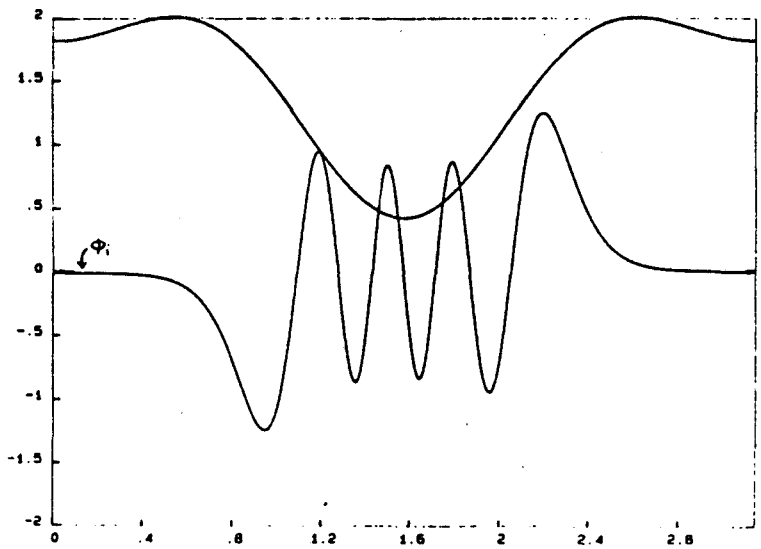

Eigenvector ϕ_i is plotted beneath the potential curve. ϕ_i is mostly localized in the acetylene well.

Figure #2.8b

Below is an example of the intensity spectrum for vinylidene with one excitation in the CH_s stretch mode.

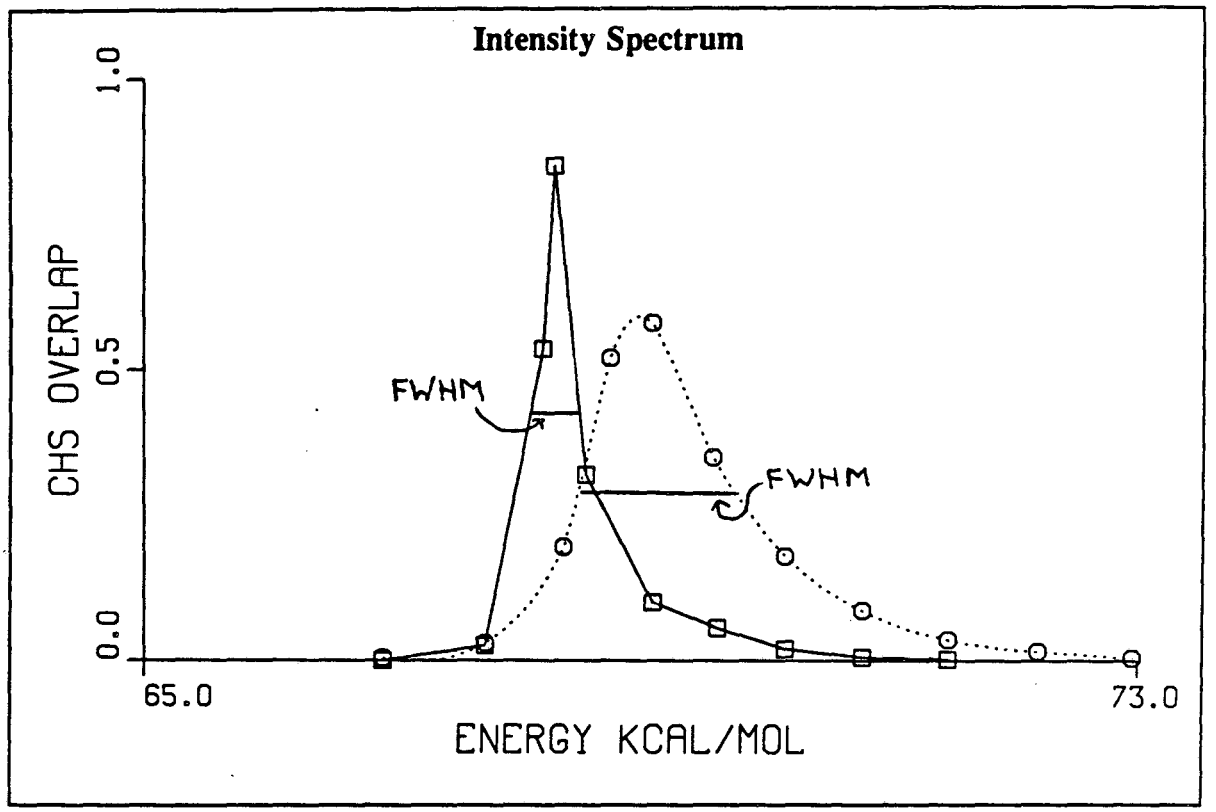

$|\langle\phi_v|\phi_i\rangle|^2$ plotted over the energy spectrum. The Full-Width-Half-Maximum determines the lifetime of the state. Solid lines depict overlap with the ground state of vinylidene; Dashed curves represent overlaps with the first excited state.

Figure 2.9

We first examined the uncoupled adiabatic Hamiltonian by setting $B_{k,\gamma}$ to zero in Equation 2.21. There exists an *effective* barrier height with the inclusion of the bath modes zero point energies because the frequencies of the bath modes at the transition state differ from those at the equilibrium. Of the four bath modes, the C-H symmetric stretch (CH_s; cf. Figure 2.7) frequency changes the most between the two local minima. Addition of this mode results in a decrease of the barrier by 1.0 kcal/mol, a nar-

rowing of the well, and an decrease in the lifetime of vinylidene and is solely due to the adiabatic effect of the bath frequencies as opposed to coupling to the reaction coordinate. The CH_2 scissors mode and the out-of-plane mode also decrease the barrier height (by 0.7 and 0.4 kcal/mol respectively) and narrow the wells. On the other hand, the C-C stretch and the C-H asymmetric stretch (CH_a) increase the barrier height by ~0.4 kcal/mol.

Based solely on these adiabatic effects, the relative effects on the lifetime of vinylidene goes as: $CH_s > CH_{scis} > C–C, CH_a >$ Out-of-plane. The CH_s mode decreases the lifetime by approximately 1¼ times. The scissors mode decreases it by a factor of two. Although the CH_a and C-C bath modes are good modes for forming the transition state, they hardly affect the lifetime at this adiabatic level.

By including the coupling term $B_{k,\gamma}$ we can examine how nonadiabatic couplings influence the lifetime of vinylidene. Table 2.4 summarizes these effects. Column 1 indicates how many quanta are in the reaction coordinate, column 2 indicates how many quanta are in one of the bath modes, column 3 gives the lifetime of vinylidene, column 4 tells how the rate of the isomerization compares with the ground state rate of vinylidene given by the first row, and column 5 indicates how the rate varies from its first excited state given by the seventh row. Column 6 gives the lifetime of vinylidene if there is no coupling to the out-of-plane mode.

It is found that the size of the kinetic coupling term is approximately 1/10 the size of the adiabatic kinetic expression. This coupling value varies as a function of γ but, in general, the CH_s mode has the smallest kinetic coupling (although it has the largest adiabatic change) and the scissors mode has the largest coupling.

We calculate the lifetime of the ground state of vinylidene to be 0.08 psec. This compares with the value of 0.14 psec of Burnett et al. and of 0.12 psec of Carrington et al. The lifetime of vinylidene with one quanta in the reaction coordinate is deter-

mined by comparing the FWHM values for the ground state with that for excited state of this mode. Excitation by one quanta increases the mean time of isomerization by a factor of three. The fact that it increases it rate makes intuitive sense since this is the isomerization coordinate itself. The amount of this increase is smaller than that which was found by Carrington et al On the other hand, when the out-of-plane mode is decoupled (Column 6) the rate increases to a factor of six, in agreement with Carrington et al In fact, the absolute rates calculated by excluding the out-of-plane mode tend to agree better with the results of Carrington et al. than those with all of the bath modes included. However, the qualitative results are the same: the Scissors mode and reaction coordinate decrease the lifetime while the C-C mode increases it (see Column 4). We find that the out-of-plane mode also decreases the lifetime (increases the rate) by a factor of two or three. Table 2.10 also indicates that the CH_s mode appears to increase the lifetime of vinylidene, in contradiction to its adiabatic effect. However, the effects of the two C-H stretches are not as clearly defined as the other modes, and we hesitate to assert what their effects are.

TABLE 4

Lifetimes					
Rxn	N. Mode	Γ(psec)	$*k_o$	$*k_1$	Γ′(psec)
0	0	0.08	1.0	-	0.15
	1 Scis	0.03	2.7	-	0.05
	1 out	0.15	2.7	-	-
	1 C-C	0.15	0.5	-	0.20
	1 CH_s	0.25	0.3	-	0.20
	1 CH_a	-	-	-	-
1	0	0.02	3.5	1.0	0.03
	1 Scis	0.012	6.7	1.8	0.012
	1 out	0.014	5.7	1.6	-
	1 C-C	0.04	2.0	0.6	0.085
	1 CH_s	0.04	2.0	0.6	0.10
	1 CH_a	0.03	2.6	0.8	-

Columns 1 & 2 give quantum number for normal mode. Column 3 gives lifetime. Column 4 gives multiple of ground state rate of isomerization. Column 5 gives multiple of the rate from one excitation in the reaction coordinate. Column 6 gives lifetime for isomerization restricted in the plane.

An interesting aspect that was uncovered during our eigenvalue calculations were the eigenstates localized near the vinylidene wells [cf. Figure 2.8a]. The two lowest energy states of these have symmetric and asymmetric symmetry due to the symmetry of the potential, and have an energetic splitting of 8-11 kcal/mol. The energy of these states lies approximately 16,000 cm^{-1} above the acetylene ground state. Therefore, there may be some possibility of seeing either this splitting or some ramification of it for highly excited acetylene states.

It might also be instructive to view these high energy states as being more in character with a C-H stretch or bend as opposed to the normal modes of acetylene.

Abramson, Field, Irme, Innes, and Kinsey[9g] have seen symmetric near degenerate pairs of lines at 11,500 cm-1 which may indicate the existence of local C-H benders. They also report that the C-H local stretch is free of strong perturbations up to 16,000 cm-1 (ν_{CH}=5,6) while the C-C and trans/bend states are massively perturbed at energies near 11,500 cm-1 which is another indication for possible C-H character at high energies. The overlap of our eigenstates at these high energies with harmonic or morse oscillators for the C-H bond may be able to illuminate this possibility.

Furthermore, the dependence of the potential surface on the angles θ_1 and θ_2 may help discern if it is possible for the concerted H motion to be a conserved dynamical quantity.

2.6 Multiple Pathways

As was mentioned above, the potential energy surfaces presented in Figure 2.5 illustrate the existence of several reaction paths on a single potential energy surface. Section 2.2 of this Chapter discusses the fact that these pathways are equally energetically viable, but that each has a different physical interpretation for the conversion between vinylidene and acetylene. They are all accessible and to neglect any of them is to neglect information about the total surface. This section briefly describes how to incorporate the effects of a second reaction pathway.

When two paths are present on a potential surface one needs to consider the following three characteristics. First, there are three Hamiltonians:

$$H_a = \text{Hamiltonian for path A only}$$

$$H_b = \text{Hamiltonian for path B only}$$

$$H = \text{full Hamiltonian}$$

$$H = H_a + V = H_b + V' \quad .$$

H_a is the Hamiltonian for path A (when one ignores the existence of path B), and vice versus for H_b. The Hamiltonians for the two separate paths in Figure 2.5, for example, will have similar forms although, for the type of expansion given in Eqn. 2.6, they will have different coefficients due to the differing orientations of the eigenvectors along the path. Therefore, the generation of the second path, H_b, is not any more difficult than for the first path H_a. The full Hamiltonian includes the coupling of the interacting paths which alters the shape of the potential. For example, although it may be sufficient to represent the orthogonal degree of freedom Q by a harmonic oscillator when there is only one reaction path, this may not be true for when there are two. The repulsive wall of the harmonic well about one path will relax as it approaches the local minimum of the second path. These anharmonicities are not included by a simple harmonic expression in Q.

The second characteristic is the presence of two different coordinate systems, $\{s_a, Q_a\}$ and $\{s_b, Q_b\}$ for path A and path B respectively. A single point **x** can now be described with respect to *either* of these two reaction paths.

Thirdly, one needs to decide in which coordinate system to express the basis set to diagonalize the full Hamiltonian. One solution is to write basis set functions as a linear combination of wavefunctions from each of these two paths. This is similar to writing molecular orbitals as linear combination of atomic orbitals. Specifically,

$$
\begin{aligned}
H\Psi_k &= E_k\Psi_k \\
\Psi &= c_a\psi_a + c_b\psi_b \\
H_a\psi_a &= \varepsilon_a\psi_a
\end{aligned}
\tag{2.26}
$$

ψ_a = wavefunction for H_a

ψ_b = wavefunction for H_b

Ψ_k = wavefunction for full H

By choosing the basis set $\{\Psi_k\}$ as shown above, the Hamiltonian matrix can be written:

$$
\mathbf{H} = \begin{bmatrix} H_{aa} & H_{ab} \\ H_{ba} & H_{bb} \end{bmatrix}
$$

where

$$
\begin{aligned}
H_{aa} &= \langle\psi_a|H|\psi_a\rangle = \langle\psi_a|H_a|\psi_a\rangle + \langle\psi_a|V|\psi_a\rangle \\
H_{bb} &= \langle\psi_b|H|\psi_b\rangle \\
H_{ba} &= \langle\psi_b|H|\psi_a\rangle
\end{aligned}
\tag{2.27}
$$

The first term for H_{aa} in Eqn. 2.27 is the straightforward matrix element for path A (as if the other path did not exist) which gives the eigenvalues ε_a. The second term is the coupling matrix element and can be evaluated if V is known. One can approximate V as a polynomial in Q_a. This is a good approximation in the vicinity of the reaction paths where potential values can be accurately fitted. Although the fit may not be as accurate far from the path, both the coupling strength and the amplitude of

the wavefunction ψ_a decrease which results in the matrix element of V becoming small in these regions (approaching zero as ψ_a approaches zero). Therefore, a polynomial fit in Q_a for V should be a good approximation far as well as near the reaction path.

ψ_a can also be expressed in a basis:

$$\begin{aligned} \psi_a &= \sum_n a_n |\Phi_{na}> = \sum_n a_n |n_a> \\ \Phi_{na} &= \chi_n(s_a) \prod_k \phi_n(Q_{ka}) \end{aligned} \tag{2.28}$$

where $\chi(s_a)$ and $\phi(Q_{ka})$ are harmonic oscillators, for example. If these forms are used when the coupling term, V, is written as a function of raising and lowering operators for the A-path (i.e., as a polynomial in Q_a), the coupling matrix elements become

$$\begin{aligned} <\Phi_{ma}|V|\Phi_{na}> &= <m_a|\sum_n c_n (a^+ + a)^n |n_a> \\ &= \sum_{n'} d_{n'} <m_a|n'_a> \\ H_{aa} &= \varepsilon_n^a + \sum_{n'} dn' <m_a|n'_a> \end{aligned} \tag{2.29}$$

It turns out that the matrix elements of H_{ba} are not much more difficult to obtain than those for H_{aa}, especially if V is written as a polynomial in Q_a. And, once again, writing V as a polynomial in Q_a is not a bad approximation if ψ_a goes to zero at distances far from the path. Therefore,

$$H_{ba}^{mn} = \varepsilon_n^a \sum\sum a_{mb} a_{na} <m_b|n_a> + \sum_{n'} f_{n'} <m_b|n'_a> \tag{2.30}$$

Eqns. 2.29 and 2.30 indicate that the Hamiltonian matrix elements H_{aa} and H_{ba} can be reduced to the energies for the separate paths plus the overlap matrix of Φ_{ma}

$$
\begin{aligned}
<m_b|n_a> &= \int dx\, \Phi^*_{mb} \Phi_{na} \\
&= \int dx \int ds_a \int dQ_a\, \delta(s_a - s_a(x))\, \delta(Q_a - Q_a(x)) \\
&\quad \cdot \int ds_b \int dQ_b\, \delta(s_b - s_b(x))\, \delta(Q_b - Q_b(x))\, \Phi^*_{mb} \Phi_{na} \\
&= \int dx \int ds_a \int dQ_a \int ds_b \int dQ_b\, \delta(x - x(s_a,Q_a)) \frac{\partial(x)}{\partial(s_a,Q_a)} \\
&\quad \cdot \delta(x - x(s_b,Q_b)) \frac{\partial(x)}{\partial(s_b,Q_b)} \Phi^*_{mb} \Phi_{na}
\end{aligned}
\tag{2.31}
$$

and Φ_{mb}. This overlap can be calculated in the following manner:

$$
= \int ds_a \int ds_b \int dQ_a \int dQ_b \frac{d(x)}{\partial(s_a,Q_a)} \frac{\partial(x)}{\partial(s_b,Q_b)} \delta_F(x(s_a,Q_a) - x(s_b,Q_b))\, \Phi^*_{mb} \Phi_{na} \; .
$$

The Jacobians in Eqn. 2.31 result from the transformation between cartesian coordinates $\{x\}$ and reaction path coordinates $\{s, Q_k\}$. The delta function avoids double counting when integrating over the two paths A and B and can be written as integrals in the usual fashion for F degrees of freedom. Therefore,

$$
\begin{aligned}
x_a &= a(s_a) + L_a \cdot Q_a \\
\frac{\partial(x)}{\partial(s_a,Q_a)} &= \left[1 + \sum_k B^a_{ks} Q_{ka}\right]. \\
\delta_F(x_a - x_b) &= \frac{1}{(2\pi)^F} \int d_F k\, e^{-i k \cdot (x_a - x_b)}
\end{aligned}
\tag{2.32}
$$

The resulting overlap integral is given by the following expression.

$$<m_b|n_a> = \frac{1}{(2\pi)^F} \int ds_a \chi_n(s_a) \int ds_b \chi_m(s_b) \int d_F k \; e^{-i\mathbf{k}\cdot(\mathbf{a}_a-\mathbf{a}_b)} \tag{2.33}$$

$$\cdot \int dQ_a [1+\mathbf{B}_a\cdot\mathbf{Q}_a] \phi_n(Q_a) e^{-i(\mathbf{k}\cdot\mathbf{L}_a)Q_a} \int dQ_b [1+\mathbf{B}_b\cdot\mathbf{Q}_b] \phi_m(Q_b) e^{+i(\mathbf{k}\cdot\mathbf{L}_b)Q_b}$$

One can regroup each dQ_k integral and write them in terms of a newly defined momentum wavefunction $\bar{\phi}$:

$$\begin{aligned} \int dQ_k \, [1 + B_{ks}Q_k] \phi_n(Q_k) \, e^{-i(\mathbf{k}\cdot\mathbf{L})Q_k} &= \left[1 + i B_{ks} \frac{\partial}{\partial(\mathbf{k}\cdot\mathbf{L})}\right] \bar{\phi}_{nk}(\mathbf{k}\cdot\mathbf{L}) \\ &= \left[1 + i B_{ks} \frac{\bar{\phi}'_{nk}(\mathbf{k}\cdot\mathbf{L})}{\bar{\phi}_{nk}(\mathbf{k}\cdot\mathbf{L})}\right] \bar{\phi}_{nk}(\mathbf{k}\cdot\mathbf{L}) \end{aligned} \tag{2.34}$$

where

$$\bar{\phi}_{nk}(\mathbf{k}\cdot\mathbf{L}) \equiv \int dQ_k \, e^{-i(\mathbf{k}\cdot\mathbf{L})Q_k} \, \phi_n(Q_k)$$

The final result for the overlap matrix is:

$$<m_b|n_a> = \int ds_a \int ds_b \, \chi_n(s_a) \, \chi_m(s_b) \, \frac{1}{(2\pi)^F} \int_F dk \; e^{-i\mathbf{k}\cdot(\mathbf{a}_a-\mathbf{a}_b)}$$

$$\cdot \prod_{n,m} \bar{\phi}_n(\mathbf{k}\cdot\mathbf{L}_a) \, \bar{\phi}_m(-\mathbf{k}\cdot\mathbf{L}_b) \left[1 + i\mathbf{B}_a \frac{\bar{\phi}'_n(\mathbf{k}\cdot\mathbf{L}_a)}{\bar{\phi}_n(\mathbf{k}\cdot\mathbf{L}_a)}\right]\left[1 - i\mathbf{B}_b \frac{\bar{\phi}'_m(\mathbf{k}\cdot\mathbf{L}_b)}{\bar{\phi}_m(\mathbf{k}\cdot\mathbf{L}_b)}\right] . \tag{2.35}$$

Just what are these terms? The first two integrals in Eqn. 2.35 are the overlaps of the basis functions for the reaction coordinates, s_a and s_b. The latter two terms contain the B_{ks} coupling of the reaction coordinate to the orthogonal bath modes. These result from the Jacobian transformation. The integral over dk integrates the momentum wavefunctions $\bar{\phi}(\mathbf{k}\cdot\mathbf{L})$. Let's take a closer look at these momentum wavefunctions:

$$
\begin{aligned}
\bar{\phi}(\mathbf{k}\cdot\mathbf{L}) &= \int dQ_k\, e^{-i(\mathbf{k}\cdot\mathbf{L})Q_k}\, \phi_n(Q_k) \\
\mathbf{k}\cdot\mathbf{L} &= \mathbf{p}\cdot\mathbf{L} = \dot{\mathbf{x}}\cdot\mathbf{L} \quad (\text{for } m = h = 1) \\
\mathbf{x} &= \mathbf{a}(s) + \sum_k \mathbf{L}_k(s)\, Q_k \\
\dot{\mathbf{x}} &= \dot{s}\left[\frac{\partial \mathbf{a}}{\partial s} + \sum \frac{\partial \mathbf{L}_k}{\partial s}\, Q_k\right] + \sum \mathbf{L}_k P_k \\
\mathbf{p}\cdot\mathbf{L}_{k'} &= \dot{s} \sum_k \mathbf{L}_k\cdot\mathbf{L}'_{k'}\, Q_k + P_{k'}
\end{aligned}
\tag{2.36}
$$

where we have used the identities $\sum \mathbf{L}_k\mathbf{L}_{k'}=\partial_{kk'}$ and $\mathbf{a}'\cdot\mathbf{L}_k=\mathbf{L}_s\cdot\mathbf{L}_k=0$. Now if the basis functions in Q are harmonic oscillators, then for $n_a=m_b=0$:

$$
\begin{aligned}
\bar{\phi}(\mathbf{k}\cdot\mathbf{L}) &= \int dQ\, e^{-i(\mathbf{k}\cdot\mathbf{L})Q} \left(\frac{\omega}{\pi}\right)^{1/4} e^{-\frac{Q^2}{2\omega}} \\
&= \left(\frac{4\pi}{\omega}\right)^{1/4} e^{-\frac{1}{2\omega}(\mathbf{k}\cdot\mathbf{L})^2} \\
\bar{\phi}'(\mathbf{k}\cdot\mathbf{L}) &= -\frac{\mathbf{k}\cdot\mathbf{L}}{\omega}\, \bar{\phi}(\mathbf{k}\cdot\mathbf{L})
\end{aligned}
\tag{2.37}
$$

Specifically for $B_{ks}=0$ one finds

$$
\begin{aligned}
<0_a|0_b> &= \frac{1}{(2\pi)^F}\frac{(4\pi)^{\frac{F-1}{2}}}{\prod_k(\omega_{ak}\omega_{bk})^{1/4}}\iint ds_a\, ds_b\, \chi(s_a)\chi(s_b) \\
&\quad \cdot \int d_F p\, e^{-i\,p\cdot\Delta a}\, e^{-\frac{1}{2}p\cdot[\sum_k \frac{\cdot L_{ka}L_{ka}\cdot}{\omega_{ak}} + \sum_k \frac{\cdot L_{kb}L_{kb}\cdot}{\omega_{bk}}]\cdot p} \qquad (2.38) \\
&= \frac{1}{(2\pi)^F}\frac{(4\pi)^{\frac{F-1}{2}}}{\prod_k(\omega_{ak}\omega_{bk})^{1/4}}\iint ds_a\, ds_b\, \chi(s_a)\,\chi(s_b)\int d_F p\, e^{-i\,p\cdot\Delta a}\, e^{-\frac{1}{2}p\cdot A\cdot p}
\end{aligned}
$$

which contains a multidimensional gaussian integral that can be integrated analytically to give

$$
\begin{aligned}
<0_a|0_b> &= \frac{1}{\sqrt{2\pi}}\prod_k^{F-1}\left[\frac{\omega_k^a\omega_k^b}{4}\right]^{-1/4} \\
&\quad \cdot \frac{1}{\sqrt{\det A}}\int ds_a \int ds_b\, \chi(s_a)\chi(s_b)\, e^{-\frac{1}{2}\Delta a(s)\cdot A^{-1}(s)\cdot\Delta a(s)}. \qquad (2.39)
\end{aligned}
$$

Now consider two reaction paths that are circles. (This could be an approximation to the paths drawn in Figure 2.5a.)

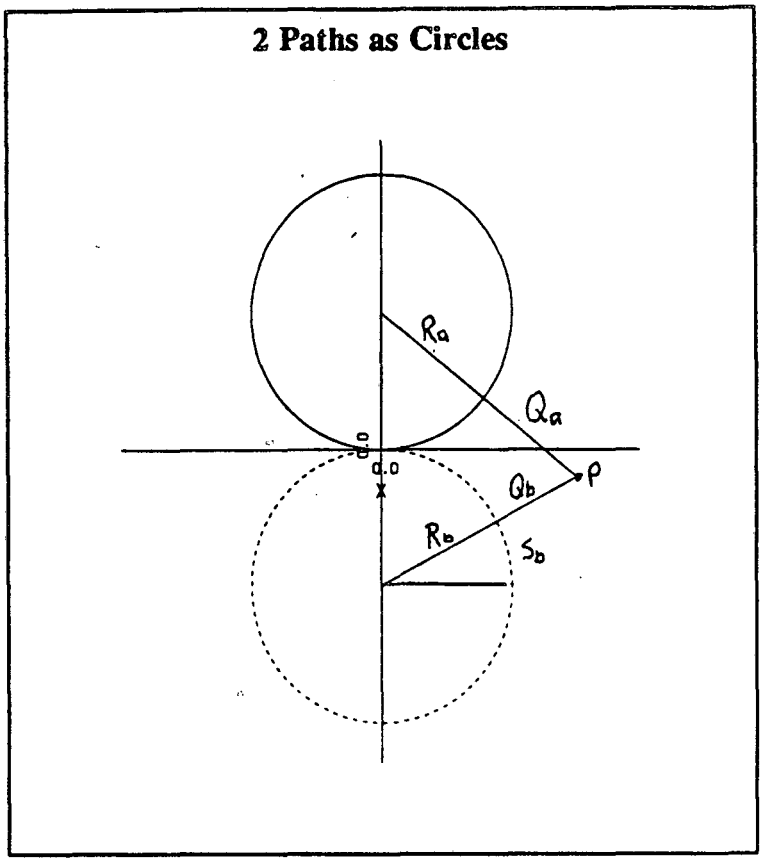

Two reaction paths are depicted as circles intersecting at the origin. Any point P can be represented by either of the two coordinate systems (s_a,Q_a) or (s_b,Q_b) as indicated in the figure.

Figure 2.10

In this case, the reaction coordinate s is the arc length along one circle and the normal coordinate Q is the distance off the circle along the direction of its radius, R. We can explicitly write the transformation between cartesian {x,y} coordinates and the reaction path coordinates {s,Q}

$$
\begin{aligned}
r &= R + Q \\
s &= R\cdot\theta \\
x &= r_a \sin\theta_a &&= r_b \sin\theta_b \\
y &= r_a \cos\theta_a - R &&= r_b \cos\theta_b + R \\
x &= (R+Q_a)\sin(\frac{s_a}{R}) &&= (R+Q_b)\sin(\frac{s_b}{R}) \\
y &= (R+Q_a)\cos(\frac{s_a}{R}) - R &&= (R+Q_b)\cos(\frac{s_b}{R}) + R
\end{aligned}
\tag{2.40}
$$

Rearranging gives

$$
\begin{aligned}
x &= R\sin(\frac{s_a}{R}) + Q_a \sin(\frac{s_a}{R}) = a_x(s_a) + L_x(s_a)\,Q_a \\
y &= R\cos(\frac{s_a}{R}) - R + Q_a \cos(\frac{s_a}{R}) = a_y(s_a) + L_y(s_a)\,Q_a \\
\frac{\partial(x,y)}{\partial(s,Q)} &= \left[\cos^2(\frac{s}{R}) + \frac{Q}{R}\cos^2(\frac{s}{R})\right] - \left[-\sin^2(\frac{s}{R}) - \frac{Q}{R}\sin^2(\frac{s}{R})\right] \\
&= \left[1 + \frac{Q}{R}\right]
\end{aligned}
$$

$$
\begin{aligned}
<0_a|0_a> &= \frac{1}{(2\pi)^2}\iint ds_a\, ds_b\, \chi(s_a)\chi(s_b) \iint dk_x\, dk_y \\
&\cdot\ e^{-i\mathbf{k}\cdot\Delta\mathbf{a}}\left[1 - i\frac{Q_a}{(R\omega_a)}\mathbf{k}\cdot\mathbf{L}_a\right]\left[1 + i\frac{Q_b}{(R\omega_b)}\mathbf{k}\cdot\mathbf{L}_b\right] e^{-\frac{1}{2}\mathbf{k}\cdot\mathbf{A}\cdot\mathbf{k}}
\end{aligned}
\tag{2.41}
$$

where only the even power terms in k survive. We have an expression for the overlap matrix in terms of the eigenvectors and frequencies of the bath modes about the two separate paths so that the Hamiltonian matrix includes both reaction paths can be evaluated.

2.7 Concluding Remarks

We have shown how to construct a two-dimensional potential energy surface for a polyatomic, specifically for the isomerization process of vinylidene and acetylene. A one-dimensional coupled Hamiltonian resulted by identifying one of the several pathways that are viable on this surface that describes the rotation of the hydrogens about the carbons as the 1,2 hydrogen shift occurs.

The lifetime of vinylidene was calculated and its sensitivity to the coupling of the various vibrational modes to the reaction coordinate was examined. The scissors mode couples most strongly to the isomerization reaction coordinate and decreases the lifetime of vinylidene while excitation of the C-C mode actually increases the lifetime. The large effect of these modes indicates a significant nonadiabatic coupling effect.

Finally a suggestion was outlined as to how to take more than one reaction path into account. This allows one to incorporate bifurcations in the path with only the need to calculate the overlaps of the basis functions for the two separate pathways.

Appendix 2.1

Experiments on vinylidene (cf. Ref. #9):

1970 Skell and Plonka
1972 Skell, Havel and McGlouchey
1972 Skell, Fagone, Klabarde
1979 Reiser et. al: IR
1980 Reiser and Steinfeld: multiple IR photon excitation
1983 Burnett et. al: photodetachment of anion

Theoretical treatment of vinylidene and barrier height (cf. Ref. #7a-e,8):

1980 Osamura et. al.	DZP+CI:	8.6-2.0 kcal/mol
1981 Krishnan, Frisch and Pople	MP2:	0.9
1981 Harding	POL-CI:	5.0-21.6
1983 Frenking	4-31G:	3.3
1984 Carrington et. al.	TZP+CI:	6.3-2.4

Theoretical treatments on triplet and anion (cf. Ref. #7d-i):

1977 Davis et. al	
1977 Kenney et. al.	
1977 Dykstra and Schaefer	DZ-P
1978 Conrad and Schaefer	DZ-PCI
1981 Osamura and Schaefer	DZ-PCI
1983 Frenking	MP2/6-31G*

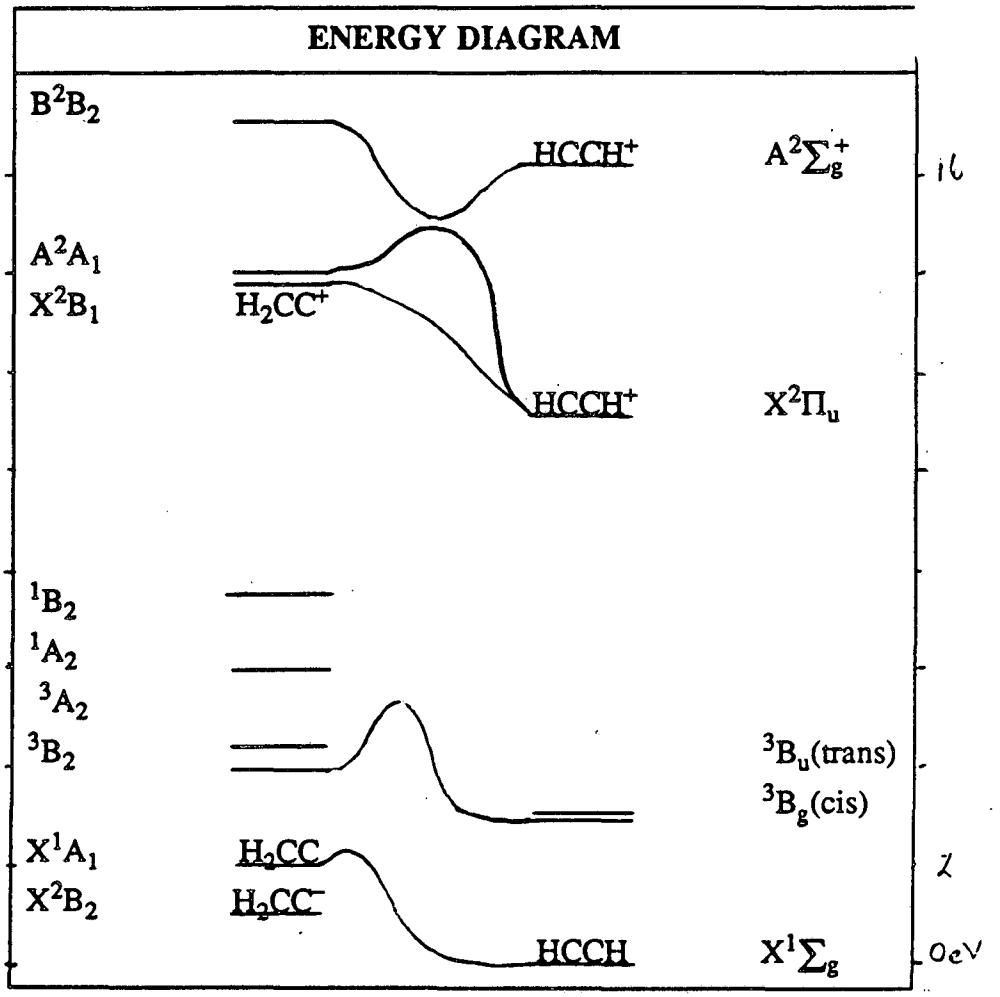

Energy diagram for vinylidene and acetylene compiled from references on previous page.

Figure A2.1

Appendix 2.2

Basis Set

The 3-21G basis set is a linear combination (or contraction) of three primatives/gaussians for the inner shells, two primatives for the inner valence shells, and one for the outer valence shells. The 3-21G basis set tends to have an accuracy comparable to the DZ basis set (±2-4 kcal/mol) but is easier to use. It can be considered as a split valence DZ basis because the valence shells are doubled (i.e., there are two functions for each minimal basis function, as is done for the DZ basis set), but the inner shell orbitals remain a single function since they contribute less to chemical properties. Carbon is assigned five types of orbitals (ϕ_{1s}, ϕ_{2s}, $\phi_{2s'}$, ϕ_{2p}, $\phi_{2p'}$) and hydrogen has two (ϕ_{1s}, $\phi_{1s'}$). This gives seven different types of orbitals. Because there is one basis function per ϕ_s and three per ϕ_p, each hydrogen will have two basis functions and each carbon nine. In the case of vinylidene, the result is a total of 22 basis functions.

Carbon:

Inner:

$$\phi_{1s} = \sum_{i=1}^{3} d_{i,1s}\, g_{1s}(\alpha_{i,1s})$$

Outer:

$$\phi_{2s} = \sum_{i=1}^{2} d_{i,2s}\, g_{1s}(\alpha_{i,2sp})$$

$$\phi_{2s'} = g_{1s}(\alpha_{2sp})$$

$$\phi_{2p} = \sum_{i=1}^{2} d_{i,2p}\, g_{2p}(\alpha_{i,2sp})$$

$$\phi_{2p'} = g_{2p}(\alpha_{2sp})$$

Hydrogen:

Outer:

$$\phi_{1s} = \sum_{i=1}^{2} d^{H}_{i,1s}\, g^{H}_{1s}(\alpha_{i,1s'})$$

$$\phi_{1s'} = g^{H}_{1s}(\alpha_{1s})$$

With this particular basis set, the coefficients d_i and exponents α_i are explicitly varied to minimize the energy of each atom. In this manner, the functions are first contracted and then optimized. (As opposed to obtaining d_i and α_i from a least squares fit to the appropriate slater orbital and then using them in the linear combination as is done for minimal basis sets.) For 3-21G, the exponent $\alpha_{i,2sp}$ is the same for the 2s and 2p orbitals.

Contour Coefficients

The explicit form for the 2-dimensional contour plot of Figure #2.2 is:

$$\begin{aligned} V_o = {} & A_0 \\ & + A_{1,0}\cos(\Delta\theta) && + A_{2,0}\cos(2\Delta\theta) \\ & + A_{0,1}\cos(\theta) && + A_{0,2}\cos(2\theta) \\ & + A_{1,1}\cos(\Delta\theta)\cos(\theta) && + A_{1,2}\cos(\Delta\theta)\cos(2\theta) \\ & + A_{2,1}\cos(2\Delta\theta)\cos(\theta) && + A_{2,2}\cos(2\Delta\theta)\cos(2\theta) \end{aligned}$$

where

A_0	= −76.23608	$A_{1,1}$	= −0.0774467
$A_{1,0}$	= −0.0723965	$A_{1,2}$	= 0.00425823
$A_{2,0}$	= 0.0518914	$A_{2,1}$	= −0.0523514
$A_{0,1}$	= −0.014805	$A_{2,2}$	= −0.00295178
$A_{0,2}$	= −0.0012972		

1-Dimensional Coefficients

The functional form for the 1-dimensional plot of Figure #2.5 is:

$$V_o = \sum_{n=0}^{2} a_{2n} \cos(2n\gamma)$$

where

$$a_o = 0.0531997 \text{ au}$$
$$a_2 = 0.03489 \text{ au}$$
$$a_4 = 0.0183097 \text{ au}$$

Appendix 2.3

We want to prove that, to a first approximation, the intensity spectra I(E) of state *i* is a Lorentzian, and that the width of this Lorentzian, Γ, is associated with a lifetime of the state. We begin by stating the fact that the survival probability of a state *i* is given by the square of the overlap of the intial state *i* with itself after a time *t* while under the influence of a Hamiltonian H

$$\text{Prob} = |\langle i|e^{-iHt/h}|i\rangle|^2 \ .$$

Then, by regarding the energy of this single state as a complex number E=E + ½ *i* Γ the survival probability becomes an exponential decay $e^{-\Gamma t/h}$ with a lifetime of τ=h/Γ.

The Lorentzian shape (with width Γ) of the absorbtion spectrum results from the fact that the survival amplitude can be determined via the imaginary part of the Green's function $(E-H)^{-1}$.

$$\langle i|e^{-iHt/h}|i\rangle = \frac{1}{2\pi i}\int_c dE e^{-iEt/h}\langle i|(E-H)^{-1}|i\rangle \qquad \text{(A2.1)}$$

Proof of Eqn. #A2.1:

Take the Laplace Transform (*LT*) of the time dependent Schrodinger equation (for a time independent Hamiltonian):

$$LT[-ih\frac{\partial}{\partial t}\Psi] \qquad = LT[H\Psi]$$

$$-ih\int_0^\infty e^{-\lambda t}\frac{\partial}{\partial t}\Psi\, dt \ = H\cdot LT[\Psi]$$

and integrate by parts:

$$-ih\left[\Psi e^{-\lambda t}\right]_0^{\infty} - ih\int \lambda \Psi e^{-\lambda t}\,dt = H \cdot LT[\Psi]$$

$$ih\,\Psi(0) + ih\,\lambda LT[\Psi] = H \cdot LT[\Psi]$$

which implies that

$$LT[\Psi] = ih\frac{\Psi(0)}{[H - ih\lambda]} \quad .$$

Transform back

$$\Psi(t) = \frac{1}{2\pi i}\int_c \frac{ih\,\Psi(0)}{[H - ih\lambda]} e^{\lambda t}\,d\lambda$$

and change variables $E = ih\lambda$ to give

$$\Psi(t) = \frac{1}{2\pi i}\int_{c-i\infty}^{c+i\infty} \Psi(0)\,[H-E]^{-1} e^{-iEt/h}\,dE \quad . \qquad \text{(A2.2)}$$

One also knows that the time dependent wavefunction can be written as the intial wavefunction propagated by the Hamiltonian,

$$\Psi(t) = e^{-iHt/h}\Psi(0)$$

which implies the following relation:

$$e^{-iHt/h} = \frac{1}{2\pi i}\int_{c-i\infty}^{c+i\infty} dE\, e^{-iEt/h}[H-E]^{-1}$$

$$<i|e^{-iHt/h}|i> = \frac{1}{2\pi i}\int_{c-i\infty}^{c+i\infty} dE <i|e^{-iEt/h}[H-E]^{-1}|i> \quad \text{Q.E.D.}$$

Once we know the above relation, the next step towards obtaining a Lorentzian lineshape is to determine the matrix element of the Green's function. If an initial state i decays by coupling to n other states via H_{in}, one finds the Green's function by inverting the matrix **M = (E1-H)**:

$$M = \begin{bmatrix} E-(E_i+\frac{i\Gamma}{2}) & H_{in} \\ H_{ni} & E-(E_n+\frac{i\Gamma}{2}) \end{bmatrix}$$

$$M^{-1} = \left[E - E_i - \frac{i\Gamma_i}{2} - \sum_n \frac{|H_{in}|^2}{E-E_n+\frac{i\Gamma_n}{2}}\right]^{-1}$$

$$= <\phi_i|\frac{1}{[E-H]}|\phi_i> \qquad \text{(A2.3)}$$

where one assumes that the separate n states do not decay via direct coupling between themselves [i.e., H_{nn}=0]. Eqn. #A2.1 becomes

$$<i|e^{-iHt/h}|i> = \frac{1}{2\pi i}\int_c \frac{e^{-iEt/h}}{E-E_i+\frac{i\Gamma_i}{2}+\sum_n \frac{|H_{in}|^2}{E-E_n+\frac{i\Gamma_n}{2}}}$$

$$= e^{i(E_{pole}-\frac{i\Gamma_{pole}}{2})t/h} \quad \text{(for } H_{in}=0\text{)} \tag{A2.4}$$

Eqn. #A2.4 indicates that the survival probability for $H_{in}=0$ is a single exponential decay Prob = $e^{-\Gamma_{pole}t/h}$ with a lifetime $\tau = h/\Gamma$ as was mentioned earlier. If, however, $H_{in}\neq 0$, the following three assumptions are needed to give the final Lorentzian expression for Eqn. #2.24:

A) Assume a 1 pole approximation to the contour integral of Eqn. #A2.4 and treat the summation over n as a perturbation such that

$$E_{pole}(\text{1st order}) = E_i - \frac{i\Gamma_i}{2}$$

$$E_{pole}(\text{2nd order}) = E_i - \frac{i\Gamma_i}{2} - \sum_n \frac{|H_{in}|^2}{(E_i-\frac{i\Gamma_i}{2}) - E_n + \frac{i\Gamma_n}{2}},$$

and therefore

$$\mathrm{Re}\,(E_{pole}) = E_i + \sum_n \frac{|H_{in}|^2(E_i-E_n)}{(E_i-E_n)^2 + (\frac{\Gamma_n-\Gamma_i}{2})^2}$$

$$= E_i + E_{nonad}$$

$$\mathrm{Im}\,(E_{pole}) = \tfrac{1}{2}\Gamma_i + \tfrac{1}{2}\sum_n \frac{|H_{in}|^2(\Gamma_n-\Gamma_i)}{(E_i-E_n)^2 + (\frac{\Gamma_n-\Gamma_i}{2})^2}$$

$$= \tfrac{1}{2}\Gamma_{pole}$$

B) Assume coupling to a continuum of states to change the sum over n to an integral over final states; and

C) Set Γ_i to zero to neglect the radiative lifetime while finding the nonradiative one to give:

$$\Gamma_{pole} = \int dE\, \rho(E)\, |H_{iE}|^2 \frac{\frac{1}{2}\Gamma(E)}{(\frac{1}{2}\Gamma(E))^2 + (E_i - E)^2} \tag{A2.5}$$

Plotting the integrand as a function of energy gives the spectral intensity profile of Eqn. #A2.1.

Chapter 3

CARTESIAN REACTION PATH

3.1 Introduction

Once again, we are interested in describing polyatomic reactions without resorting to a full 3N-6 *ab initio* quantum chemistry calculation. In this chapter, rather than use the Reaction Surface Hamiltonian as was presented in Chapter 2, we present a new class of models for describing dynamics in polyatomic systems that reduces to the expansion about a one-dimensional reaction coordinate, but which is much easier to generate and use in dynamical calculations than is the minimum energy path.

As was said earlier, there are some difficulties with using the minimum energy path description for hydrogen atom transfer reactions. An example of this type of process (other than the vinylidene-acetylene isomerization problem) is the intramolecular hydrogen transfer in malonaldehyde.[5,14]

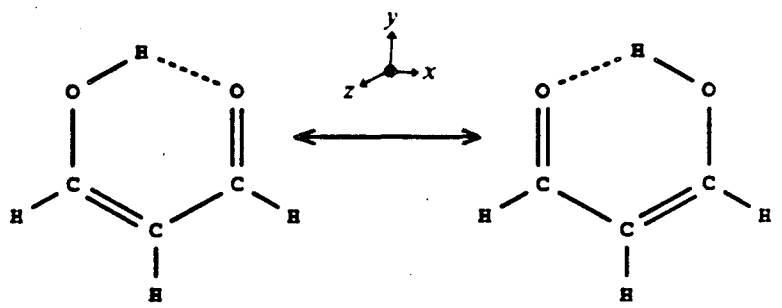

(3.1)

This reactive process is the motion of essentially only one hydrogen atom, H_1, with the other degrees of freedom playing a modest role. The problem with the minimum energy reaction path description here is that the reaction path always arrives at the reactant and product wells along the normal mode of *lowest frequency* of the appropriate sym-

metry [cf. Appendix 3.1]. It was explained in the Introductory Chapter how, for the above example in Equation 3.1, the lowest frequency is associated with some floppy skeletal vibrational motion that is quite unrelated to the motion of atom H_1, while the relevant vibration is the O-H_1 stretch, which is the *highest* frequency of the reactant. This results in curvature coupling elements in the reaction path Hamiltonian[2] that are large and difficult to deal with.

Another drawback of the reaction path (or surface) model is that the reaction path is mass-dependent. Thus, if one wishes to treat isotopically related reactions, an entire recalculation of the minimum energy path (and force constant matrix along it) is required for each new isotopic species. It would simplify calculations if the potential energy surface "input" to the dynamical treatment was independent of the nuclear masses.

The new model presented here is totally cartesian in structure and, thus, much simpler to deal with than the earlier reaction path Hamiltonian. One relies on "chemical intuition" to select which one (or more) cartesian coordinate is treated for arbitrarily large displacements, as opposed to the other coordinates which move only slightly. For Equation 3.1, for example, it is only the x-coordinate of hydrogen atom H_1 that undergoes large displacement; although all the other atoms (and the y and z coordinate of H_1) move, they do not move very much. Thus, the potential energy in the 3N-1 remaining cartesian coordinates can be adequately approximated by a quadratic expansion about some reference configuration. The Hamiltonian now has the generic form of a "system", H_{1x}, which is linearly coupled to a harmonic "bath", as has been so commonly assumed for many model studies.[15] It is much easier to describe the coupling between the "system" and "bath" here than it is in the reaction path Hamiltonian where the coupling arises from curvature coupling effects in the kinetic energy[2]. The potential energy surface information required for this cartesian model is itself simpler to generate than that for the reaction path Hamiltonian, and it is also mass-independent

so that different isotopes of the same system do not require new potential energy surface calculations. Finally, we mention that conservation of total angular momentum is accounted for approximately (but adequately for H-atom transfer processes).

The cartesian reaction path model is developed in Section 2. Section 3 describes the theoretical methods used to treat the dynamics. Application to a model of H-atom transfer in malonaldehyde is presented in Section 4.

3.2 A Cartesian Model for Reaction Dynamics

Frozen Bath Version

We start with the Hamiltonian for an N-atom polyatomic system expressed in the full set of 3N cartesian coordinates

$$H = \sum_{i=1}^{3N} \frac{p_i^2}{2m_i} + V(x_i) \quad . \tag{3.2}$$

The first step in defining the model is to identify which cartesian coordinate(s) one wishes to describe for arbitrarily large displacements. For Equation 3.1 one could choose the x coordinate of hydrogen atom H_1; a more accurate model would be to treat both the x and y coordinates of H_1 for arbitrarily large displacements. Let **r** denote the one or two (or maybe three) cartesian coordinates to be described for arbitrary displacements and **R** denote the remaining 3N-1 or 3N-2 cartesian coordinates that do not move very much during the reaction of interest. The **R**-dependence of the potential energy, V=V(**r**,**R**) is expanded in a Taylor series to second order about a reference geometry $\mathbf{R}_o$:

$$V(\mathbf{r},\mathbf{R}) = V(\mathbf{r},\mathbf{R}_o) + \frac{\partial V(\mathbf{r},\mathbf{R}_o)}{\partial \mathbf{R}_o}\cdot(\mathbf{R}-\mathbf{R}_o) + \frac{1}{2}(\mathbf{R}-\mathbf{R}_o)\cdot\frac{\partial^2 V(\mathbf{r},\mathbf{R}_o)}{\partial \mathbf{R}_o \partial \mathbf{R}_o}\cdot(\mathbf{R}-\mathbf{R}_o) \quad . (3.3)$$

Equation 3.3 is the essence of the model: the exploitation of the fact that most of the coordinates [i.e., atoms] do not move very much during the reaction. With Equation 3.3 the Hamiltonian takes the form:

$$\begin{aligned} H(\mathbf{p},\mathbf{r},\mathbf{P},\mathbf{R}) &= [\tfrac{1}{2}\mathbf{p}\cdot\mathbf{m}^{-1}\cdot\mathbf{p} + V(\mathbf{r},\mathbf{R}_o)] \\ &+ [\tfrac{1}{2}\mathbf{P}\cdot\mathbf{m}^{-1}\cdot\mathbf{P} + \frac{1}{2}(\mathbf{R}-\mathbf{R}_o)\cdot K(\mathbf{r})\cdot(\mathbf{R}-\mathbf{R}_o)] \\ &- f(\mathbf{r})\cdot(\mathbf{R}-\mathbf{R}_o) \end{aligned} \quad (3.4)$$

where the quantities in Equation 3.4 are recognizable as:

$$\begin{aligned} K(\mathbf{r}) &= \frac{\partial^2 V(\mathbf{r},\mathbf{R}_o)}{\partial \mathbf{R}_o \partial \mathbf{R}_o} \\ f(\mathbf{r}) &= -\frac{\partial V(\mathbf{r},\mathbf{R}_o)}{\partial \mathbf{R}_o} \\ \mathbf{m} &= \text{diagonal matrix of atomic masses} \end{aligned}$$

Equation 3.4 is essentially the generic Hamiltonian for a (low-dimensional) "system" [the **r** degree(s) of freedom] coupled to a "bath" of harmonic oscillators [the **R** degrees of freedom]. The coupling [the last term in Equation 3.4] is linear in the bath coordinates **R**. This describes "solvent-reorganization" effects, i.e., the change in the bath coordinates' instantaneous equilibrium positions as the system dynamics takes place. There is another type of coupling between the system and bath because the force constant matrix of the bath, K(**r**), is a function of the system coordinate **r**, this results because the instantaneous vibrational frequencies and normal mode eigenvectors change

with the system dynamics. One who is familiar with the reaction path formalism will immediately recognize how much more readily one can deal with system-bath coupling with this new Hamiltonian, Equation 3.4, than with that in the reaction-path Hamiltonian.[2]

The reader will also note that the required input from *ab initio* quantum chemistry calculations is much easier to generate for the Hamiltonian in Equation 3.4 than it is for the reaction path Hamiltonian. What is required for Equation 3.4 is the energy, gradient and force constant matrix of the potential energy surface for a *frozen* bath ($\mathbf{R}=\mathbf{R}_o$), as a function of $\mathbf{r}$. Geometry optimization is not required. If $\mathbf{r}$ is only one coordinate, for example, this means that one requires an energy gradient and force constant matrix at, say, ten predetermined geometries.

Conservation of Total Angular (and Linear) Momentum

Our initial inclination was to ignore the fact that this model does not conserve total angular and linear momentum (owing to the fact that the approximation to the potential surface, Equation 3.3, destroys rotational and translational invariance). Jaquet and Miller[16] had used essentially this model to treat H-atom diffusion on a tungsten surface, and there, of course, one does not need to be concerned with rotation and translation of the (infinite) surface of tungsten atoms. In malonaldehyde (Equation 3.1), however, the "surface" is composed of all atoms except the tunneling hydrogen and is therefore not infinite. It seemed to us that it was sufficiently more massive than the single H atom that tunnels and that one could thus ignore rotation and translation. Unfortunately, test calculations convinced us that this is not the case, at least for malonaldehyde; the low frequencies of the bath [those that should be zero, i.e., pure rotations and translations] mix in an unphysical way with the true low vibrational frequencies of the molecule. It was thus deemed necessary to project out six pure rotational and translational degrees of freedom.

To separate the rotational motion rigorously requires use of curvilinear coordinates [i.e., Euler angles][17], thus destroying the cartesian form of the Hamiltonian (Equation 3.4). Chapter 4 presents a Hamiltonian which eliminates rotation explicitly. To avoid this for the present cartesian model, and also because we are developing the model for application to large molecular systems for which rotational motion is not of interest, we present here one possible way to eliminate rotation approximately by projecting out infinitesimal rotation and translation of the N-1 atom "substrate" formed by excluding the tunneling hydrogen atom. This allows one to construct a simplified Hamiltonian that accounts for the recoil effect of the substrate atoms when the H atom moves.

To be specific, we refer to Equation 3.2 with $r=x_{H_1}$ chosen as the (one) "system" coordinate. Then, with indices i=1-3 referring to the three cartesian coordinates of atom H_1, the matrix elements

$$U_{ik}^{sub} = \begin{cases} i=4,\ldots,3N \\ k=4,\ldots,3N-6 \end{cases} \tag{3.5}$$

denote the eigenvectors of the projected, mass-weighted force constant matrix of the N-1 atom substrate [all atoms except H_1],

$$(1-\mathbf{P})\cdot \mathbf{m}^{-\frac{1}{2}}\cdot \mathbf{K}_o\cdot \mathbf{m}^{-\frac{1}{2}}\cdot(1-\mathbf{P}) \ . \tag{3.6}$$

Here $\mathbf{K}_o=\mathbf{K}(x_1^o)$; x_1^o is some convenient intermediate value of the system coordinate x_1; **m** is the (3N-3) x (3N-3) matrix of masses for the (N-1) atom substrate; and **P** is the (3N-3) x (3N-3) matrix that projects onto the six degrees of freedom that are infinitesimal rotations and translations of the (N-1) atom substrate. The explicit form of **P** has been given before[2] and is a function only of the geometry of the substrate. The

factor (1-P) in Equation 3.6 insures that the projected, mass-weighted force constant matrix will have six zero eigenvalues corresponding to infinitesimal rotations and translations and 3(N-1)-6 non-zero eigenvalues that describe vibration of the (N-1) substrate atoms about their reference positions.

The matrix $\mathbf{U}_{sub}$ from Equation 3.5 is now augmented by the other cartesian coordinates of atom H_1 which have not been taken as system coordinates; e.g., with $\mathbf{r}$ chosen as the $x_{H_1}=x_1$, the coordinates $y_{H_1}=x_2$ and $z_{H_1}=x_3$ are part of the bath. The final U matrix is

$$\mathbf{U}_{i,k} = \begin{bmatrix} 1 & 0 & \\ 0 & 1 & 0 \\ 0 & & \mathbf{U}_{sub} \end{bmatrix}_{\substack{i=2,\ldots,3N \\ k=2,\ldots,3N-6}} \tag{3.7}$$

The (3N-1) cartesian bath coordinates $\mathbf{R}$ can now be expressed in terms of the 3N-7 normal mode bath coordinates $\mathbf{Q}$ which have the six rotations and translations of the substrate eliminated,

$$(\mathbf{R} - \mathbf{R}_o) = \mathbf{m}^{1/2} \cdot \mathbf{U} \cdot \mathbf{Q} \tag{3.8}$$

with $\mathbf{U}$ given by Equation 3.7. The Hamiltonian of Equation 3.4 becomes (with $\mathbf{r}=x_1$)

$$\begin{aligned} H(p_1,x_1,\mathbf{P},\mathbf{Q}) &= [\frac{p_1^2}{2m_1} + V_{eff}(x_1)] \\ &+ [\sum_{k=2}^{3N-6} \tfrac{1}{2}P_k^2 + \frac{1}{2}\mathbf{Q}\cdot\mathbf{K}_{eff}(x_1)\cdot\mathbf{Q}] - \mathbf{f}_{eff}(x_1)\cdot\mathbf{Q} \end{aligned} \tag{3.9a}$$

where $\mathbf{K}_{eff}$ and $\mathbf{f}_{eff}$ are the (3N-7) matrix and vector, respectively,

$$\mathbf{K}_{\mathrm{eff}}(x_1) = \mathbf{U}^{+} \cdot \mathbf{m}^{-1/2} \cdot \mathbf{K}(x_1) \cdot \mathbf{m}^{-\frac{1}{2}} \cdot \mathbf{U} \tag{3.9b}$$

$$\mathbf{f}_{\mathrm{eff}}(x_1) = \mathbf{f}(x_1) \cdot \mathbf{m}^{-\frac{1}{2}} \cdot \mathbf{U} \tag{3.9c}$$

and

$$V_{\mathrm{eff}}(x_1) = x_1, \mathbf{R}_o) \tag{3.9d}$$

This Hamiltonian, Equation 3.9, is for one system coordinate. It should be clear how Equations 3.5-9 are modified if the system coordinate(s) **r** is chosen to be x_1 and $x_2=y_H$, say. [Note that $\mathbf{K}_{\mathrm{eff}}(x_1)$ is not diagonal because **U** was obtained by diagonalizing $\mathbf{K}(x_1)$ at the fixed value $x_1=x_1^o$.]

The transformations described by Equation 3.5-9 for eliminating overall translation and rotation of the substrate must be re-done for different isotopic species; i.e., the matrix $\mathbf{K}_{\mathrm{eff}}(x_1)$ and coupling vector $\mathbf{f}_{\mathrm{eff}}(x_1)$ in Equation 3.9 depend on the atomic masses. It should be noted, however, that the mass dependence on the projected (3N-3) x (3N-3) substrate portion of $\mathbf{K}_{\mathrm{eff}}(x_1)$ corresponds to secondary isotope effects. Primary isotope substitutions are simply incorporated *via* the identity portion of the matrix **U**. Both of these mass variations are simple, though. The important matter is that the original **K** and **f** of Equation 3.9, which are obtained from *ab initio* quantum chemistry calculations, are mass-independent. Also important for treating the dynamics of the "system-bath" Hamiltonian [Equation 3.9] is that its cartesian and linear coupling form has been maintained by the (approximate) way that we have eliminated overall translation and rotation.

Flexible Bath

In some cases one may wish to allow the reference geometry of the bath to vary with the system coordinate **r** [e.g., so that the equilibrium geometries of the reactants

and products are accurately reproduced by the model]. It is actually possible to generalize the above treatment in a simple way to incorporate this and still maintain the simple form of the resulting Hamiltonian.

Thus, let $\mathbf{R}_o(\mathbf{r})$ be the reference geometry of the bath as a function of the system coordinate(s) $\mathbf{r}$. We envision, for example, that $\mathbf{R}_o(\mathbf{r})$ may be chosen simply to interpolate between the reactant and product geometries of the bath variables. A Taylor series expansion of $\mathbf{R}$ about $\mathbf{R}_o(\mathbf{r})$, as in Equation 3.3, is still possible:

$$V(\mathbf{r},\mathbf{R}) = V(\mathbf{r},\mathbf{R}_o(\mathbf{r})) + \left[\frac{\partial V(\mathbf{r},\mathbf{R})}{\partial \mathbf{R}}\right]_{\mathbf{R}=\mathbf{R}_o(\mathbf{r})} \cdot (\mathbf{R} - \mathbf{R}_o(\mathbf{r}))$$

$$+ \frac{1}{2}(\mathbf{R} - \mathbf{R}_o(\mathbf{r})) \cdot \left(\frac{\partial^2 V(\mathbf{r},\mathbf{R})}{\partial \mathbf{R}\partial \mathbf{R}}\right)_{\mathbf{R}=\mathbf{R}_o(\mathbf{r})} \cdot (\mathbf{R} - \mathbf{R}_o(\mathbf{r})) \tag{3.10}$$

and this can be combined with the cartesian kinetic energy to form a Hamiltonian like that of Equation 3.4.

To maintain the simple form of the resulting Hamiltonian it is still necessary to project out rotations and translations of the *frozen* substrate. Therefore, the transformation matrix $\mathbf{U}$ is defined as above [Equation 3.5-7] but with $\mathbf{K}_o = \mathbf{K}(x_1^o,\mathbf{R}_o(x_1^o))$, where x_1^o is again a fixed value of the system coordinate x_1. The projector $\mathbf{P}$ is also defined at the frozen substrate geometry $\mathbf{R}_o(x_1^o)$. The relation between the (3N-1) coordinates $\mathbf{R}$ (for $\mathbf{r}=x_1$) and the (3N-7) coordinates $\mathbf{Q}$ is thus

$$\mathbf{R} - \mathbf{R}_o(x_1^o) = \mathbf{m}^{-1/2} \cdot \mathbf{U} \cdot \mathbf{Q} \tag{3.11}$$

so that $\mathbf{R} - \mathbf{R}_o(x_1)$ in Equation 3.10 (with $\mathbf{r}=x_1$) is given by

$$\mathbf{R} - \mathbf{R}_o(x_1) = \mathbf{R}_o(x_1^o) - \mathbf{R}_o(x_1) + \mathbf{m}^{-1/2} \cdot \mathbf{U} \cdot \mathbf{Q}\ . \tag{3.12}$$

Using Equation 3.12 in Equation 3.10 gives the same form of Hamiltonian as before (Equation 3.9a) now with

$$\mathbf{K}_{\mathrm{eff}}(x_1) = \mathbf{U}^{+} \cdot \mathbf{m}^{-1/2} \cdot \mathbf{K}(x_1) \cdot \mathbf{m}^{-1/2} \cdot \mathbf{U} \tag{3.9b'}$$

$$\mathbf{f}_{\mathrm{eff}}(x_1) = \left[\mathbf{f}(x_1) + (\mathbf{R}_o(x_1) - \mathbf{R}_o(x_1^o)) \cdot \mathbf{K}(x_1)\right] \cdot \mathbf{m}^{-1/2} \cdot \mathbf{U} \tag{3.9c'}$$

$$\begin{aligned} V_{\mathrm{eff}}(x_1) &= V(x_1,\mathbf{R}_o(x_1)) - \mathbf{f}(x_1) \cdot (\mathbf{R}_o(x_1) - \mathbf{R}_o(x_1^o)) \\ &+ \tfrac{1}{2}(\mathbf{R}_o(x_1) - \mathbf{R}_o(x_1^o)) \cdot \mathbf{K}(x_1) \cdot (\mathbf{R}_o(x_1) - \mathbf{R}_o(x_1^o)) \end{aligned} \tag{3.9d'}$$

where

$$\mathbf{K}(x_1) = \left[\frac{\partial^2 V(x_1,\mathbf{R})}{\partial \mathbf{R} \partial \mathbf{R}}\right]_{\mathbf{R}=\mathbf{R}_o(x_1)}$$

$$\mathbf{f}(x_1) = -\left[\frac{\partial V(x_1,\mathbf{R})}{\partial \mathbf{R}}\right]_{\mathbf{R}=\mathbf{R}_o(x_1)}$$

These expressions revert to Equation 3.9 in the rigid bath limit, where $\mathbf{R}_o(x_1)=\mathbf{R}_o$.

To conclude this description of the model we summarize the advantages that it has over earlier reaction path modes: (1) Most important is that it contains the physically correct picture of the dynamics, clearly identifying the relevant coordinates of the process. The intrinsic reaction path for these heavy-light-heavy mass combinations leads to unphysical reaction paths[4]; (2) It is considerably easier to treat the dynamics of the resulting Hamiltonian which has the coupling in the *potential* energy rather than that for the reaction path Hamiltonian that has the coupling in the *kinetic* energy; (3) It is relatively simple to do calculations for different isotopes; and (4) It is much simpler to generate the *ab initio* quantum chemistry "input" for the model.

Disadvantages of the model, on the other hand, are that we are able to separate off overall rotational motion only approximately if we wish (as we do) to maintain the simple form of the Hamiltonian; this seems to be a minor error, particularly so if the "substrate" is large. Finally, the model requires that one invoke "chemical intuition" to choose the cartesian coordinates that constitute the "system"; one may view this as an advantage or a disadvantage.

3.3 System-Bath Dynamics

Basic Method

Having defined the model Hamiltonian in the previous section, one is now ready to treat its dynamics. The most elegant and rigorous way to treat these system-harmonic bath Hamiltonians is *via* Feynman path integral methods[18a]. This permits one to take into account the effect of the bath on the system exactly. There is currently a great deal of progress being made in this direction[18], but these approaches are at present not available for practical calculations with real chemical systems. In this paper, therefore, we utilize an approximate treatment due to Makri and Miller[15] that has been shown to do a good job for including the effect of coupling to a bath on the tunneling in a double-well system, as is the process in Equation 3.1. We first summarize the basic ideas of this approach and then describe some necessary extensions for the present application.

The basis set method of Makri and Miller chooses basis functions for the total system-bath Hamiltonian in the form

$$\Psi_{i,n}(r,Q) = \chi_i(r)\,\Phi_n^i(Q) \tag{3.13}$$

where $\{\chi_i(r)\}$ is a set of localized functions in the "system" coordinate and $\{\Phi_n^i(Q)\}$ are the eigenfunctions of the "bath" Hamiltonian that results when the total Hamiltonian is averaged over basis function $\chi_i(r)$. $\Phi_n^i(Q)$ is obtainable analytically because the resulting "bath" Hamiltonian is that of linearly coupled harmonic oscillators. We have taken the set $\{\chi_i\}$ as the distributed Gaussians of Hamilton and Ligh<t[19], as used by Makri and Miller. The matrix of the total system-bath Hamiltonian, $H1_{i'n',in}$, is constructed in this basis, and the *zeroth-order effective system Hamiltonian* of ref. (16) is defined by taking the part of the Hamiltonian matrix that is diagonal in the bath quantum numbers, i.e., by setting $\mathbf{n}'=\mathbf{n}$. This effective system Hamiltonian has a dimension only of the number of system basis functions $\{\chi_i\}$ and is of the form

$$H_{i',i}^{n} = H_{i'n,in} = F_{i',i}^{n}\, h_{i',i}^{n} \qquad (3.14)$$

where $h_{i',i}^{n}$ is a one-dimensional-like Hamiltonian matrix and $F_{i',i}^{n}$ is the Franck-Condon factor between the oscillator functions Φ_n^i and $\Phi_n^{i'}$,

$$F_{i',i}^{n} = \int \Phi_{i'n}(Q)\, \Phi_{in}(Q)\, dQ\ . \qquad (3.15)$$

Most of the effects of the bath on the system dynamics are contained in the Franck-Condon factor. [i.e., it describes the "solvent relaxation", or polaronic effects of the bath on the system.] Makri and Miller found that this approximation, i.e., taking the bath quantum numbers to be diagonal, worked quite well provided that the basis functions $\{\chi_i\}$ are localized. The reader should see ref. (16) for discussion of the reasons for this as well as further aspects of the approach.

Extensions

Makri and Miller considered a system-bath Hamiltonian with a *constant* force constant matrix, **K**, so their treatment must be generalized in order to apply it to the present Hamiltonian (Equation 3.9a). Specifically, the Frank-Condon factor of Equation 3.15 in the present case is given more explicitly by

$$F^{n}_{i',i} = \int \prod_{k} \phi_{n_k}(q_{i'k})\, \phi_{n_k}(q_{ik})\, dQ \tag{3.16}$$

where $\phi_{n_k}(q_k)$ are ordinary one-dimensional harmonic oscillator wavefunctions, and the coordinates q_i (and $q_{i'}$) are the linear combinations of **Q** that diagonalize the oscillator potentials

$$V_i = \tfrac{1}{2}\, Q \cdot K_i \cdot Q - f_i \cdot Q \tag{3.17}$$

where

$$\begin{aligned} K_i &= \langle \chi_i | K_{eff} | \chi_i \rangle \\ f_i &= \langle \chi_i | f_{eff} | \chi_i \rangle \end{aligned}$$

More specifically, if L_i is the (3N-7) x (3N-7) matrix of eigenvectors of K_i, then $\omega_i^2 \cdot 1 = L_i^+ \cdot K_i \cdot L_i$ are the diagonal frequencies of the bath modes associated with the Gaussian χ_i localized at r_i, and q_i is given in terms of **Q** by

$$q_i = L_i^+ \cdot Q - \omega_i^{-2} \cdot L_i^+ \cdot f_i \,. \tag{3.18}$$

Because the matrices L_i and $L_{i'}$ are different (owing to the fact that the force constant

matrices $\mathbf{K}_i$ and $\mathbf{K}_{i'}$ are different) the integrals in Equation 3.16 do not factorize into a product of one-dimensional integrals, but they have the form of a multidimensional Gaussian integral (times powers). There have, however, been a number of papers describing the efficient evaluation of these multidimensional harmonic Franck-Condon factors using generating function, recursion, and iterative methods.[20]. We used a method similar to that of ref. (21a).

With this more generalized Franck-Condon factor, the effective system Hamiltonian which results from the system-bath Hamiltonian of Equation 3.9a is given explicitly by

$$\begin{aligned} H^{n}_{i',i} &= F^{n}_{i',i} <\chi_{i'}|\frac{p_1^2}{2m_1} + V_{eff(x_1)}|\chi_i> + \frac{1}{2}<\chi_{i'}|\chi_i><\Phi^{i'}_n|P^2|\Phi^i_n> \\ &+ \frac{1}{2}<\Phi^i_n|Q\cdot K_{i'i}\cdot Q|\Phi^i_n> - f_{i'i}\cdot<\Phi^{i'}_n|Q|\Phi^i_n> \end{aligned} \tag{3.19}$$

where

$$\mathbf{K}_{i'i} = <\chi_{i'}|\mathbf{K}_{eff}(x_1)|\chi_i>$$

$$\mathbf{f}_{i'i} = <\chi_{i'}|\mathbf{f}_{eff}(x_1)|\chi_i> .$$

The last three terms in Equation 3.19 are multidimensional Gaussians times powers and are evaluated by methods similar to those used for the Franck-Condon factor.

3.4 Application to Three-atom Model of Malonaldehyde

Before applying this cartesian path methodology to an *ab initio* treatment of

malonaldehyde (Equation 3.1) we consider here a simple three-atom model of this reaction that can be treated exactly (because it is a triatomic system). It is important to test both the cartesian reaction path model described in Section 2 and the dynamical treatment summarized in Section 3.

The three-atom model we consider is the O-H-O part of Equation 3.1,

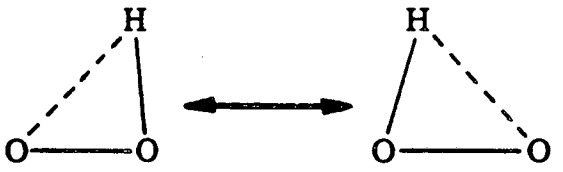

(3.20)

with a potential energy function that has the general form of the double-well potential of Janoschek *et al.*,[21] generalized to include bending motion:

$$V = a_1 + a_2Q_a^2 + a_3Q_a^4 + a_4Q_s^2 + a_5Q_a^2Q_s + a_6Q_s^2 + \frac{1}{2}K_\gamma(\gamma-\gamma_o)^2 \qquad (3.21)$$

where γ is the angle between the two OH bonds. The coefficients (in a.u.) have been chosen to approximate the energetics and geometry of reaction 3.1:

$$\begin{aligned} a_1 &= 0.01338 & a_4 &= -0.02745 \\ a_2 &= -0.03603 & a_5 &= 0.03695 \\ a_3 &= 0.02425 & a_6 &= 0.07786 \\ \gamma_o &= 158^\circ & K_\gamma &= 0.20000 \\ Q_a &= \sqrt{\frac{1}{2}}(r_1-r_2) \\ Q_s &= \sqrt{\frac{1}{2}}(r_1+r_2) \end{aligned} \qquad (3.22)$$

The "bare" barrier height [i.e., with no zero-point energy corrections] for this po-

tential is 6.88 kcal/mol, in qualitative agreement with what is thought to be the correct value for malonaldehyde.[14] Table 1 compares the equilibrium and transition state geometries for this potential to the corresponding quantities for malonaldehyde..

TABLE 1

Comparison of Geometries				
	Equilibrium		Transition State	
internal coordinates[a]	three-atom model	malonaldehyde[b]	three-atom model	malonaldehyde[b]
r_1	0.82 A	0.99	1.20	1.20
r_2	1.46 A	1.69	1.20	1.20
r_3	2.23 A	1.22	2.36	2.36
γ	158.°	155.	158.	158.

[a] r_1 and r_2 are OH bond lengths; r_3 is the O-O bond length; γ is the angle between the two OH bonds. [b] See ref. (18) and (19).

The cartesian reaction model of Section 2 was now applied, with the x coordinate of the H-atom as the "system" coordinate. Both the frozen reference geometry for the bath (Section 2a) and a flexible reference geometry (Section 2c) were used to test the sensitivity of the results to how well the bath is modeled.

TABLE 2

Tunneling splitting (cm^{-1})				
	Reference geometry of bath			
isotope	transition state[a]	equilibrium[a]	flexible[b]	exact[c]
OHO	81 (156)[d]	76 (63)	66 (95)	76
ODO	23 (30)	9 (18)	7 (22)	9

[a] Frozen reference geometry [see Sec 2a]. [b] Flexible reference geometry [see Sec 2c]. [c] Exact values of the tunneling splitting (for this model). [d] Values in parentheses are tunneling splittings given by the one-dimensional vibrational adiabatic approximation.

Table 2 gives the tunneling splitting for the ground vibrational state of this double well potential, as calculated by the basis set method described in Section 3. Results in Table 2 are given for the principal isotope, and also for the deuterated system, each for three different choices of the reference geometry of the bath: "transition state" refers to a frozen reference geometry of the bath which is that of the transition state, "equilibrium" also refers to a frozen reference geometry but one that is the average of the two equilibrium geometries, and "flexible" refers to the variable reference geometry [Section 2c] that interpolates between the transition state and the equilibrium geometries. The "exact" values given in Table 2 were calculated by the method of Carter and Handy[22], which is readily applied to any triatomic system. Finally, the values given in parentheses in Table 2 are the results obtained from the one-dimensional vibrationally adiabatic approximation, and are thus a measure of how much adiabatic coupling affects the tunneling.

From the results in Table 2 one sees that the bath has a very significant effect on the tunneling dynamics *viz* the error in the values given by the one-dimensional vibrationally adiabatic approximation [those in parentheses are in error by 50 to 100%].

The adiabatic error for the equilibrium geometry is the smallest, while that for the transition state is the largest. In fact, one also sees from Table 2 that the fixed equilibrium geometry for the bath does a better job of describing the dynamics of H-atom transfer [i.e., the tunneling splitting] than does a frozen transition state reference geometry. It thus appears that a quadratic expansion of the potential in bath coordinates about a *frozen* reference geometry can be sufficient if the geometry of the bath does not relax very much during the reaction. A flexible reference is necessary, however, if there is a lot of relaxation in the bath. Fortunately, the flexible bath model of Section 2c is not any more difficult to apply than is the frozen bath treatment of Section 2a.

3.5 Concluding Remarks

The cartesian reaction path model presented in Section 2 provides a much simpler description of the interaction between the "system" [the reaction coordinate] and the "bath" [the remaining degrees of freedom] than does a reaction path model based on the (curvilinear) minimum energy [i.e., steepest descent] path. Also, as discussed above, this description is often a more physically correct picture of the dynamics (as, for example, in the case of H-atom transfer where the minimum energy reaction path is very sharply curved). It is also gratifying that the kind of *ab initio* quantum chemistry calculations that are necessary to apply this model are simpler to generate than for the steepest descent path.

The Hamiltonian that results from this cartesian reaction path model has the generic form of a cartesian "system" linearly coupled to a harmonic "bath". The most powerful way for treating the dynamics of such a system is Feynman path integral methodology, but it is encouraging to see that the simpler basis set method summar-

ized in Section 3 does quite a good job of describing how coupling to the bath affects the H-atom transfer dynamics. We thus believe that the overall approach described herein will be useful for treating a variety of polyatomic reaction processes.

Appendix 3.1

Here we show briefly (this is not a formal proof) why the reaction coordinate always approaches a stationary point from the lowest frequency mode.

For the path of steepest descent

$$\frac{\partial \alpha}{\partial s} = \frac{-\left[\frac{\partial V}{\partial x}\right]_{x=\alpha}}{\left|\frac{\partial V}{\partial x}\right|_{x=\alpha}} \tag{A3.1}$$

where α contains the cartesian coordinates of the reaction path as a function of the reaction coordinate *s*. Consider a potential $V = V_o + \frac{1}{2}\sum_{i=1}^{2}\omega_i^2 x_i^2$. The ratio of Equation A3.1 for the two degrees of freedom can be written:

$$\frac{\frac{\partial \alpha_i}{\partial s}}{\frac{\partial \alpha_j}{\partial s}} = \frac{\left[\frac{\partial V}{\partial x_i}\right]_{x_i=\alpha_i}}{\left[\frac{\partial V}{\partial x_j}\right]_{x_j=\alpha_j}} = \frac{\omega_i^2 \alpha_i}{\omega_j^2 \alpha_j} ,$$

$$\int \frac{1}{\alpha_i}\frac{\partial \alpha_i}{\partial s} ds = \int \left[\frac{\omega_i}{\omega_j}\right]^2 \frac{1}{\alpha_j}\frac{\partial \alpha_j}{\partial s} ds ,$$

and

$$\ln \alpha_i = \left[\frac{\omega_i}{\omega_j}\right]^2 \ln \alpha_j .$$

Therefore,

$$\alpha_i = \alpha_j^{(\frac{\omega_i}{\omega_j})^2} \quad \textit{along the path} \tag{A3.2}$$

Let's examine two possible cases: (a) $\omega_i > \omega_j$ and (b) $\omega_i < \omega_j$. One can see that for Case a α_i is greater than α_j and for Case b α_i is less than α_j,

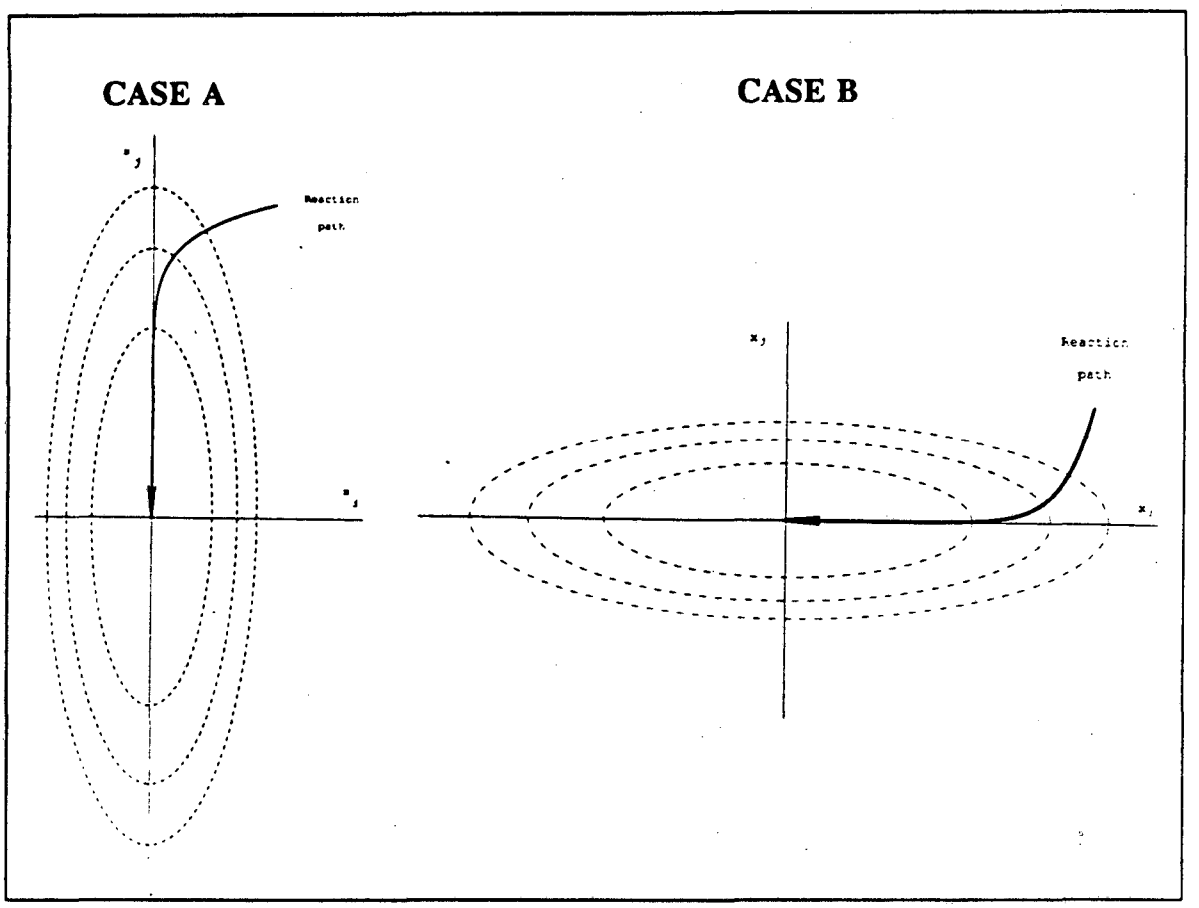

Reaction paths approach stationary state along lowest frequency mode.
CASE A: $\omega_i > \omega_j$. CASE B: $\omega_j > \omega_i$.

Figure A3.1

The path of steepest descent approaches the stationary point from the mode of lowest frequency: α_j for Case a and α_i for Case b.

Chapter 4

DIABATIC HAMILTONIAN

4.1 Introduction

An alternative method on which to base the dynamical model of H-atom transfer reactions in polyatomic systems is based on a previously suggested[23a] *straight-line cartesian path*[23] The purpose of this chapter is to develop this idea of a linear path in a more rigorous fashion than before, correctly incorporating conservation of total angular (and, trivially, linear) momentum. We also show rigorously how all coupling in the *kinetic* energy part of the Hamiltonian can be eliminated, to then appear in the *potential* energy. For this reason we have termed this model a *diabatic* reaction path Hamiltonian in analogy with the adiabatic/diabatic language used for describing systems with electronic and nuclear [i.e., vibration, rotation, translation] degrees of freedom.[24] Following this analogy, the earlier reaction path Hamiltonian[2] would be called the *adiabatic* reaction path Hamiltonian because the local vibrational modes orthogonal to the reaction path are the exact normal modes for a fixed value of the reaction coordinate [i.e., a fixed position on the reaction path] with the coupling between these modes and the reaction coordinate appearing in the kinetic energy, just as does the coupling between nuclear degrees of freedom and adiabatic electronic states. In the model developed in this chapter, the coupling between the reaction coordinate and perpendicular modes has been transformed from the kinetic to the potential energy, the same as for a diabatic electronic representation.

Section 2 first describes the linear reaction path and how it is defined so that no linear or angular momentum is generated along it. Construction of the Hamiltonian

then follows very closely the procedures used for the original (adiabatic) reaction path Hamiltonian, and this is carried out in Section 3. It is shown in Section 4 how to eliminate the coriolis couplings between the reaction coordinate and the orthogonal vibrational modes, so that the resulting Hamiltonian (for J=0) has a totally cartesian kinetic energy [i.e., a sum of squares of the momenta, with no coordinate dependence]. The straight-line Hamiltonian is applied to a polyatomic system in Section 5.

To conclude the Introduction it is useful to discuss qualitatively why we think a linear reference, or reaction path, will be useful for H-atom transfer reactions whereas it was asserted that the minimum energy reaction path would not.

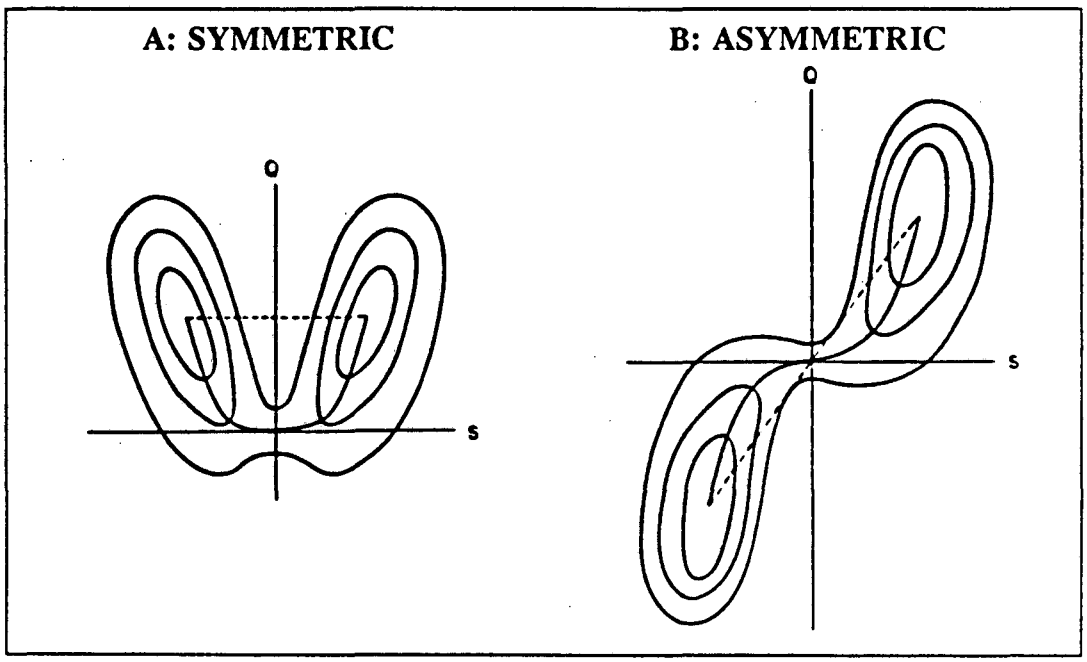

Potential energy contours for H-L-H system illustrating curvature of the reaction coordinate for symmetric coupling and asymmetric coupling.

Figure 4.1

Figure 1a shows the sketch of a potential energy contour typical of a collinear heavy + light-heavy system, like reaction 1.2. As mentioned in the Introduction of Chapter 1, it is well known[4] in such cases that the tunneling dynamics does not follow

the minimum energy path (the full line) but rather "cuts to corner". One can take advantage of this fact and view the linear path from reactants to products as the extreme version of corner cutting. Figure 1a also pertains to certain modes in a polyatomic system that have a predominantly symmetric type of coupling. For example, the 2-dimensional potential surface for hydrogen transfer in malonaldehyde

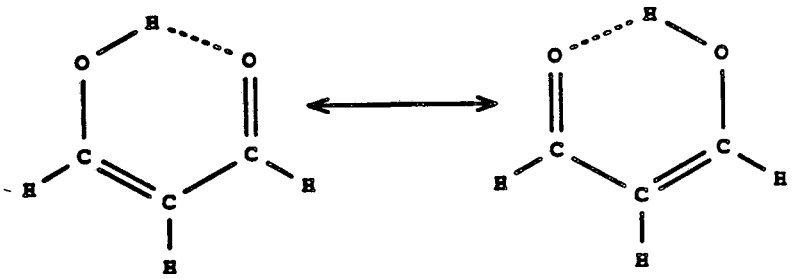

(4.1)

looks qualitatively like Figure 1a when the reaction coordinate is taken as the s-coordinate and the O-O stretch as the Q-coordinate.

Figure 1b, on the other hand, is for a mode with predominantly *asymmetric* coupling to the reaction coordinate, one for which the potential well in the reaction coordinate is asymmetric for a fixed (non-zero) value of the other coordinate. The minimum energy path in this case will also be sharply curved and not useful for defining a reaction coordinate. The straight-line path in this case "cuts" both corners, passing through the transition state. An example of this situation is the double H-atom transfer in formic acid dimer,

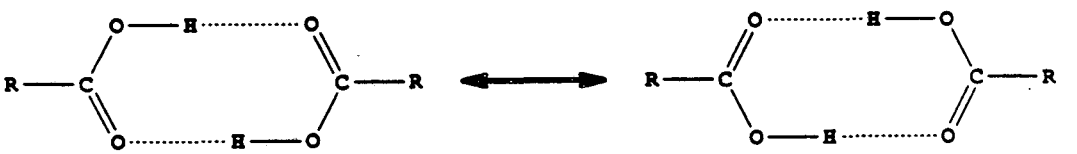

(4.2)

where the coordinate {s} of Figure 1b is the concerted motion of the two hydrogen atoms and Q the asymmetric O-C-O stretch that is coupled strongly to it.

4.2 The Linear Reference Path

First some comments on notation because we will switch on occasion between vector notation and component notation. Three-dimensional cartesian vectors are indicated as bold-face quantities with an over arrow. Thus, $\vec{\mathbf{R}}_i$, i=1-N, are the three cartesian coordinates of the N atoms; and $\vec{\mathbf{x}}_i$ are the corresponding mass-weighted coordinates

$$\vec{\mathbf{x}}_i = \sqrt{m_i}\,\vec{\mathbf{R}}_i\,. \tag{4.2}$$

Bold-face $\mathbf{x}$ with no index is the 3N-dimensional vector $\mathbf{x}=\{x_{i\gamma}\}$, with γ=x,y,z and i=1-N. Thus in component notation Equation 2.1a is

$$x_{i\gamma} = \sqrt{m_i}\,R_{i\gamma}\,. \tag{4.3}$$

The *linear reference path* is defined by linear interpolation between reactant and product geometry, i.e.,

$$\begin{aligned} \mathbf{x}_o(s) &= \tfrac{1}{2}(\mathbf{x}_r+\mathbf{x}_p) + (\mathbf{x}_p-\mathbf{x}_r)\left(\frac{s}{\Delta s}\right) \\ \Delta s &= |\mathbf{x}_p-\mathbf{x}_r| \end{aligned} \tag{4.4}$$

where $\mathbf{x}_r \equiv \{\, x_{i\gamma} \,\}$, and $\mathbf{x}_p \equiv x_{i\gamma}^{(p)}$ are the 3N mass-weighted cartesian coordinates of the atoms for the equilibrium geometry of the reactants and products, respectively. In terms of the coordinates $\vec{\mathbf{R}}_i$, Equation 4.4 is

$$\vec{\mathbf{R}}_i^{(o)}(s) = \tfrac{1}{2}(\vec{\mathbf{R}}_i^{(r)} + \vec{\mathbf{R}}_i^{(p)}) + (\vec{\mathbf{R}}_i^{(p)} - \vec{\mathbf{R}}_i^{(r)})\left(\frac{s}{\Delta s}\right). \tag{4.5}$$

where s, the reaction coordinate, is the distance along this linear path. As s varies from -½Δs to +½Δs the reference geometry varies from that of reactants to products. We note that

$$x_o'(s) = \frac{(x_p - x_r)}{\Delta s}\ , \tag{4.6}$$

so that

$$|x_o'(s)| = 1;$$

where the prime denotes $(\frac{\partial}{\partial s})$.

To make the above definitions concrete we must specify how the axis system which defines product coordinates $\vec{R}_i^{(p)}$ is related to the axis used to define the reactant coordinates $\vec{R}_i^{(r)}$. This is intimately connected with the requirement[25] that the reference path $x_o(s)$ be one for which *no linear or angular momentum be generated* for displacements along it. To use the Hougen-Bunker-Johns[25] methodology, the path $x_o(s)$ must satisfy the following conditions:

$$\sum_i m_i \vec{R}_i'^{(o)}(s) = 0 \tag{4.7a}$$

$$\sum_i m_i \vec{R}_i^{(o)}(s) \times \vec{R}_i'^{(o)}(s) = 0 \tag{4.7b}$$

The first requirement, Equation 4.7a insures that no linear momentum is generated along the path, and this is easily satisfied by choosing the reactant and product coordinates so that the center of mass in each case is at the origin. This means that

$$\sum_i m_i \vec{R}_i^{(r)} = \sum_i m_i \vec{R}_i^{(p)} = 0\ . \tag{4.8}$$

If the reactant coordinates, for example, are originally given so that Equation 4.8 is not true, then one re-defines them by

$$\vec{R}_i^{(r)} \rightarrow \vec{R}_i^{(r)} - \vec{R}_{com}^{(r)} \tag{4.9}$$

where

$$\vec{R}_{com}^{(r)} = \frac{\sum_i m_i \vec{R}_i^{(r)}}{\sum_i m_i} .$$

Multiplying Equation 4.5 by m_i and summing over *i* gives (using Equation 4.8)

$$\sum_i m_i \vec{R}_i^{(o)}(s) = 0 , \tag{4.10}$$

and Equation 4.7a easily follows.

Insuring no angular momentum along the linear reference path is trickier. Substituting the linear path, Equation 4.5, into Equation 4.7b leads to the following equation

$$\sum_i m_i \left(\vec{R}_i^{(r)} \times \vec{R}_i^{(p)} \right) = 0 \tag{4.11}$$

as the condition that the total angular momentum remains zero along the path. Equation 4.11 will not be true unless the product axis system is *oriented* in precisely the correct way with respect to the reactant one. (The two axis systems have already been chosen so that the center of mass of both is at the origin.)

Thus suppose that Equation 4.11 is not true for the initial orientation of the product axis system with respect to the reactant one. One then rotates the product axis by

replacing the product coordinates

$$\vec{R}_i^{(p)} \rightarrow T \cdot \vec{R}_i^{(p)} , \tag{4.12}$$

where T is the 3x3 cartesian rotation matrix[26] parametrized by three Euler angles that specify the rotation. These three Euler angles are chosen so that the three equations in Equation 4.11 are satisfied.

It is useful to see explicitly how this works for the case that reactant and product molecule are *planar*, e.g., as for reactions 4.1 and 4.2. the reactant and product coordinate vectors thus have the form

$$\vec{R}_i^{(r)} = \begin{bmatrix} X_i^{(r)} \\ Y_i^{(r)} \\ 0 \end{bmatrix} , \qquad \vec{R}_i^{(p)} = \begin{bmatrix} X_i^{(p)} \\ Y_i^{(p)} \\ 0 \end{bmatrix} , \tag{4.13}$$

and it is then easy to show that Equation 4.11 reduces to the single equation

$$\sum_i m_i \left(X_i^{(r)} Y_i^{(p)} - Y_i^{(r)} X_i^{(p)}\right) \equiv \sum_i m_i \left(\vec{R}_i^{(r)} \times \vec{R}_i^{(p)}\right)_z = 0 \ . \tag{4.14}$$

If Equation 4.14 is not true, then the product axis system needs to be rotated by an angle ϕ about the z-axis, whereby $\vec{R}_i^{(p)}$ of Equation 4.13 is replaced by

$$\begin{bmatrix} X_i^{(p)} \\ Y_i^{(p)} \\ 0 \end{bmatrix} \rightarrow \begin{bmatrix} \cos\phi\, X_i^{(p)} + \sin\phi\, Y_i^{(p)} \\ -\sin\phi\, X_i^{(p)} + \cos\phi\, Y_i^{(p)} \\ 0 \end{bmatrix} . \tag{4.15}$$

With this replacement it is a simple calculation to show that Equation 2.14 becomes

$$0 = -\sin\phi \sum_i m_i (X_i^{(r)} X_i^{(p)} + Y_i^{(r)} Y_i^{(p)}) + \cos\phi \sum_i m_i (X_i^{(r)} Y_i^{(p)} - Y_i^{(r)} X_i^{(p)}) \quad (4.16)$$

which is satisfied by the choice

$$\phi = \tan^{-1}\left[\frac{\sum_i m_i (\vec{R}_i^{(r)} \times \vec{R}_i^{(p)})_z}{\sum_i m_i \vec{R}_i^{(r)} \cdot \vec{R}_i^{(p)}}\right] . \quad (4.17)$$

Therefore, if the original product coordinates $\vec{R}_i^{(p)}$ do not satisfy Equation 4.14, they are rotated according to Equation 4.16 with the angle ϕ given by Equation 4.17.

The requirement of no linear and angular momentum along the reaction path given by Equation 4.14, thus uniquely defines the axis system for the product coordinates with respect to that for the reactant.

4.3 The Straight-Line Reference Path Hamiltonian

With the linear reaction path defined as in the previous section, one can proceed to construct the Hamiltonian in precisely the same manner as for the original reaction path Hamiltonian.[2] Thus $\{P_{i\gamma,i'\gamma}\}$,

$$P_{i\gamma,i'\gamma}(s) = \sum_{k=3N-6}^{3N} L_{i\gamma,k}(s) L_{i'\gamma,k}(s) , \quad (4.18)$$

is the projector onto the seven directions that are pure translations and rotations of the N atom system, plus the direction along the linear reaction path. The six 3N dimen-

sional vectors $\{L_{i\gamma,k}(s)\}$, k=3N-7...3N that correspond to pure translations and rotations are as given before,[2] and the one for k=3N-6

$$L_{i\gamma,3N-6}(s) = x'^{(o)}_{i\gamma}(s) \tag{4.19}$$

is the direction along the reaction path.

The (3N-7) eigenvectors $\{L_{i\gamma,k}(s)\}$, k=1...3N-7 that are orthogonal to the reaction path (and contain no translations or rotations) are determined by diagonalizing the projected force constant matrix

$$\mathbf{K}_{proj} = [1-\mathbf{P}(s)] \cdot \mathbf{K}(s) \cdot [1-\mathbf{P}(s)] \ , \tag{4.20}$$

where

$$K_{i\gamma,i'\gamma}(s) = \left[\frac{\partial^2 V}{\partial x_{i\gamma} \partial x_{i'\gamma}} \right]_{\mathbf{x}=\mathbf{x}_o(s)} .$$

The 3N-7 non-zero eigenvalues of the projected force constant matrix are $\omega_k^2(s)$, k=1...3N-7. The 3N cartesian coordinates $\mathbf{x}$ are given in terms of $(s,\{Q_k\})$, k=1...3N-7 by

$$x_{i\gamma} = x^{(o)}_{i\gamma}(s) + \sum_{k=1}^{3N-7} L_{i\gamma,k}(s)\, Q_k \tag{4.21}$$

where $\{Q_k\}$ are local normal coordinates for the 3N-7 directions that are orthogonal to the reaction path (and which carry no linear or angular momentum). We note for later use two orthogonality relations,

$$\begin{aligned} \sum_{i\gamma} L_{i\gamma,k}(s)\, L_{i\gamma,k'}(s) &= \delta_{k,k'} \\ \sum_{k=1}^{3N-7} L_{i\gamma,k}(s)\, L_{i'\gamma,k}(s) &= \delta_{i\gamma,i'\gamma} - P_{i\gamma,i'\gamma}(s) \end{aligned} \quad , \tag{4.22}$$

or in matrix notation

$$\begin{aligned} \mathbf{L}^T(s)\cdot\mathbf{L}(s) &= 1 \\ \mathbf{L}(s)\cdot\mathbf{L}^T(s) &= 1 - \mathbf{P}(s) \end{aligned}$$

where it is understood here that the index k ranges only over the values k=1...3N-7. **L**(s) is thus a 3N x (3N-7) rectangular matrix. We note also the identity which follows from the second relation of Equation 4.22 since $\mathbf{P}^2 = \mathbf{P}$ for any projector

$$\mathbf{P}(s)\cdot\mathbf{L}(s) = 0 \; .$$

The reaction path Hamiltonian for J=0 is then

$$\begin{aligned} H(p_s,s,p_k,Q_k) &= \tfrac{1}{2}\left[P_s - \sum_{k,k'=1}^{3N-7} Q_k P_{k'} B_{k,k'}(s)\right]^2 + V_o(s) \\ &+ \sum_{k=1}^{3N-7} \left[\, \tfrac{1}{2}P_k^2 - f_k(s)\, Q_k + \tfrac{1}{2}\omega_k^2(s)\, Q_k^2 \,\right] \end{aligned} \tag{4.23a}$$

where

$$\begin{aligned} f_k(s) &= -\sum_{i\gamma} D_{i\gamma}(s)\, L_{i\gamma,k}(s) \\ D_{i\gamma}(s) &= \left[\frac{\partial V}{\partial x_{i\gamma}}\right]_{x=x_o(s)} \\ B_{k,k'}(s) &= \sum_{i\gamma} L'_{i\gamma,k}(s)\, L_{i\gamma,k'}(s) \end{aligned} \quad . \tag{4.23b}$$

Equation 4.23a is the same as the original reaction path Hamiltonian[2] with two exceptions. First, because the reaction path is straight, the curvature coupling elements are zero [i.e., $B_{k,3N-6}(s)\equiv 0$] so the first term in the present Hamiltonian does not have the factor

$$\left[1 + \sum_{k=1}^{3N-7} Q_k B_{k,3N-6}(s)\right]^2 \tag{4.24}$$

that appears in the denominator of the previous result.[2] Second, since the present linear reaction path is not the minimum energy path, the potential energy has a term that is linear in the coordinates $\{Q_k\}$. We note also that cubic and quartic terms in coordinates $\{Q_k\}$ can readily be added to Equation 4.23 if the third and fourth cartesian derivatives of the potential are evaluated along the reaction path. The cubic term, for example, is

$$\frac{1}{6} \sum_{k,k',k''=1}^{3N-7} Q_k Q_{k'} Q_{k''} C_{kk'k''}(s) \,, \tag{4.25}$$

where

$$C_{kk'k''}(s) = \sum_{i\gamma}\sum_{i'\gamma'}\sum_{i''\gamma''} \left[\frac{\partial^3 V}{\partial x_{i\gamma}\partial x_{i'\gamma}\partial x_{i''\gamma''}}\right]_{x=x_o(s)} L_{i\gamma,k}(s)\, L_{i'\gamma',k'}(s)\, L_{i''\gamma'',k''}(s)$$

and the quartic term is similar. It is, of course, possible to include such higher order terms in only some modes k and not in others.

Finally, we note that the Hamiltonian for J>0 is also constructed in the present case in the same manner as before.[3]

4.4 Elimination of Kinetic Energy Coupling

The final step in obtaining the diabatic reaction path Hamiltonian is to eliminate the "coriolis" coupling terms in Equation 4.23 which involve the coupling elements $B_{k,k'}(s)$. This procedure has been carried out before,[3b] so we briefly summarize it here.

F_2 *Transformation*

One makes an s-dependent linear transformation of the $\{Q_k\}$ coordinates to new coordinates $\{\overline{Q}_k\}$ defined by

$$\overline{Q}_k = \sum_{k'} Q_{k'} U_{k',k}(s) \ , \tag{4.26}$$

or in matrix notation

$$\overline{\mathbf{Q}} = \mathbf{U}^T(s) \cdot \mathbf{Q}$$

where all indices k, k' take on values 1 to 3N-7. The (3N-7)x(3N-7) matrix **U** is an orthogonal matrix [i.e., $\mathbf{U}^T \cdot \mathbf{U} = \mathbf{U} \cdot \mathbf{U}^T = 1$]. The generating function which accomplishes this transformation from the "old" variables (p_s, s, **P**, **Q**) to the "new" ones ($\overline{p}_s, \overline{s}, \overline{\mathbf{P}}, \overline{\mathbf{Q}}$) is of the F_2-type[12]

$$F_2(s\,\mathbf{Q}, \overline{p}_s \overline{\mathbf{P}}) = s\,\overline{p}_s + \mathbf{Q}^T \cdot \mathbf{U}(s) \cdot \overline{\mathbf{P}} \ . \tag{4.27}$$

With the standard defining equations[12]

$$p_s = \frac{\partial F_2}{\partial s} \quad ; \qquad \bar{s} = \frac{\partial F_2}{\partial \bar{p}_s}$$

$$\mathbf{P} = \frac{\partial F_2}{\partial \mathbf{Q}} \quad ; \qquad \bar{\mathbf{Q}} = \frac{\partial F_2}{\partial \bar{\mathbf{P}}}$$

one finds the following relations between the "old" and "new" variables

$$\begin{aligned} p_s &= \bar{p}_s + \mathbf{Q}^T \cdot \mathbf{U}'(s) \cdot \bar{\mathbf{P}} \\ \mathbf{P} &= \mathbf{U}(s) \cdot \bar{\mathbf{P}} \\ \bar{s} &= s \\ \bar{\mathbf{Q}} &= \mathbf{U}^T \cdot \mathbf{Q} \end{aligned} \tag{4.28}$$

If the transformation matrix $\mathbf{U}(s)$ is chosen to satisfy the equation

$$\mathbf{U}'(s) = \mathbf{B}(s) \cdot \mathbf{U}(s) \ , \tag{4.29}$$

where $\mathbf{B}(s) \equiv \{B_{k,k'}(s)\}$ is the coupling matrix of Equation 4.23b, then the Hamiltonian of Equation 4.23a takes the following form in terms of the new variables:

$$H(\bar{p}_s, \bar{s}, \bar{\mathbf{p}}, \bar{\mathbf{Q}}) = \tfrac{1}{2}\bar{p}_s^2 + V_o(\bar{s}) + \sum_{k=1}^{3N-7} \left[\tfrac{1}{2}\bar{P}_k^2 - \bar{f}_k(\bar{s})\, \bar{Q}_k \right] + \sum_{k,k'=1}^{3N-7} \tfrac{1}{2}\bar{Q}_k\, \Lambda_{k,k'}(\bar{s})\, \bar{Q}_k \tag{4.30a}$$

where

$$\begin{aligned} \bar{f}_k(\bar{s}) &= \sum_{k'=1}^{3N-7} f_{k'}(\bar{s})\, U_{k',k}(\bar{s}) \\ \Lambda_{k,k'}(\bar{s}) &= \sum_{k''=1}^{3N-7} U_{k'',k}(\bar{s})\, \omega_{k''}(\bar{s})^2\, U_{k'',k'}(\bar{s}) \end{aligned} \tag{4.30b}$$

In matrix notation we note that $\bar{\mathbf{f}}(s)$ and $\Lambda(s)$ of Equations 4.30b can be written as

$$\begin{aligned} \bar{\mathbf{f}}^T(s) &= \mathbf{f}^T(s)\cdot\mathbf{U}(s) \\ \Lambda(s) &= \mathbf{U}^T\cdot\omega^2(s)\cdot\mathbf{U}(s) \end{aligned} \tag{4.30c}$$

and in light of Equation 4.23b and the fact that $\mathbf{L}^T\cdot\mathbf{K}(s)\cdot\mathbf{L}(s) = \omega(s)^2$, Equation 4.30c reads

$$\begin{aligned} \bar{\mathbf{f}}^T(s) &= -\mathbf{D}^T(s)\cdot\mathbf{L}(s)\cdot\mathbf{U}(s) \\ \Lambda(s) &= \mathbf{U}^T(s)\cdot\mathbf{L}^T(s)\mathbf{K}(s)\cdot\mathbf{L}(s)\cdot\mathbf{U}(s) \end{aligned} \tag{4.30d}$$

Therefore, in matrix notation the Hamiltonian Equation 4.30a becomes (dropping the over bars from the "new" coordinates and momenta):

$$H(p_s,s,\mathbf{P},\mathbf{Q}) = \left[\tfrac{1}{2}p_s^2 + V_o(s)\right] + \left[\tfrac{1}{2}\mathbf{P}^T\cdot\mathbf{P} - \mathbf{f}(s)^T\cdot\mathbf{Q} + \tfrac{1}{2}\mathbf{Q}^T\cdot\Lambda\cdot\mathbf{Q}\right] \tag{4.31a}$$

with

$$\begin{aligned} \mathbf{f}^T(s) &= -\mathbf{D}^T(s)\cdot\mathbf{M}(s) \\ \Lambda(s) &= \mathbf{M}^T(s)\cdot\mathbf{K}(s)\cdot\mathbf{M}(s) \\ \mathbf{M}(s) &\equiv \mathbf{L}(s)\cdot\mathbf{U}(s) \end{aligned} \tag{4.31b}$$

Equation 4.31a is the desired "diabatic" Hamiltonian: The kinetic energy is now totally cartesian and the coupling has been transformed from it to the off-diagonal elements $\Lambda_{k,k'}(s)$ in the potential energy. The matrix $\mathbf{M}(s)$ is the 3N x (3N-7) transformation matrix and $\mathbf{D}(s)$ and $\mathbf{K}(s)$ are the cartesian gradient and force constant matrix of Equations 4.23b and 4.20. We emphasize that it is the *combination*

$\mathbf{L}(s)\cdot\mathbf{U}(s) \equiv \mathbf{M}(s) \equiv \{M_{i\gamma,k}(s)\}$ that is required to construct the quantities that go in the Hamiltonian. We will discuss in more detail below how this transformation matrix $\mathbf{M}(s)$ is determined.

The procedure for constructing the Hamiltonian is, therefore, as follows: First the linear reaction path is properly determined as in Section 2 from the reactant and product equilibrium geometries. One then computes the energy $V_o(s)$, cartesian gradient $\mathbf{D}(s)$, and cartesian force constant matrix $\mathbf{K}(s)$ along this path (and also higher derivatives of the potential, e.g., Equation 4.25, if these are desired). The transformation matrix $\mathbf{M}(s)$ is then determined as is shown below and the quantities $\mathbf{f}(s)$ and $\Lambda(s)$ are computed via Equation 4.31b. If cubic, quartic, etc., terms in the potential are required, then the cartesian forms as given by Equation 4.25 are also transformed from cartesian space to Q_k-space via the matrix $\mathbf{M}(s)$.

M-Matrix

To conclude this section we show a simple procedure for determining the transformation matrix $\mathbf{M}(s)$ of Equation 4.31b. To make the notation below less cluttered we do not always denote the explicit s-dependence of the quantities $\mathbf{L}$, $\mathbf{M}$, and $\mathbf{U}$. The first step is to obtain the differential equation for $\mathbf{M}(s)$ that results from Equation 4.31b

$$\mathbf{M}' = \mathbf{L}'\cdot\mathbf{U} + \mathbf{L}\cdot\mathbf{U}' \,. \tag{4.32}$$

Using Equation 4.29 for $\mathbf{U}'$ and Equation 4.23b for $\mathbf{B}$ gives

$$\mathbf{M}' = \mathbf{L}'\cdot\mathbf{U} + \mathbf{L}\cdot\mathbf{L}^T\cdot\mathbf{L}\cdot\mathbf{U} \,. \tag{4.33}$$

Differentiating Equation 4.22 gives:

$$\mathbf{L}'\cdot\mathbf{L}^T + \mathbf{L}\cdot\mathbf{L}^T = -\mathbf{P}'$$

or

$$\mathbf{L}\cdot\mathbf{L}^T = -\mathbf{L}'\cdot\mathbf{L}^T - \mathbf{P}'$$

so that Equation 4.33 becomes

$$\begin{aligned}\mathbf{M}' &= \mathbf{L}'\cdot\mathbf{U} - \left[\mathbf{L}'\cdot\mathbf{L}^T + \mathbf{P}'\right]\cdot\mathbf{L}\cdot\mathbf{U} \\ &= \mathbf{L}'\cdot\mathbf{U} - \mathbf{L}'\cdot(\mathbf{L}^T\cdot\mathbf{L})\cdot\mathbf{U} - \mathbf{P}'\cdot\mathbf{L}\cdot\mathbf{U}\end{aligned}$$

Using $\mathbf{L}^T\cdot\mathbf{L}=\mathbf{1}$ and $\mathbf{M} = \mathbf{L}\cdot\mathbf{U}$ finally gives

$$\mathbf{M}'(s) = -\mathbf{P}'(s)\cdot\mathbf{M}(s) \tag{4.34}$$

as the fundamental defining equation for $\mathbf{M}(s)$. One needs only to supplement it with a boundary or initial condition such as

$$\mathbf{M}(0) = \mathbf{L}(0)\cdot\mathbf{U}(0)\ .$$

If we choose $\mathbf{U}(0) = \mathbf{1}$ then the initial condition is

$$\mathbf{M}(0) = \mathbf{L}(0) \tag{4.35}$$

where $\mathbf{L}(0)$ is obtained by diagonalizing the force constant matrix at the single position s=0. With Equation 4.35 as the initial condition for $\mathbf{M}(s)$, the differential equation Equation 4.34 determines $\mathbf{M}$ at all other values of s.

One way to obtain $\mathbf{M}$ over a grid of values in s is to integrate Equation 4.34 over a short increment (s_{k-1},s_k). This gives

$$\mathbf{M}_k - \mathbf{M}_{k-1} = -(\mathbf{P}_k - \mathbf{P}_{k-1}) \cdot \mathbf{M}_{k-1} \tag{4.36}$$

where

$$\mathbf{M}_k = \mathbf{M}(s_k)$$

$$\mathbf{P}_k = \mathbf{P}(s_k)$$

etc.

Then, since $\mathbf{P}(s) \cdot \mathbf{M}(s) = 0$ for all s (because $\mathbf{P}(s) \cdot \mathbf{L}(s) = 0$ from the orthogonality relations given by Equation 4.22), Equation 4.36 becomes

$$\mathbf{M}_k = (1 - \mathbf{P}_k) \cdot \mathbf{M}_{k-1} \ . \tag{4.37}$$

Iterating this relation gives

$$\mathbf{M}_k = (1 - \mathbf{P}_k) \cdot (1 - \mathbf{P}_{k-1}) \cdots (1 - \mathbf{P}_1) \cdot \mathbf{M}_0 \tag{4.38}$$

as a simple way to compute **M** over a grid of $\{s_k\}$ values, given the initial condition M(0) from Equation 4.35.

A more accurate approximate for integrating Equation 4.34 is to use the following equation instead of Equation 4.36.

$$\mathbf{M}_k - \mathbf{M}_{k-1} = -(\mathbf{P}_k - \mathbf{P}_{k-1}) \cdot \frac{1}{2}(\mathbf{M}_k + \mathbf{M}_{k-1}) \ . \tag{4.39}$$

This can be rearranged (because $\mathbf{P}_k \cdot \mathbf{M}_k = \mathbf{P}_{k-1} \cdot \mathbf{M}_{k-1} = 0$) to give

$$(1 - \tfrac{1}{2}\mathbf{P}_{k-1}) \cdot \mathbf{M}_k = (1-\tfrac{1}{2}\mathbf{P}_k) \cdot \mathbf{M}_{k-1} \ . \tag{4.40}$$

One can show that

$$(1 - \tfrac{1}{2}\mathbf{P}_{k-1})^{-1} = (1 + \mathbf{P}_{k-1})$$

so that from Equation 4.40 one obtains

$$\mathbf{M}_k = [1 - \tfrac{1}{2}(1+\mathbf{P}_{k-1}) \cdot \mathbf{P}_k] \cdot \mathbf{M}_{k-1} \tag{4.41}$$

which should be more accurate than Equation 4.37. Equation 4.37 can then be iterated to give

$$\mathbf{M}_k = [1-\tfrac{1}{2}(1+\mathbf{P}_{k-1})\cdot\mathbf{P}_k] \cdot [1-\tfrac{1}{2}(1+\mathbf{P}_{k-2})\cdot\mathbf{P}_{k-1}] \cdots [1-\tfrac{1}{2}(1+\mathbf{P}_0)\cdot\mathbf{P}_1] \cdot \mathrm{M}_0 \tag{4.42}$$

instead of Equation 4.38.

In summary then, the matrix M(s) that transforms from the cartesian space $\{i\gamma\}$ to the diabatic space $\{k\}$ is given by Equation 4.38 or 4.42, where the initial value $\mathbf{M}(0) \equiv \mathbf{L}(0)$ [Equation 4.35] is determined by diagonalizing the projected force constant matrix at the one position s=0. It is not necessary to diagonalize the projected force constant matrix at any other values as only the projectors $\mathbf{P}(s_k)$ are needed at the various values of the reaction coordinate in Equation 4.38.

4.5 Application

This straight line reaction Hamiltonian was applied to the isomerization process of Equation 4.1. An STO-3G basis set was used to generate *ab initio* energies, first, and second derivatives. These values are given in Appendix 4.1 along with the reactant and transition state geometries used for the interpolation procedure. After eliminating the kinetic energy coupling to obtain a Hamiltonian of the form in Equation 4.31a, $V_0(s)$, f(s) and Γ were fitted to a cubic spline.

The barrier for the 1-dimensional potential $V_0(s)$ is 24.5 kcal/mol because $V_0(s)$ does not pass through the true transition state of the many dimensional isomerization. The tunneling splitting of this 1-dimensional double well is 0.04 cm^{-1}. When the bath modes are added, the barrier is lowered by the nonzero first and second derivatives. Although the most rigorous method to include the effects of all of the other vibrational modes is to use Feynman path integrals, as was mentioned in Section 3.3, we present here results from inclusion of one important mode. The O-O stretch is the strongest coupled bath mode. Three other modes which couple strongly are the high frequency stretch of the y-coordinate of the tunneling proton, the y-stretch of the molecule, and the lowest frequency mode. The eigenvectors for these modes are pictured in Figure 4.2.

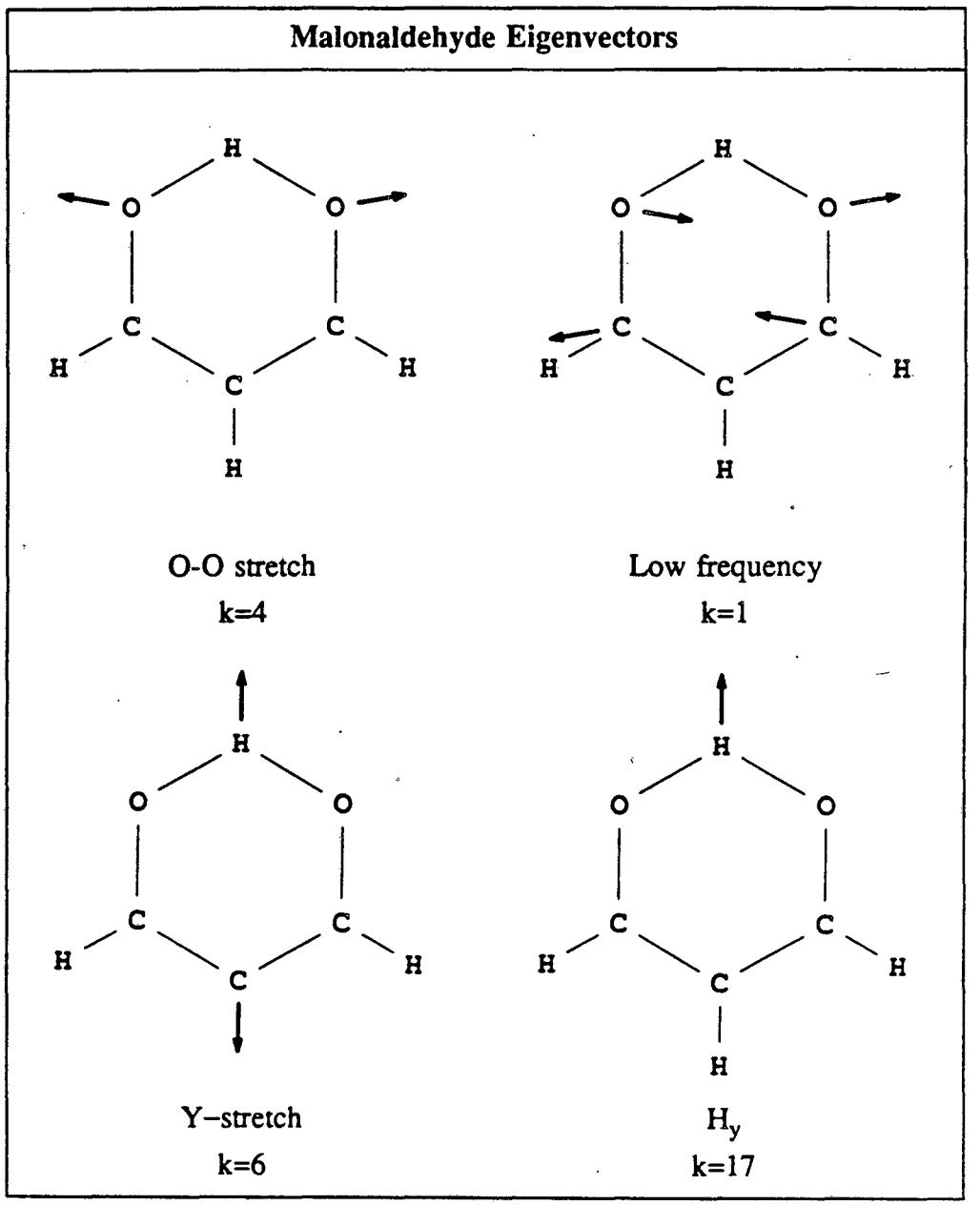

Four normal modes that are strongly coupled to the reaction coordinate. Only the largest components of the eigenvectors are illustrated.

Figure #4.2

A plot of the potential as a function of the reaction coordinate s and the O-O mode is shown in Figure 4.3.

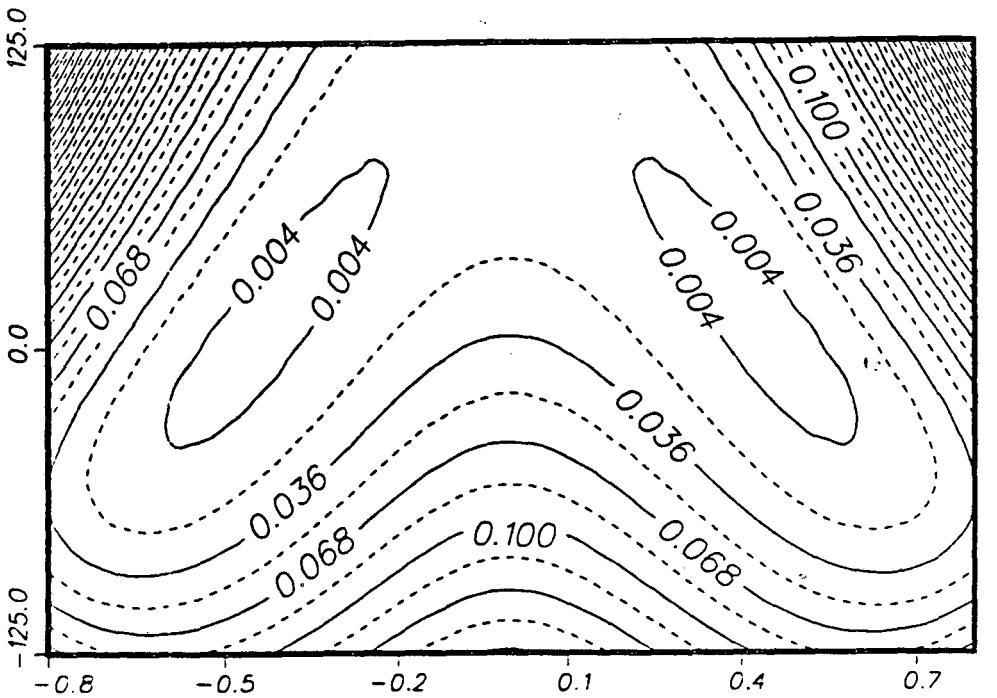

Contour plot for malonaldehyde. X-axis is reaction coordinate. Y-axis is O-O stretch bath mode.

Figure 4.3

The symmetric O-O stretch lowers the barrier to 3.82 kcal/mol. The result is a tunneling splitting of 11.8 cm^{-1} as compared to the experimentally determined tunneling splitting of 21 cm^{-1}. Thus, addition of this bath mode increases the 1-dimensional splitting by a factor of 250 to within a factor of two of the true value.

4.6 Concluding Remarks

We have shown how to construct a diabatic reaction path Hamiltonian, based on a

straight line that interpolates linearly from the reactant to the product geometry of the molecular system. Conservation of total linear and angular momentum are correctly incorporated. For J=0 the resulting Hamiltonian involves only the 3N-6 internal degrees of freedom, (s, $\{Q_k\}$ k=1,3N-7) where s is the distance along the reaction path and $\{Q_k\}$ are the coordinates for motion orthogonal to it. Equations 4.31a and 4.31b summarize the basic result for the Hamiltonian (for J=0), where Equation 4.38 or 4.42 show how the transformation matrix M(s) can be calculated. The kinetic energy term in the Hamiltonian is cartesian-like because the coriolis-type coupling terms have been transformed into potential energy coupling (hence the term "diabatic").

Throughout this paper we have implicitly assumed the use of classical mechanics. However, because the resulting Hamiltonian, Equation 4.31a, has a cartesian kinetic energy, though, it is trivial to transform the result [Equation 4.31a] to a quantum mechanical Hamiltonian operator by making the standard replacements

$$\begin{aligned} \tfrac{1}{2}p_s^2 &\rightarrow -\tfrac{1}{2}h^2\frac{\partial^2}{\partial s^2} \\ \tfrac{1}{2}P_k^2 &\rightarrow -\tfrac{1}{2}h^2\frac{\partial^2}{\partial Q_k^2} \end{aligned} \tag{4.43}$$

As discussed in the Introduction of this chapter, this diabatic reaction path Hamiltonian should be especially useful for describing H-atom transfer reactions in molecular systems. An example has been given for the H-atom transfer in the isomerization of malonaldehyde.

Appendix 4.1

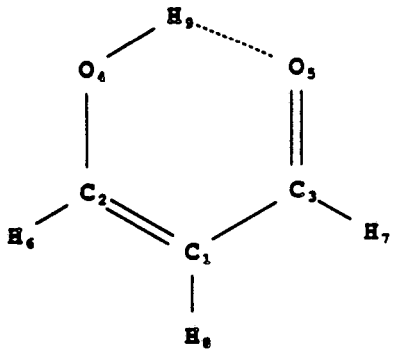

MALONALDEHYDE TRANSITION GEOMETRY (au)			
Atom	X(I)	Y(I)	Z(I)
C_1	0.0000000000	0.0000000000	0.0000000000
C_2	2.2277042514	1.4300312524	0.0000000000
C_3	-2.2277042514	1.4300312524	0.0000000000
O_4	2.1668312726	3.8637010892	0.0000000000
O_5	-2.1668312726	3.8637010892	0.0000000000
H_6	4.0850731790	0.4990275371	0.0000000000
H_7	-4.0850731790	0.4990275371	0.0000000000
H_8	0.0000000000	-2.0258755801	0.0000000000
H_9	0.0000000000	4.2733368674	0.0000000000
MALONALDEHYDE EQUILIBRIUM GEOMETRY			
C_1	0.0000000000	0.0000000000	0.0000000000
C_2	2.1459625195	1.3226355177	0.0000000000
C_3	-2.4479322539	1.3671248465	0.0000000000
O_4	2.2774372896	3.8994283798	0.0000000000
O_5	-2.5713262285	3.6944844190	0.0000000000
H_6	3.9955913063	0.4079992978	0.0000000000
H_7	-4.1755989146	0.2012422145	0.0000000000
H_8	0.0000000000	-2.0337690050	0.0000000000
H_9	0.4717004984	4.4454312787	0.0000000000

STO-3G *ab initio* geometries of stationary states. Origin of coordinate axis is located on C_1. Transition State energy is -262.1453248054 au. Equilibrium energy is -262.1558074974 au.

Linear Reference Potential for Malonaldehyde

S	Energy (au)
0.0	-262.1168443113
0.05	-262.1178165327
0.10	-262.1206078797
0.15	-262.1248832012
0.20	-262.1301856824
0.25	-262.1360147848
0.30	-262.1418692180
0.35	-262.1472606966
0.40	-262.1517113440
0.45	-262.1547436882
0.50	-262.1558674974
0.55	-262.1545647701
0.60	-262.1502726914
0.70	-262.1301212797
0.80	-262.0891444320
0.90	-262.0185581101
1.00	-261.9055824980

First Derivatives

First derivative for bath = 1

0.00642709	0.00406706	0.00243116	0.00129877	0.00051991
0.00023181	0.00000000	-0.00018146	-0.00031693	-0.00040950
-0.00046116	-0.00047303	-0.00044572	-0.00038006	-0.00027860
-0.00014782	0.00000000	0.00014782	0.00027860	0.00038006
0.00044572	0.00047303	0.00046116	0.00040950	0.00031693
0.00018146	0.00000000	-0.00023181	-0.00051991	-0.00129877
-0.00243116	-0.00406706	-0.00092065		

First derivative for bath = 4

0.00419621	0.00264371	0.00158639	0.00085937	0.00035394
0.00016121	0.00000000	-0.00013481	-0.00024737	-0.00034114
-0.00041905	-0.00048348	-0.00053617	-0.00057811	-0.00060932
-0.00062891	-0.00063564	-0.00062891	-0.00060932	-0.00057811
-0.00053617	-0.00048348	-0.00041905	-0.00034114	-0.00024737
-0.00013481	0.00000000	0.00016121	0.00035394	0.00085937
0.00158639	0.00264371	-0.00320928		

First derivative for bath = 6

-0.00255844	-0.00157100	-0.00092065	-0.00048742	-0.00019644
-0.00008822	0.00000000	0.00007184	0.00012994	0.00017649
0.00021335	0.00024214	0.00026418	0.00028052	0.00029191
0.00029869	0.00030095	0.00029869	0.00029191	0.00028052
0.00026418	0.00024214	0.00021335	0.00017649	0.00012994
0.00007184	0.00000000	-0.00008822	-0.00019644	-0.00048742
-0.00092065	-0.00157100	0.00000000		

First derivative for bath = 17

-0.00998441	-0.00577968	-0.00320928	-0.00161724	-0.00062089
-0.00027387	0.00000000	0.00021430	0.00038044	0.00050765
0.00060357	0.00067455	0.00072585	0.00076174	0.00078540
0.00079891	0.00080331	0.00079891	0.00078540	0.00076174
0.00072585	0.00067455	0.00060357	0.00050765	0.00038044
0.00021430	0.00000000	-0.00027387	-0.00062089	-0.00161724
-0.00320928	-0.00577968	0.00001831		

Second derivatives

Second derivatives are printed out in matrix format at 33 reaction coordinate values. The derivatives are taken with respect to the bath modes k=1, 4, 6, 17 of Figure #4.2. The matrix elements are arranged in ascending order. For example, the (2,4) matrix element is the second derivative of the potential with respect to k=4 and k=17.

Second Derivatives for s = -1.00

0.00014346	0.00009443	-0.00006320	-0.00030168
0.00009443	0.00006125	-0.00003555	-0.00015758
-0.00006320	-0.00003555	0.00003866	0.00006027
-0.00030168	-0.00015758	0.00006027	0.00005973

Second Derivatives for s = -0.90

0.00010610	0.00006537	-0.00004148	-0.00017827
0.00006537	0.00004197	-0.00002255	-0.00009477
-0.00004148	-0.00002255	0.00003171	0.00003413
-0.00017827	-0.00009477	0.00003413	0.00006353

Second Derivatives for s = -0.80

0.00007884	0.00004535	-0.00002734	-0.00010409
0.00004535	0.00002930	-0.00001433	-0.00005761
-0.00002734	-0.00001433	0.00002759	0.00001953
-0.00010409	-0.00005761	0.00001953	0.00007455

Second Derivatives for s = -0.70

0.00005934	0.00003165	-0.00001813	-0.00005930
0.00003165	0.00002102	-0.00000910	-0.00003536
-0.00001813	-0.00000910	0.00002516	0.00001128
-0.00005930	-0.00003536	0.00001128	0.00008478

Second Derivatives for s = -0.60

0.00004514	0.00002217	-0.00001201	-0.00003197
0.00002217	0.00001557	-0.00000573	-0.00002171
-0.00001201	-0.00000573	0.00002372	0.00000649
-0.00003197	-0.00002171	0.00000649	0.00009184

Second Derivatives for s = -0.55

0.00003939	0.00001852	-0.00000973	-0.00002254
0.00001852	0.00001355	-0.00000451	-0.00001691
-0.00000973	-0.00000451	0.00002322	0.00000488
-0.00002254	-0.00001691	0.00000488	0.00009409

Second Derivatives for s = -0.50

0.00003429	0.00001542	-0.00000783	-0.00001517
0.00001542	0.00001190	-0.00000351	-0.00001307
-0.00000783	-0.00000351	0.00002283	0.00000362
-0.00001517	-0.00001307	0.00000362	0.00009557

Second Derivatives for s = -0.45

0.00002970	0.00001277	-0.00000625	-0.00000944
0.00001277	0.00001053	-0.00000269	-0.00000997
-0.00000625	-0.00000269	0.00002252	0.00000264
-0.00000944	-0.00000997	0.00000264	0.00009642

Second Derivatives for s = -0.40

0.00002550	0.00001051	-0.00000492	-0.00000506
0.00001051	0.00000940	-0.00000201	-0.00000747
-0.00000492	-0.00000201	0.00002227	0.00000187
-0.00000506	-0.00000747	0.00000187	0.00009675

Second Derivatives for s = -0.35

0.00002161	0.00000858	-0.00000381	-0.00000181
0.00000858	0.00000848	-0.00000146	-0.00000546
-0.00000381	-0.00000146	0.00002208	0.00000127
-0.00000181	-0.00000546	0.00000127	0.00009671

Second Derivatives for s = -0.30

0.00001796	0.00000694	-0.00000290	0.00000046
0.00000694	0.00000774	-0.00000102	-0.00000384
-0.00000290	-0.00000102	0.00002192	0.00000082
0.00000046	-0.00000384	0.00000082	0.00009643

Second Derivatives for s = -0.25

0.00001450	0.00000553	-0.00000215	0.00000188
0.00000553	0.00000716	-0.00000067	-0.00000257
-0.00000215	-0.00000067	0.00002179	0.00000050
0.00000188	-0.00000257	0.00000050	0.00009603

Second Derivatives for s = -0.20

0.00001122	0.00000431	-0.00000154	0.00000255
0.00000431	0.00000673	-0.00000041	-0.00000159
-0.00000154	-0.00000041	0.00002170	0.00000027
0.00000255	-0.00000159	0.00000027	0.00009562

Second Derivatives for s = -0.15

0.00000819	0.00000321	-0.00000105	0.00000257

0.00000321	0.00000643	-0.00000022	-0.00000087
-0.00000105	-0.00000022	0.00002162	0.00000013
0.00000257	-0.00000087	0.00000013	0.00009528

Second Derivatives for s = -0.10

0.00000559	0.00000216	-0.00000066	0.00000205
0.00000216	0.00000625	-0.00000009	-0.00000038
-0.00000066	-0.00000009	0.00002158	0.00000005
0.00000205	-0.00000038	0.00000005	0.00009505

Second Derivatives for s = -0.05

0.00000376	0.00000110	-0.00000032	0.00000113
0.00000110	0.00000616	-0.00000002	-0.00000009
-0.00000032	-0.00000002	0.00002155	0.00000001
0.00000113	-0.00000009	0.00000001	0.00009492

Second Derivatives for s = -0.00

0.00000309	0.00000000	0.00000000	0.00000000
0.00000000	0.00000613	0.00000000	0.00000000
0.00000000	0.00000000	0.00002154	0.00000000
0.00000000	0.00000000	0.00000000	0.00009489

Second Derivatives for s = 0.05

0.00000376	-0.00000110	0.00000032	-0.00000113
-0.00000110	0.00000616	-0.00000002	-0.00000009
0.00000032	-0.00000002	0.00002155	0.00000001
-0.00000113	-0.00000009	0.00000001	0.00009492

Second Derivatives for s = 0.10

0.00000559	-0.00000216	0.00000066	-0.00000205
-0.00000216	0.00000625	-0.00000009	-0.00000038
0.00000066	-0.00000009	0.00002158	0.00000005
-0.00000205	-0.00000038	0.00000005	0.00009505

Second Derivatives for s = 0.15

0.00000819	-0.00000321	0.00000105	-0.00000257
-0.00000321	0.00000643	-0.00000022	-0.00000087
0.00000105	-0.00000022	0.00002162	0.00000013
-0.00000257	-0.00000087	0.00000013	0.00009528

Second Derivatives for s = 0.20

0.00001122	-0.00000431	0.00000154	-0.00000255
-0.00000431	0.00000673	-0.00000041	-0.00000159
0.00000154	-0.00000041	0.00002170	0.00000027
-0.00000255	-0.00000159	0.00000027	0.00009562

Second Derivatives for s = 0.25

0.00001450	-0.00000553	0.00000215	-0.00000188
-0.00000553	0.00000716	-0.00000067	-0.00000257
0.00000215	-0.00000067	0.00002179	0.00000050
-0.00000188	-0.00000257	0.00000050	0.00009603

Second Derivatives for s = 0.30

0.00001796	-0.00000694	0.00000290	-0.00000046
-0.00000694	0.00000774	-0.00000102	-0.00000384
0.00000290	-0.00000102	0.00002192	0.00000082
-0.00000046	-0.00000384	0.00000082	0.00009643

Second Derivatives for s = 0.35

0.00002161	-0.00000858	0.00000381	0.00000181
-0.00000858	0.00000848	-0.00000146	-0.00000546
0.00000381	-0.00000146	0.00002208	0.00000127
0.00000181	-0.00000546	0.00000127	0.00009671

Second Derivatives for s = 0.40

0.00002550	-0.00001051	0.00000492	0.00000506
-0.00001051	0.00000940	-0.00000201	-0.00000747
0.00000492	-0.00000201	0.00002227	0.00000187
0.00000506	-0.00000747	0.00000187	0.00009675

Second Derivatives for s = 0.45

0.00002970	-0.00001277	0.00000625	0.00000944
-0.00001277	0.00001053	-0.00000269	-0.00000997
0.00000625	-0.00000269	0.00002252	0.00000264
0.00000944	-0.00000997	0.00000264	0.00009642

Second Derivatives for s = 0.50

0.00003429	-0.00001542	0.00000783	0.00001517
-0.00001542	0.00001190	-0.00000351	-0.00001307
0.00000783	-0.00000351	0.00002283	0.00000362
0.00001517	-0.00001307	0.00000362	0.00009557

Second Derivatives for s = 0.55

0.00003939	-0.00001852	0.00000973	0.00002254
-0.00001852	0.00001355	-0.00000451	-0.00001691
0.00000973	-0.00000451	0.00002322	0.00000488
0.00002254	-0.00001691	0.00000488	0.00009409

Second Derivatives for s = 0.60

0.00004514	-0.00002217	0.00001201	0.00003197
-0.00002217	0.00001557	-0.00000573	-0.00002171
0.00001201	-0.00000573	0.00002372	0.00000649
0.00003197	-0.00002171	0.00000649	0.00009184

Second Derivatives for s = 0.70

0.00005934	-0.00003165	0.00001813	0.00005930
-0.00003165	0.00002102	-0.00000910	-0.00003536
0.00001813	-0.00000910	0.00002516	0.00001128
0.00005930	-0.00003536	0.00001128	0.00008478

Second Derivatives for s = 0.80

0.00007884	-0.00004535	0.00002734	0.00010409
-0.00004535	0.00002930	-0.00001433	-0.00005761
0.00002734	-0.00001433	0.00002759	0.00001953
0.00010409	-0.00005761	0.00001953	0.00007455

Second Derivatives for s = 0.90

0.00010610	-0.00006537	0.00004148	0.00017827
-0.00006537	0.00004197	-0.00002255	-0.00009477
0.00004148	-0.00002255	0.00003171	0.00003413
0.00017827	-0.00009477	0.00003413	0.00006353

Second Derivatives for s = 1.00

0.00014346	-0.00009443	0.00006320	0.00030168
-0.00009443	0.00006125	-0.00003555	-0.00015758
0.00006320	-0.00003555	0.00003866	0.00006027
0.00030168	-0.00015758	0.00006027	0.00005973

Chapter 5

EMPIRICAL VALENCE BOND MODEL

5.1 Introduction

This chapter combines a minimal amount of *ab initio* information with empirical data to form a simple and effective model for polyatomic systems. This model approximates an adiabatic potential by two simple potential curves that interact with each other. This idea comes from work by A. Warshel and R. M. Weiss[27] concerned with solvent and enzymatic effects on chemical reactions. They assign one empirically derived potential to each resonance structure involved in the reaction of interest [e.g., reactants and products with and without solvent effects] and represent the full chemical reaction by the interaction of these potentials. It is also analogous with valence bond theory where a system is represented by the interaction of wavefunctions generated for each separate nucleus of a molecule. It is for this reason that Warshel and Weiss refer to their work as the Empirical Valence Bond model. We adapt this empirical valence bond model to describe chemical reactions of bound states in the gas phase.

Section 2 presents the theory of this model as well as several options for the form of these potentials and their coupling, and Section 3 illustrates applications to 1-d problems while commenting on the extensions needed for larger systems. (I note here that applications to large systems are currently being done in our research group by Y. T. Chang.)

5.2 Theory

The first step in this theory is to select potentials which describe the isolated reactants and products, called V_{11} and V_{22} respectively. They can be harmonic or Morse potentials, for example. Or, for the empirical valence bond model as we present it here, V_{11} and V_{22} are defined as empirical potentials for the isolated reactants and products and are functions of internal coordinates. These two potentials cross and interact by the coupling term V_{12}, and the energy of the system is the solution to the following two state secular equation:

$$\begin{vmatrix} V_{11}-W & V_{12} \\ V_{12} & V_{22}-W \end{vmatrix} = 0$$

$$W_{\pm} = \frac{V_{11} + V_{22}}{2} \pm \sqrt{\left[\frac{V_{11}-V_{22}}{2}\right]^2 + V_{12}^2} \tag{5.1}$$

where it is assumed that the overlap integral of the two potentials, $S_{12} = \langle \psi_{11} | \psi_{22} \rangle$, is negligible. Figure 5.1 plots W in dotted lines and V_{11} and V_{22} by solid curves.

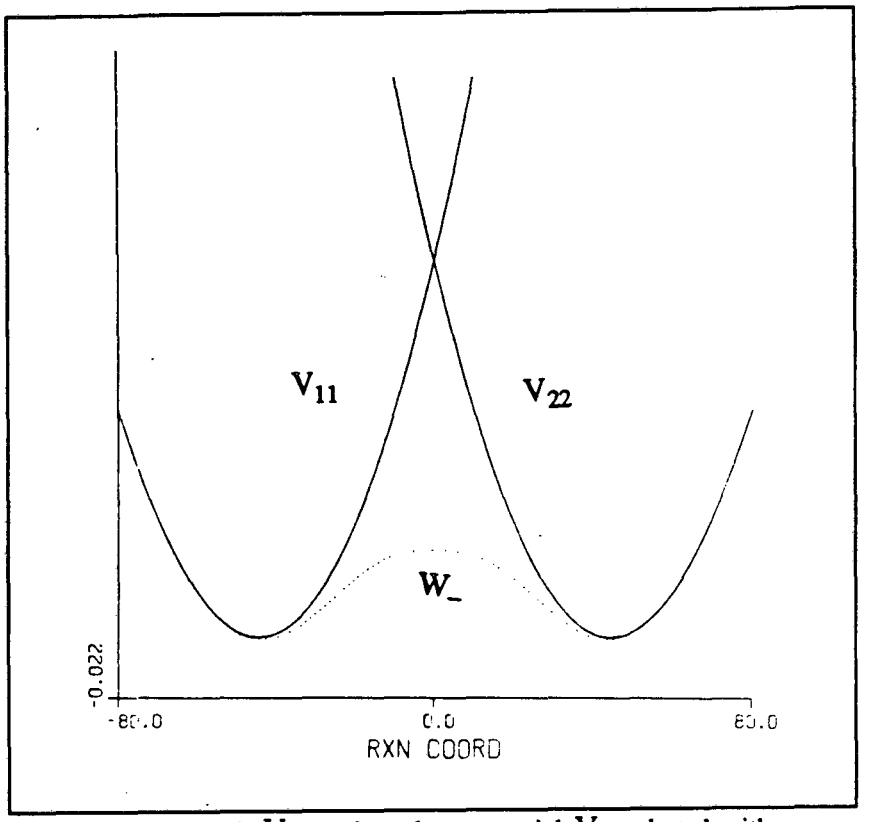

Reactant potential, V_{11} and product potential V_{22} plotted with new approximated adiabatic potential W.

Figure 5.1

As can be seen in Figure 5.1 the lowest surface W_ forms a double-well potential. In order for W to accurately reproduce the adiabatic double well potential of the true system, V_{11}, V_{22}, and V_{12} need to satisfy the following:

1) *At the minimum*: V_{11} and V_{22} approximate the adiabatic potential near their respective minima and V_{12} tends to zero.

2) *At the transition state*: V_{12} gives the accurate barrier height.

Three appropriate forms for V_{11} and V_{22} were mentioned above [e.g., empirical forms, harmonic oscillators, or Morse oscillators]. V_{12}, however, depends upon the choice of V_{11} and V_{22} as well as the system of interest. This dependency is illustrated

by rearranging Equation 5.1 to solve for V_{12}:

$$V_{12}^2 = (V_{11} - W)(V_{22} - W) \tag{5.2}$$

One possible form for V_{12} can be derived by expanding (to second order) the chosen functions of V_{11} and V_{22} and the unknown W about a geometry $q^\dagger$:

$$\begin{aligned} V_{11} &= V_{11}^\dagger(q^\dagger) + D_{11}(q^\dagger)\Delta q + \tfrac{1}{2}\Delta q K_{11}(q^\dagger)\Delta q \\ V_{22} &= V_{22}^\dagger(q^\dagger) + D_{22}(q^\dagger)\Delta q + \tfrac{1}{2}\Delta q K_{22}(q^\dagger)\Delta q \quad . \\ W &= W^\dagger(q^\dagger) + D(q^\dagger)\Delta q + \tfrac{1}{2}\Delta q K(q^\dagger)\Delta q \end{aligned} \tag{5.3}$$

D_{ii} and K_{ii} are the first and second derivatives of V_{ii} respectively, while D contains the first derivatives and K the second derivatives of W. $W^\dagger$, D and K may be determined from *ab initio* calculations. For example, if $q^\dagger$ is the transition state then $W^\dagger$ is the barrier height, $D(q^\dagger)$ is zero, and $K(q^\dagger)$ are the transition state frequencies. V_{12} can now be determined to second order in Δq using Equation 5.2 to give:

$$\begin{aligned} V_{12}^2 &= (V_{11}^\dagger - W^\dagger)(V_{22}^\dagger - W^\dagger) \\ &+ \Delta q\,[V_{11}^\dagger D_{22} + V_{22}^\dagger D_{11} - W^\dagger(D_{11}+D_{22})] \\ &+ \tfrac{1}{2}\Delta q\Delta q\,[2W^\dagger K - W^\dagger(K_{11}+K_{22}) - K(V_{11}^\dagger+V_{22}^\dagger) \\ &\qquad + V_{11}^\dagger K_{22} + V_{22}^\dagger K_{11} + 2D_{11}D_{22}] \\ V_{12}^2 &= A + \Delta q AB + \Delta q(AC + \tfrac{1}{2}ABB)\Delta q \end{aligned} \tag{5.4}$$

if

$$A = (V_{11}^{\dagger} - W^{\dagger})(V_{22}^{\dagger} - W^{\dagger})$$

$$B = \frac{[V_{11}^{\dagger}D_{22} + V_{22}^{\dagger}D_{11} + W^{\dagger}(D_{11}+D_{22})]}{(V_{11}^{\dagger} - W^{\dagger})(V_{22}^{\dagger} - W^{\dagger})}$$

$$AC = K[W^{\dagger} - \tfrac{1}{2}(V_{11}^{\dagger}+V_{22}^{\dagger})] + \tfrac{1}{2}K_{22}(V_{11}^{\dagger}-W^{\dagger}) + \tfrac{1}{2}K_{11}(V_{22}^{\dagger}-W^{\dagger}) - \frac{1}{2A}D_{11}^{2}(V_{22}^{\dagger}-W^{\dagger})^2 - \frac{1}{2A}D_{22}^{2}(V_{11}^{\dagger}-W^{\dagger})^2$$

Equation 5.4 can be factored to resemble a series expansion of an exponential (to second order)

$$V_{12}^2 = A\,[1 + B\Delta q + \Delta q C \Delta q + \tfrac{1}{2}(B\Delta q)^2] \tag{5.5}$$

so that V_{12} becomes

$$V_{12}^2 = Ae^{(B\Delta q + \Delta q C \Delta q)} \tag{5.6}$$

There have not been any restrictions in the dimensionality of the system. V_{11} and V_{22} can be functions of all the internal degrees of freedom of the problem, V_{12} can be a multidimensional exponential and, therefore, W given by Equation 5.1 can represent a global potential energy surface of many dimensions. The accuracy of this global surface is limited by the second order approximation made in Equation 5.3, but its applicability extends to many dimensions.

5.3 Applications

When V_{11} and V_{22} are written as harmonic potentials, $V = \frac{1}{2}m\omega^2(q \pm a)^2$, V_{12} becomes a gaussian that strongly couples the two potentials V_{11} and V_{22} at the transition state while becoming negligible near the minimum values for each.

$$V_{12}(q) = V_{12}^{\dagger} e^{\frac{-q^2}{2V_{12}^{\dagger 2}}\left[K_{11}(\frac{1}{2}\omega^2 a^2 + W^{\dagger}) + KV_{12}^{\dagger}\right]} \tag{5.7}$$

If the transition state forces K are not known, V_{12} can be generated by an iterative process. This procedure is as follows: A constant value for V_{12} is chosen [e.g., $V_{12} = V_{11} - V_{barrier}$] to calculate an expression for W via Equation 5.1 from which an approximation to K can be determined via Equation 5.3; the values for W and K are substituted into Equation 5.7 to yield a new expression for V_{12}; which is used to determine the next value of W to continue the process until V_{12} stops changing.

1-Dimension

Four 1-dimensional potentials were used to test the accuracy of Equation 5.7 and the iterative process outlined above. They are: 1) The straight line potential for malonaldehyde given by Equation 4.31a; 2) Hutchinson's LEPS potential for malonaldehyde (see Appendix 5.1); 3) Janoschek's adapted potential of Equation 3.21; and 4) an empirical potential for malonaldehyde calculated from an Amber/MM2 program[28] (see Appendix 5.1). Figure 5.2 shows the convergence of these iterations for one potential but is representative of all four.

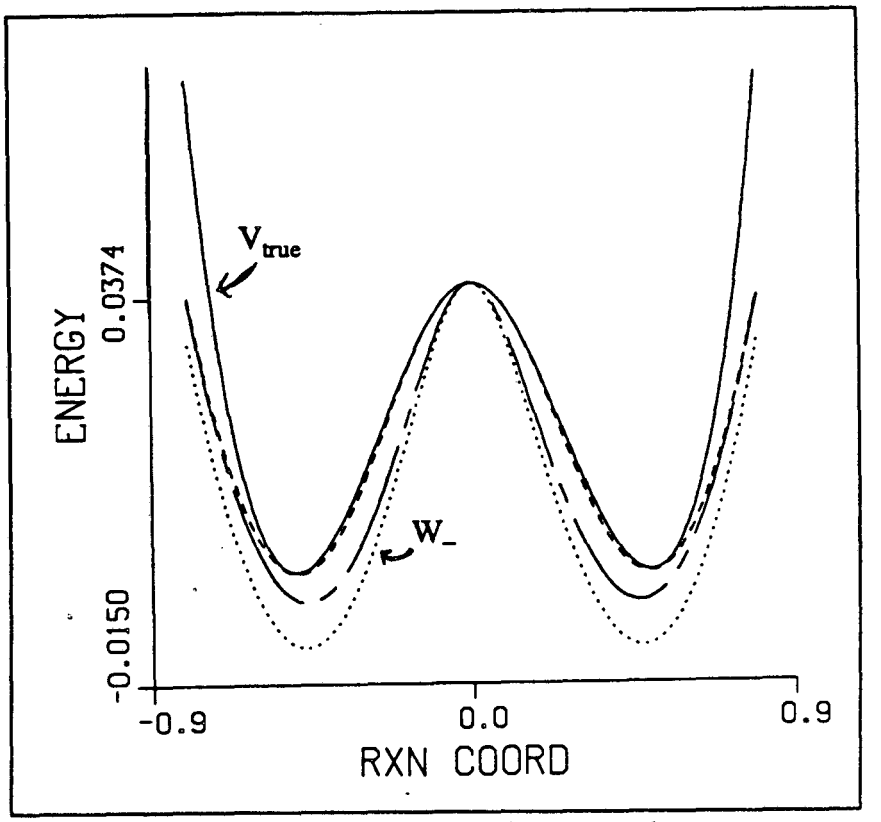

Broken lines show convergence of potential W towards to true potential plotted by the solid line.

Figure 5.2

The optimal width of a gaussian expression for V_{12} calculated by the iterative process is that which is generated by Equation 5.7. Figure 5.2 also reveals that a constant value for V_{12} may be sufficient for qualitative properties with W.

The accuracy of using the harmonic approximation of Equation 5.6 is quite good, as can be seen in Figure 5.3 which plots the four known potentials and their corresponding approximations. The tunneling splitting of the harmonic approximation to the straight line reference potential is 0.037 cm^{-1} and of the empirically determined malonaldehyde potential is 0.039 cm^{-1}. This compares very well with the true 1-dimensional splitting of 0.04 cm^{-1}.

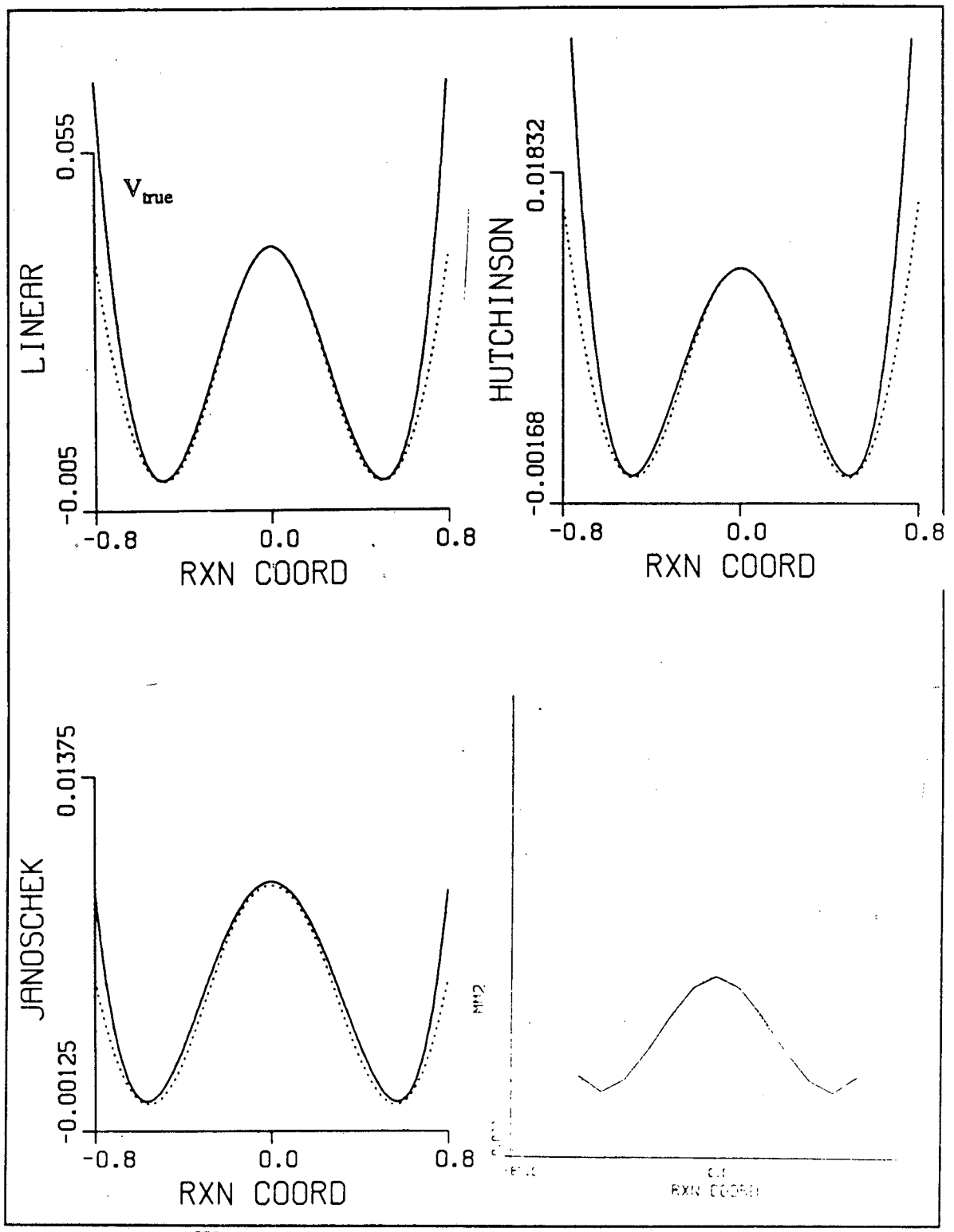

Comparison of W_- (dotted lines) calculated from Eqn. #5.1 with four different potentials V_{true} (solid curve).

Figure #5.3

Extensions

The test cases presented thus far are for 1-dimensional potentials. Below is an example for modeling the 2-dimensional surface plotted in Figure 4.2, reproduced below for convenience.

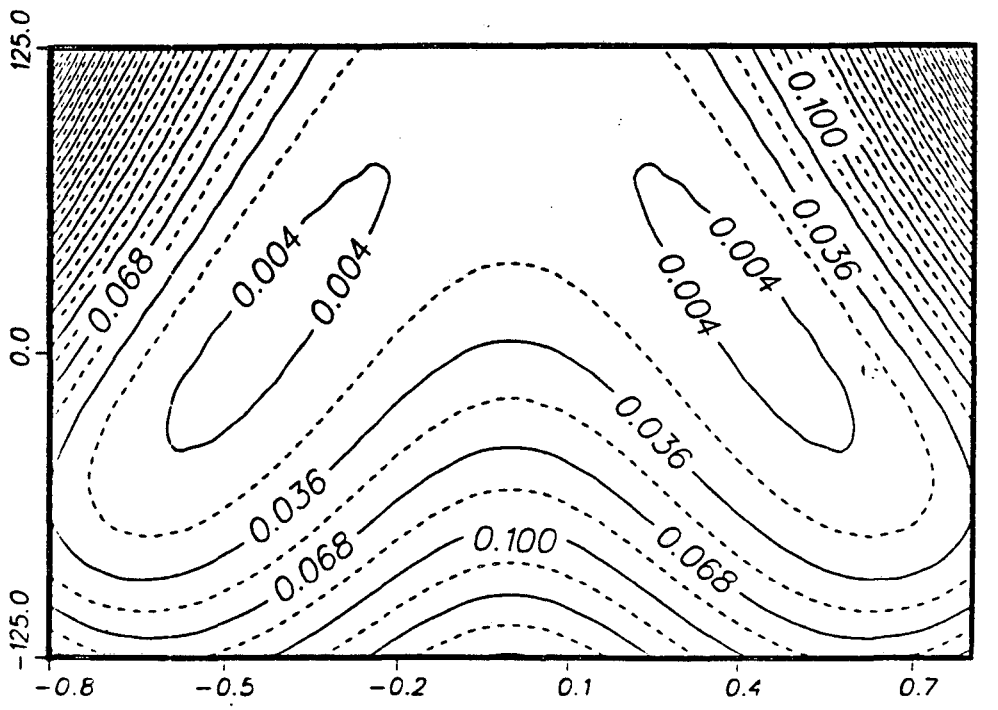

2-dimensional potential for H-atom transfer in malonaldehyde coupled with the O-O stretch vibrational mode.

Figure 5.4

Although one can still use Equation 5.6 for V_{12}, the appropriate coordinates for V_{11} and V_{22} are not the reaction coordinate s and the bath mode Q. Instead, the coupling between s and Q necessitates rotating the coordinate system. The new coordinates (x,y) are the eigenvectors of the diagonalized force constant matrix K at the equilibrium geometry and are written as:

$$
\begin{aligned}
x &= K_{11}(s-s_{eq}) + K_{12}(Q-Q_{eq}) \\
y &= K_{21}(s-s_{eq}) + K_{22}(Q-Q_{eq})
\end{aligned}
$$

or

$$
\begin{aligned}
x_{11} &= \cos\theta\,(s+s_{eq}) - \sin\theta\,(Q-Q_{eq}) \\
y_{11} &= \sin\theta\,(s+s_{eq}) + \cos\theta\,(Q-Q_{eq}) \\
x_{22} &= \cos\theta\,(s-s_{eq}) + \sin\theta\,(Q-Q_{eq}) \\
y_{22} &= -\sin\theta\,(s-s_{eq}) + \cos\theta\,(Q-Q_{eq})
\end{aligned}
\tag{5.8}
$$

where

$$
\begin{aligned}
V_{11} &= \tfrac{1}{2}\omega_x^2 x_{11}^2 + \tfrac{1}{2}\omega_y^2 y_{11}^2 \\
V_{22} &= \tfrac{1}{2}\omega_x^2 x_{22}^2 + \tfrac{1}{2}\omega_y^2 y_{22}^2
\end{aligned}
$$

Figure 5.5 plots the harmonic potentials of V_{11} and V_{22} as a function of the rotated coordinate system (x,y) with θ of Equation 5.8 equal to 12.78°.

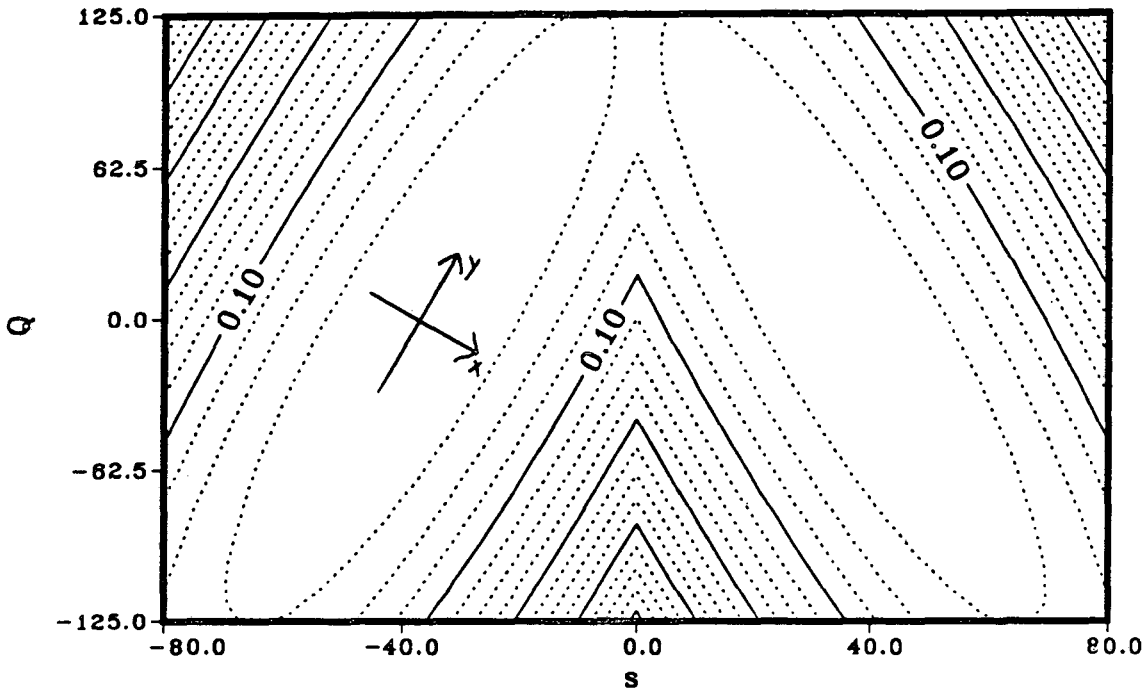

2-dimensional potential of V_{11} and V_{22} for H-atom transfer in malonaldehyde. The appropriate eigenvectors X and Y are the diagonalized eigenvectors at the minima of the reaction coordinate s coupled with the O-O stretch vibrational Q mode.

Figure 5.5

5.4 Summary

This chapter demonstrates the usefulness of the EVB method for approximating polyatomic systems. The input necessary for constructing the potential is simple, and the final potential energy surface has been shown to be accurate for four 1-dimensional double well potentials. An example of a 2-dimensional EVB potential has also been shown to be a highly accurate approximation.

Appendix 5.1

LEPS Potential for Malonaldehyde

$$V = V_{LEPS}(\text{OHOstretch}) + V_{\omega_1} + V_{\omega_2}$$

$$\begin{aligned}
V_{LEPS} &= Q_1 + Q_2 - (J_1^2 + J_2^2 - J_1 J_2)^{1/2} \\
Q_j(S_j) &= \frac{1}{2}\left[{}^2\Pi(S_j) + {}^2\Sigma(S_j)\right] \\
J_j(S_j) &= \frac{1}{2}\left[{}^2\Pi(S_j) - {}^2\Sigma(S_j)\right]
\end{aligned}$$

$$\begin{aligned}
{}^2\Pi(S_j) &= D_{2\pi}\left[e^{-2\alpha^{2\pi}(S_j - S_o^{2\pi})} - 2e^{-\alpha^{2\pi}(S_j - S_o^{2\pi})}\right] \\
{}^2\Sigma(S_j) &= D_{2\Sigma}\left[e^{-2\alpha^{2\pi}(S_j - S_o^{2\pi})} + 2e^{-\alpha^{2\pi}(S_j - S_o^{2\pi})}\right]
\end{aligned}$$

$$\begin{aligned}
V_{\omega_j}(\phi_j, S_j) &= \frac{1}{2} K_{bend}(\phi_j - \phi_o)^2 \chi(S_j) \\
\chi(S_j) &= \frac{1}{2}\left[1 - \tanh(\gamma(S_j - S_c))\right]
\end{aligned}$$

with the following parameters in atomic units:

$D_{2\pi}$	= 0.16875	$D_{2\Sigma}$	= 0.15796
$\alpha^{2\pi}$	= 1.2351	$\alpha^{2\Sigma}$	= 0.935
$S_o^{2\pi}$	= 1.836	$S_o^{2\Sigma}$	= 1.650
K_{bend}	= 0.233	S_c	= 3.5
ϕ_o	= 10.0	R_{O-O}	= 4.42
γ	= 1.815 radian		

Reactant Geometry at MM2 Minima (Angstroms)			
	X	Y	Z
C_1	-0.027	-1.112	0.000
C_2	1.144	-0.457	0.000
C_3	-1.193	-0.422	0.000
O_4	1.300	0.894	0.000
O_5	-1.266	0.787	0.000
H_6	2.087	-1.029	0.000
H_7	-2.113	-1.051	0.000
H_8	-0.035	-2.217	0.000
H_9	0.426	1.335	0.000

Product Geometry at MM2 Minima			
	X	Y	Z
C_1	0.027	-1.112	0.000
C_2	1.193	-0.422	0.000
C_3	-1.144	-0.457	0.000
O_4	1.266	0.787	0.000
O_5	-1.300	0.894	0.000
H_6	2.113	-1.051	0.000
H_7	-2.087	-1.029	0.000
H_8	0.035	-2.217	0.000
H_9	-0.426	1.335	0.00

Transition State on the Linear Path			
	X	Y	Z
C_1	0.000	-1.112	0.000
C_2	1.168	-0.439	0.000
C_3	-1.168	-0.439	0.000
O_4	1.283	0.841	0.000
O_5	-1.283	0.841	0.000
H_6	2.100	-1.040	0.000
H_7	-2.100	-1.040	0.000
H_8	0.000	-2.217	0.000
H_9	0.000	1.335	0.000

Frequencies at MM2 Minimum Geometry		
Frequency (cm-1)	Eigenvalue	
-12.7	-0.058	(Imaginary Frequency)
-7.3	-0.019	(Imaginary Frequency)
-0.5	0.000	(Imaginary Frequency)
-0.3	0.000	(Imaginary Frequency)
0.2	0.000	
9.0	0.029	
115.8	4.760	
328.7	38.345	
427.4	64.824	
455.5	73.607	
614.3	133.891	
693.3	170.560	
846.7	254.339	
1003.7	357.417	
1046.9	388.843	
1103.3	431.887	
1147.1	466.850	
1175.4	490.231	
1242.6	547.865	
1308.7	607.670	
1426.6	722.079	
1735.6	1068.790	
1948.5	1347.089	
2882.9	2948.961	
2901.7	2987.469	
2908.7	3001.912	
3546.0	4461.403	

First Derivative RMS = 3.03907 Kj/Mole

Frequencies at MM2 Transition State Geometry	
Frequency (cm-1)	Eigenvalue
-1015.1	-365.602 (Imaginary Frequency)
-623.3	-137.829 (Imaginary Frequency)
-172.4	-10.549 (Imaginary Frequency)
-0.6	0.000 (Imaginary Frequency)
0.4	0.000
0.7	0.000
221.2	17.361
376.9	50.392
507.4	91.346
605.7	130.173
762.1	206.088
831.9	245.555
1018.8	368.274
1048.6	390.161
1079.3	413.280
1152.4	471.210
1209.4	518.964
1262.7	565.964
1297.8	597.616
1345.5	642.369
1700.1	1025.529
1909.1	1293.123
2377.5	2005.530
2849.7	2881.374
2890.3	2963.959
2946.5	3080.493
7854.4	21889.2332

Frequencies at MM2 Transition State STO-3G Geometry		
Frequency (cm-1)		Eigenvalue
-1821.5	-1177.282	(Imaginary Frequency)
-1329.7	-627.375	(Imaginary Frequency)
-103.3	-3.783	(Imaginary Frequency)
-0.7	0.000	(Imaginary Frequency)
0.0	0.000	
0.7	0.000	
2908.7	3001.912	
234.7	19.550	
337.3	40.363	
545.5	105.565	
626.6	139.303	
713.7	180.713	
746.4	197.694	
875.6	272.016	
930.6	307.280	
997.0	352.681	
1028.2	375.078	
1098.6	428.212	
1199.5	510.539	
1260.3	563.529	
1276.3	577.951	
1511.6	810.731	
1570.8	875.487	
1756.3	1094.503	
2947.1	3081.663	
3038.5	3275.723	
3106.8	3424.692	
10034.4	35725.938	

First Derivative RMS =1765.09863 Kj/Mole

MM2 Potential Values for V_{11}		
Rxn Coord	MM2 min	STO-3G min
-80.0	72.73	148.73
-75.0	50.96	112.73
-70.0	33.78	83.13
-65.0	20.52	58.83
-60.0	10.88	39.62
-55.0	4.51	24.88
-50.0	1.01	14.26
-45.0	0.00	7.47
-40.0	1.07	0.00
-35.0	3.79	0.07
-30.0	7.90	2.60
-25.0	19.25	7.29
-20.0	30.79	19.52
-15.0	45.65	34.33
-10.0	65.05	54.54
-5.0	89.44	83.59
-0.0	121.42	123.00
5.0	164.07	179.66
10.0	222.39	267.48
15.0	307.69	398.01
20.0	432.88	610.55
25.0	626.74	951.25
30.0	935.33	1540.85
35.0	1457.31	2582.50
40.0	2328.12	4407.04
45.0	3849.66	7805.53
50.0	6589.36	14138.73
55.0	11557.41	23901.88
60.0	20852.45	24000.00
65.0	23901.88	24000.00
70.0	24000.00	24000.00
75.0	24000.00	24000.00
80.0	24000.00	24000.00

W calculated for $V_{barrier}$ = 20 kcal mol^{-1}	
Rxn Coord	W
-80.0	72.3001210029797221
-75.0	50.5305117547577538
-70.0	33.3508196190632589
-65.0	20.0892946248513908
-60.0	10.3864780599005826
-55.0	3.61972803011940414
-50.0	-0.550873253498707527
-45.0	-2.67007640077673614
-40.0	-3.34183101869854227
-35.0	-3.25250287458140974
-30.0	-3.06132851238749026
-25.0	2.76533140260096388
-20.0	6.65705336667623726
-15.0	10.9827765185257284
-10.0	15.3650837521211265
-5.0	18.6882389214889102
-0.0	20.0000000000000000
5.0	18.6882389214889102
10.0	15.3650837521211265
15.0	10.9827765185257284
20.0	6.65705336667623726
25.0	2.76533140260096388
30.0	-3.06132851238749026
35.0	-3.25250287458140974
40.0	-3.34183101869854227
45.0	-2.67007640077673614
50.0	-0.550873253498707527
55.0	3.61972803011940414
60.0	10.3864780599005826
65.0	20.0892946248513908
70.0	33.3508196190632589
75.0	50.5305117547577538
80.0	72.3001210029797221

Chapter 6

DENSITY MATRIX TUNNELING SPLITTINGS

6.1 Introduction

As was mentioned in Chapters 3 and 4, a rigorous method for including many degrees of freedom is to use Feynman path integrals. We present here the formalism of how to use path integrals in molecular dynamics problems, specifically for calculating tunneling splittings. First, the relation between density matrices for a polyatomic system and the splitting of the lowest two energy levels of a symmetric potential is presented in Section 2. Section 3 then combines the use of path integration techniques and statistical Monte Carlo techniques in the evaluation of the multidimensional integrals resulting from Section 2. The result is the use of traditional statistical concepts and techniques for calculating dynamical tunneling rates or splittings. Section 4 illustrates these ideas to determine the tunneling splitting of malonaldehyde.

6.2 Density Matrices

Ceperly and Jacucci[29] relate the density matrix of the crystal ^{3}He system to the frequency with which it oscillates between two arrangements (of N atoms exchanging at various lattice sites). In a similar fashion, one can relate the two lowest energy levels of a symmetric potential to the diagonal and off diagonal density matrix elements of the system.

A density matrix is analogous to a propagator in imaginary time, as can be seen by comparing Equation 6.1 to the real time propagator Equation 6.2 and setting $\beta \equiv \frac{1}{kT}$ to be $\beta = \frac{it}{\hbar}$.

$$\begin{aligned} \frac{\int dr \langle r | e^{-\beta H} f | r \rangle}{\int dr \langle r | e^{-\beta H} | r \rangle} &= \text{Thermal average of f} \\ \langle r | e^{-\beta H} | r \rangle &= \text{Diagonal density matrix} \end{aligned} \tag{6.1a}$$

$$\begin{aligned} \psi(t) &= \langle r | e^{\frac{-iHt}{\hbar}} | 0 \rangle \\ \psi(t) &= \int dr' \langle r | e^{\frac{-iHt}{\hbar}} | r' \rangle \langle r' | 0 \rangle \\ \langle r | e^{\frac{-iHt}{\hbar}} | r' \rangle &= \text{Real time propagation amplitude} \\ &\quad \text{from state } r' \text{ to } r \text{ in time } t \end{aligned} \tag{6.1b}$$

If the coordinate representation of the density matrix of a Hamiltonian H is written as a linear combination of eigenstates of the system

$$\begin{aligned} \langle r' | e^{-\beta H} | r \rangle &= \sum_{m,n} \langle r' | m \rangle \langle m | e^{-\beta H} | n \rangle \langle n | r \rangle \\ &= \sum_{m,n} e^{-\beta E_n} \langle r' | m \rangle \langle m | n \rangle \langle n | r \rangle \\ &= \sum_{m} e^{-\beta E_m} \phi_m^*(r') \phi_m(r) \end{aligned} \tag{6.2}$$

then the ratio of the off diagonal density matrix to the diagonal can be expanded as:

$$\text{Ratio} = \frac{\langle -r|e^{-\beta H}|r\rangle}{\langle r|e^{-\beta H}|r\rangle} = \frac{\sum_n e^{-\beta E_n}\phi_n^*(-r)\phi_n(r)}{\sum_n e^{-\beta E_n}\phi_n^2(r)} \tag{6.3a}$$

For a symmetric potential $\phi_n(-r) = (-1)^n\phi_n(r)$. Therefore, Equation 6.3a becomes

$$\text{Ratio} = \frac{e^{-\beta E_0}\phi_0^2\left[1 - e^{-\beta\Delta E_{01}}\left(\frac{\phi_1}{\phi_0}\right)^2 + e^{-\beta\Delta E_{12}}\left(\frac{\phi_2}{\phi_0}\right)^2 - \cdots\right]}{e^{-\beta E_0}\phi_0^2\left[1 + e^{-\beta\Delta E_{01}}\left(\frac{\phi_1}{\phi_0}\right)^2 + e^{-\beta\Delta E_{12}}\left(\frac{\phi_2}{\phi_0}\right)^2 + \cdots\right]} \tag{6.3b}$$

and if the lowest energy splitting $\Delta E_{01} \equiv E_1 - E_0$ is much smaller than ΔE_{12}

$$\begin{aligned}
\text{Ratio} &= \frac{e^{(x+\frac{\beta}{2}\Delta E_{01})} - e^{-(x+\frac{\beta}{2}\Delta E_{01})}}{e^{(x+\frac{\beta}{2}\Delta E_{01})} + e^{-(x+\frac{\beta}{2}\Delta E_{01})}} \\
&= \tanh(x + \frac{\beta}{2}\Delta E_{01}) \\
\tanh^{-1}(\text{Ratio}) &= x + \frac{\beta}{2}\Delta E_{01} + \cdots \\
\text{where } e^{-x} &\equiv \left(\frac{\phi_1}{\phi_0}\right)
\end{aligned} \tag{6.3c}$$

One restriction has been made to obtain the above expression for the density ratio in terms of the splitting:

$$e^{\beta\Delta E_{01}} \gg e^{\beta\Delta E_{12}} \tag{6.3d}$$

This inequality assures that the summation of Equation 6.3b converges after the first two elements. The result is:

$$\tanh^{-1}(\text{Ratio}) = \frac{<-r|e^{-\beta H}|r>}{<r|e^{-\beta H}|r>} = x + \frac{\beta}{2}\Delta E_{01} \tag{6.3e}$$

Equation 6.3e gives a prescription for finding the lowest energy splitting for a symmetric potential: ΔE_{01} is the slope of the inverse hyperbolic tangent of the density ratio plotted as a function of beta.

6.3 Multidimensional Integrals

Discretization

Density matrices can be evaluated by inserting N-1 complete sets of states

$$<r'|e^{-\beta H}|r> = \int dx_1 \cdots \int dx_{N-1} <r'|e^{-\frac{\beta H}{N}}|x_1>$$

$$\cdot <x_1|e^{-\frac{\beta H}{N}}|x_2> \cdots <x_{N-1}|e^{-\frac{\beta H}{N}}|r> \tag{6.4}$$

and evaluating the discretized term to first order in β with a small time approximation

($\frac{\beta}{N} \to 0$) (we use the expression for the average potential resulting from the Trapezoidal rule)

$$
\begin{aligned}
<x_i|e^{-\frac{\beta H}{N}}|x_j> &= <x_i|e^{-\frac{\beta T}{N}} e^{-\frac{\beta V}{N}} e^{-O\frac{\beta^2[T,V]}{N}}|x_j> \\
&= \int dx_o <x_i|e^{-\frac{\beta T}{N}}|x_o><x_o|e^{-\frac{\beta V}{N}}|x_j> \\
&= \int dx_o \int dp <x_i|e^{-\frac{\beta}{N}\frac{p^2}{2m}}|p><p|x_o><x_o|e^{-\frac{\beta V}{N}}|x_j> \qquad (6.5) \\
&= \int dx_o \sqrt{\frac{m}{2\pi\beta h^2}} e^{\frac{-mN}{2\beta h^2}(x_o-x_i)^2} <x_o|e^{-\frac{\beta V}{N}}|x_j> \\
&= \sqrt{\frac{m}{2\pi\beta h^2}} e^{\frac{-mN}{2\beta h^2}(x_j-x_i)^2} e^{-\frac{\beta}{2N}[V(x_i)+V(x_j)]}
\end{aligned}
$$

The result is

$$
<r'|e^{-\beta H}|r> = \left[\frac{m}{2\pi\beta h^2}\right]^{\frac{N}{2}} \int\int dx_1 \cdots dx_{N-1}
$$

$$
\cdot e^{-[\sum_{i=1}^{N}\frac{mN}{2h^2\beta}(x_i-x_{i+1})^2+\sum_{i=1}^{N}\frac{\beta}{2N}(V(x_i)+V(x_{i+1}))]} \qquad (6.6a)
$$

The kinetic energy piece of Equation 6.6a can be diagonalized to give

$$
<r'|e^{-\beta H}|r> = <r'|e^{-\beta T}|r> \cdot \frac{\int da_1 \cdots da_{N-1}\, e^{-[\sum_{k=1}^{N-1}\frac{a_k}{2} + \sum_{i=1}^{N}\frac{\beta}{2N}[V(q(s_i))-V(q(s_{i+1}))]]}}{\int da_1 \cdots da_{N-1}\, e^{-\sum_{k=1}^{N-1}\frac{a_k^2}{2}}}
$$

$$q(s_j) = r' + (r-r')(\frac{js}{\beta N}) + \sum_{k=1}^{N-1} a_k \sigma_k \sin(\frac{jk\pi s}{\beta N})$$
$$\sigma_k = \sqrt{\frac{2h^2\beta}{m}} \frac{1}{2N\sin(\frac{k\pi}{2N})} \tag{6.6b}$$

Equation 6.6b is analogous to summing over normal mode excitations where a free particle reference has been factored in front for convenience. Either of the forms for Equation 6.6 is valid. Sometimes Equation 6.6b may prove valuable for large β when domination of Equation 6.6a by the potential term leads to problems in the evaluation of the integral. We use Equation 6.6b to assist in optimizing the stepsize needed to evaluate the integral by Monte Carlo methods, as reported in Section 6.3 below.

This is equivalent to performing a Fourier path integral[30] because integrating over all points in Equation 6 is equivalent to summing over all paths between the endpoints (r,r′), The density matrices needed for Equation 6.3 are now expressed as a multidimensional integral of exponents as given by Equation 6.6 and can be evaluated with a process called *the charging algorithm.*

Charging Algorithm

The name of this method arises because it adds a perturbation to a reference Hamiltonian to yield the final Hamiltonian, i.e., it "charges up" the reference system to reach the true one. The procedure to determine any integral of the form

$$I \equiv \int dx e^{-\beta H} \tag{6.7}$$

is to separate the Hamiltonian into a known reference part H_o plus a perturbation term λH_1, to define a function

$$I(\lambda) \equiv \int dx\, e^{-\beta(H_o+\lambda H_1)}$$

and to note that

$$\frac{1}{I}\frac{dI}{d\lambda} = \frac{\int dx\,[\beta H_1] e^{-\beta(H_o+\lambda H_1)}}{\int dx\, e^{-\beta(H_o+\lambda H_1)}}$$
$$\equiv <\beta H_1>_\lambda$$

Integrating the above equation gives

$$\int_0^1 d\ln I(\lambda) = \int_0^1 d\lambda <\beta H_1>_\lambda$$
$$I(1) = I(0)\, e^{\beta\int_0^1 <H_1>_\lambda d\lambda} \tag{6.8}$$
$$I(0) = \int dx\, e^{-\beta H_o}$$

where I(0) is known for the reference Hamiltonian H_o. I(1) is the solution to Equation 6.7 and can be determined if $\int_0^1 <\beta H_1>_\lambda d\lambda$ is known. Therefore, the problem of solving for I has been transformed into solving the definite integral over $d\lambda$ given by Equation 6.8.

To solve for the density matrices of Equation 6.3 and 6.7, we rewrite Equation 6.6 as

$$<r'|e^{-\beta H}|r> = A\int\int dx e^{-\beta H(x)}$$

and use the charging algorithm to solve for

$$<r'|e^{-\beta H}|r> = I(0)\, e^{\beta\int_0^1 <H_1>_\lambda} d\lambda \tag{6.9}$$

where

$$\begin{aligned} I(0) &= <r'|e^{-\beta H_o}|r> \\ <H_1>_\lambda &= \frac{\int\int dx\, H_1(x) e^{-\beta(H_o+\lambda H_1)}}{\int\int dx e^{-\beta(H_o+\lambda H_1)}} \end{aligned} \tag{6.10}$$

Thus, the density matrices can be determined by evaluating the integral of the average of H_1 weighted by λ over the range λ=(0,1). A reference Hamiltonian needs to be known to evaluate I(0). This may simply be the free particle reference for which an analytic expression for the density matrix is known, or it can be part of the Hamiltonian for which some information is already known.

Monte Carlo Path Integration

The Monte Carlo path integral method[31] is used to evaluate Equation 6.9 by making N of Equation 6.6 large enough to validate the small time approximation (which gives a large multidimensional integral). Metropolis sampling is used to generate the paths over **dx** with the appropriate distribution probability of $e^{-\beta(H_o+\lambda H_1)}$. These appropriately distributed paths are generated by forming a Markov chain by constructing

a random walk whose conditional probability of going from one point to the next is dependent only on that time step. M different chains are constructed $H_1(x)$ is evaluated along each path, and the final value for Equation 6.10 is

$$
\begin{aligned}
<H_1>_\lambda &= \frac{\int dx\,(H_1)e^{-\beta(H_o+\lambda H_1)}}{\int dx\, e^{-\beta(H_o+\lambda H_1)}} \\
&= \frac{1}{M}\sum_{i=1}^{M}{}' H_1(x_i) \pm \frac{1}{M}\left[<H_1^2> - <H_1>^2\right]^{1/2}
\end{aligned}
\tag{6.11}
$$

The prime in the summation indicates that the sum is over accepted paths defined below. The construction of appropriately weighted paths has been outlined in Reference 31, and will briefly be described here: A path is chosen. A new path $\{x_i\}$ with a small deviation from the previous path is calculated. The value of $H_o+\lambda H_1$ at $\{x_i\}$ is compared to that for the previous path. If the new value is less than the preceding one, the new value of $H_1(x_i)$ is added to the sum of Equation 6.11 and the path $\{x_i\}$ is accepted as the reference from which the next path will be a small deviation. If, however, the new value is not smaller than the preceding value then one needs to perform a second criteria test: If the new value is smaller than a random number the new value is added and the new path is accepted. Otherwise the preceding value is added instead, the new path is rejected, and the preceding path is retained from which to form the next possible path. This ensures that paths of low energy are included but does not prevent other paths from being explored. One chooses step sizes of the coordinates x that give an acceptance rate of nearly 50 percent, and varies M until Equation 6.11 converges. It should be noted that if β is large so that there is little kinetic energy contribution to the value of $H_o+\lambda H_1$ then the choice of paths might remain

confined to a low energy region of the potential and the calculation would not contain a statistical averaging. One needs to monitor the paths to be sure that different regions of the potential are being sampled (although not necessarily accepted very often).

6.4 Application

The accuracy of Equation 6.3e is tested for the diabatic linear reference hamiltonian of malonaldehyde given by Equation 4.31. We first need to know if the previously mentioned restriction is met i.e., if the tunneling splitting is much less than ΔE_{12} such that the two-level approximation of Equation 6.3b is satisfied.

We begin with the 1-dimensional potential for the isomerization of malonaldehyde (Equation 4.1). The tunneling splitting ΔE_{01} is 0.043 cm^{-1} while ΔE_{12} is 2785 cm^{-1} so $\Delta E_{01} \ll \Delta E_{12}$ and Equation 6.3c should be satisfied. In order to test this we confirmed that convergence of Equation 6.3b is met after only two eigenstates are added. Table 6.1 also shows the values for the density matrix as a function of β, their ratios, and the value for ΔE_{01} as calculated by Equation 6.3e for several values of β.

TABLE 6.1

β	diagonal	off diagonal	$\tanh^{-1}$(Ratio)	ΔE_{01}
600	1.745e-2	3.477e-4	0.01993	
1000	1.240e-3	2.476e-5	0.01997	0.043
2000	1.668e-6	3.348e-8	0.02017	0.043
5000	4.066e-15	8.280e-17	0.02036	0.043
9000	1.334e-26	2.768e-24	0.02075	0.043

Density matrix calculations for 1-dimensional potential $H=T_s+V_s$

Although performing a Monte Carlo path integral for a 1-dimensional potential is not necessary, we did so to examine how well the tunneling splitting could be determined. The path integration method gave a tunneling splitting of 0.04 cm^{-1}.

The next step is to include the bath modes of the problem. We first include the O-O stretch mode, which is most strongly coupled to the reaction coordinate (cf. Section 4.5). The tunneling splitting for this system is 11.8 cm^{-1}. Using basis set calculated density matrices, we examine the restriction of Equation 6.3c. Convergence for the summation given by Equation 6.3b occurs for the first two eigenstates only for a value of β greater than 8000. Below that value, the two-level approximation breaks down. Therefore, the first condition is met for β >8000. Table 6.2 supports this fact. The fifth column of Table 6.2 indicates that a linear plot of Equation 6.3c occurs at β above 8000. The density matrix method is able to calculate the correct splitting, but with a restricted region of beta values for which Equation 6.3e is valid.

TABLE 6.2

β	diagonal	off diagonal	$\tanh^{-1}$(Ratio)	ΔE_{01}
4000	4.165e-13	1.104e-14	0.02851	
7000	8.614e-23	7.921e-24	0.09222	9.61
8000	5.125e-26	6.008e-27	0.1177	11.18
9000	3.053e-29	4.370e-30	0.1441	11.58
10000	1.821e-32	3.083e-33	0.1709	11.71

Density matrix for 2-dimensional potential with O-O stretch

As was mentioned at the end of Section 6.5, one would like to sample different regions of the potential. Figure 6.1 plots four Monte Carlo paths on the 2-dimensional potential for malonaldehyde.

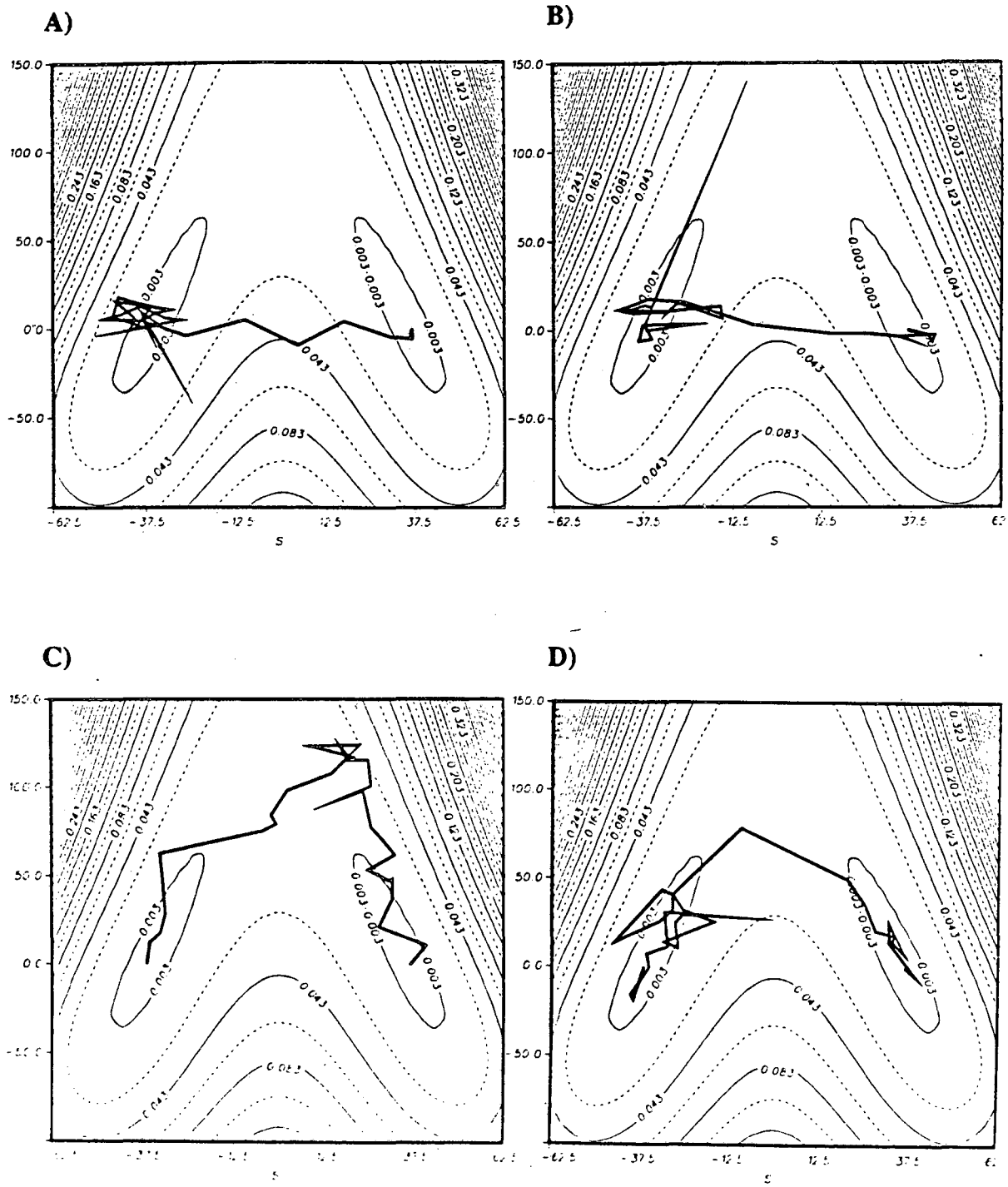

Monte Carlo paths generated for integrating Eqn. #6.11 for off diagonal matrix. Paths A and B travel straight across a high barrier. Paths C and D explore lower energy regions of the potential.

Figure 6.1

The paths were generated during the evaluation of the off diagonal density matrix element. Figure 6.1a and 6.1b plot paths that travel nearly straight across a high barrier from one well to another. Figure 6.1c and 6.1d illustrate paths that sample lower regions of the potential. These generated paths depend upon the probability distribution $e^{-\beta H_o+\lambda H_1}$ so paths similar to Figure 6.1c 6.1d occur much more frequently for values of $\lambda = 1$ than for $\lambda = 0$. This occurs because the coupling is included in the weighting of paths with $\lambda = 1$. These paths will, therefore, also depend upon the choice of reference Hamiltonian. These plots were generated using the 1-dimensional Hamiltonian as the reference H_o. Equation 6.9 becomes

$$<r'|e^{-\beta H}|r> = <r'|e^{-\beta(T_s+V_s+T_Q)}|r> \cdot e^{\beta\int_0^1 <V_Q> d\lambda} \tag{6.12}$$

The solution to the 2-dimensional problem can then be used to include another bath mode, and each mode can be added sequentially.

An alternative to adding bath modes successively is to define the reference Hamiltonian as the adiabatic Hamiltonian (cf. Section 2.4). Then one can add as many degrees of freedom at a time as are desired.

$$<r'|e^{-\beta H}|r> = <r'|e^{-\beta H_{adiab}}|r> e^{\int_0^1 <H-H_{adiab}> d\lambda} \tag{6.13}$$

6.5 Concluding Remarks

It is shown how one can determine the two lowest energy levels of a symmetric potential by calculating the ratio of the off diagonal density matrix element to the diagonal element. The density matrix elements are calculated by approximating them as the product of many discretized portions and evaluating each portion by the small time (high Temperature) limit. One can evaluate the resulting multidimensional integral by combining the charging algorithm with Monte Carlo path integral techniques. These techniques are applied to the isomerization reaction of malonaldehyde.

References

1. For early work on reaction paths and reaction coordinates see
   (a) R. A. Marcus, *J. Chem. Phys.* **45**, 4493, (1968); *J. Chem. Phys.* **45**, 4500 (1968). **49**, 2610 (1968).
   (b) S. Glasstone, K. J., Laidler, and H. Eyring, *The Theory of Rate Processes*, (McGraw-Hill, New York, 1941).
   (c) G. L. Hofacker, *Z. Naturforsch. Teil A* **18**, 607 (1963); *J. Chem. Phys.* **43**, 208 (1965); S. F. Fischer, G. L. Hofacker, and R. Seiler, *J. Chem. Phys.* **51**, 3941 (1969).
   (d) K. Fukui, S. Kato, and H. Fujimoto, *J. Am Chem. Soc.* **97**, 1 (1975); K. Yamashita, T. Yamabe, and K. Fukui, *Chem. Phys. Lett.* **84**, 123 (1981); A. K. Fukui, *Acc. Chem. Res.* **14**, 363 (1981).

2. W. H. Miller, N. C. Handy, and J. E. Adams, *J. Chem. Phys.* **72**, 99 (1980).

3. For applications of the reaction path see:
   (a) W. H. Miller, in *Tunneling*, eds. J. Jortner and B. Pullman, (D. Reidel, Boston, 1986), pp. 91-101.
   (b) W. H. Miller, in *Potential Energy Surfaces and Dynamics Calculations*, ed. D. G. Truhlar (Plenum Press, New York, 1981), p. 265.
   (c) W. H. Miller, in *The Theory of Chemical Reaction Dynamics*, ed. D.C. Clary (D. Reidel, Dordrecht, 1986), p.27.
   (d) W. H. Miller, *J. Phys. Chem.* **87**, 3811 (1983).

(e) S. K. Gray, W. H. Miller, Y. Yamaguchi and H.F. Schaefer, *J. Chem. Phys.* **73**, 2733 (1980); S. K. Gray, W. H. Miller, Y. Yamaguchi and H.F. Schaefer, *J. Am. Chem. Soc.* **103**, 1900 (1981); Y. Osamura, H. F. Schaefer, S. K. Gray and W. H. Miller, *J. Am. Chem. Soc.* **103**, 1904 (1981).

(f) W. H. Miller and S-H Shi, *J. Chem Phys.* **75**, 2258 (1981); C. J. Cerjan, S-H. Shi and W. H. Miller, *J. Phys. Chem.* **86**, 2244 (1982).

(g) W. H. Miller and S. Schwartz, *J. Chem. Phys.* **77**, 2378 (1982).

(h) B. A. Waite, S. K. Gray and W. H. Miller, *J. Chem. Phys.* **78**, 259 (1983).

(i) P. Russegger and J. Brickman, *J. Chem. Phys.* **62**, 1086 (1975); **60**, 1 (1977).

(j) M. V. Basilevsky, *Chem. Phys.* **24**, 81 (1977); **67**, 337 (1982); M. V. Basilevsky and A. G. Shamov, *Chem. Phys.* **60**, 349 (1981).

(k) X. Chapuisat, A. Nauts, and G. Durrand, *Chem. Phys.* **56**, 91 (1981); A. Nauts and X. Chapuisat, *Chem. Phys. Lett.* **85**, 212 (1982).

(l) G. A. Natanson, *Mol. Phys.* **46**, 481 (1982).

(m) S. F. Fischer and M. A. Ratner, *J. Chem. Phys.* **57**, 2769 (1972).

(n) J. Pancir, *Collect. Czech. Commun.* **40**, 1112 (1975); **42**, 16 (1977).

(o) K. Ishida, K. Morokuma, and A. Komornicki, *J. Chem. Phys.* **66**, 2153 (1977).

(p) M. Page and J. W. McIver, Jr., *J. Chem. Phys.* **88**, 922 (1988).

(q) T. H. Dunning, Jr.,and L. Harding, *Faraday Disc. Chem. Soc.* in press (1988)

(r) B. C. Garret, M. J. Redmon, R. Steckler, D. G. Truhlar, K. K. Baldridge, D. Bartol, M. W. Schmidt, and M. S. Gordon, *J. Phys. Chem.*

92, 1476 (1988).

4. For examples of corner cutting (H-L-H) see:
   (a) T. F. George and W. H. Miller, *J. Chem. Phys.* **56**, 5722 (1972); **57**, 2458 (1972).
   (b) B.C. Garrett, D.G. Truhlar, A.F. Wagner, and T.H. Dunning, Jr., *J. Chem. Phys.* **45**, 120 (1973).
   (c) J. Manz and J. Romelt, *Chem. Phys. Lett.* **81**, 179 (1981).
   (d) J. A. Kaye and A. Kuppermann, *Chem. Phys. Lett.* **77**, 573 (1981); **78**, 546 (1981).
   (e) V. K. Babamov and R. A. Marcus, *J. Chem. Phys.* **74**, 1790 (1981).
   (f) C. Hiller, J. Manz, W. H. Miller, and J. Romelt, *J. Chem. Phys.* **78**, 3850 (1983).

5. T. Carrington, Jr., and W. H. Miller, *J. Chem. Phys.* **81**, 3573 (1984); T. Carrington, Jr. and W. H. Miller, *J. Chem. Phys.* **84**, 4364 (1986).

6. For further applications see:
   (a) R. T. Skodje, D. G. Truhlar, and B. C. Garrett, *J. Phys. Chem.* **85**, 3019 (1981); R. T. Skodje, D. G. Truhlar, and B. C. Garrett, *J. Chem. Phys.* **77**, 5955 (1982); R. T. Skodje and D. G. Truhlar, and B. C. Garrett, *J. Phys. Chem.* **88**, 628 (1984).
   (b) A. D. Isaacson and D. G. Truhlar, *J. Chem. Phys.* **76**, 1380 (1982).
   (c) D. G. Truhlar, N. J. Kilpatrick, and B. C. Garrett, *J. Chem. Phys.* **78**, 2438 (1983).
   (d) B. C. Garrett and D. G. Truhlar, *J. Chem. Phys.* **81**, 309 (1984).

7. Theoretical papers on vinylidene:

(a) M. P. Conrad and H. F. Schaefer III, *J. Am. Chem. Soc.* **100,** 7820 (1978).

(b) C. E. Dykstra and H. F. Schaefer III, *J. Am. Chem. Soc.* **100,** 1378 (1978).

(c) Osamura, H. F. Schaefer III, S. K. Gray, and W. H. Miller, *J. Am. Chem. Soc.* **103,** 1904 (1981); Y. Osamura and H. F. Schaefer III, *Chem. Phys. Lett.* **79,** 412 (1981).

(d) L. B. Harding, *J. Am. Chem. Soc.* **103,** 7469 (1981).

(e) P. Rosmus, P. Botschwina and J. P. Moier, *Chem. Phys. Lett.* **84,** 71 (1981).

(f) G. Frenking, *Chem. Phys. Lett.* **100,** 484 (1983).

(g) K. A. White and G. C. Shatz, *J. Phys. Chem.* **88,** 2049 (1984).

8. R. Krishnan, M. J. Frisch, J. A. Pople , P von R Schleyer, *Chem. Phys. Lett.* **79,** 408 (1981).

9. For experimental work on vinylidene and its derivatives, see:

(a) P. S. Skell and J. H. Planda, *J. Am. Chem. Soc.* **92,** 5620 (1970); P. S. Skell, F. A. Fagone, H. J. Klabundre, *J. Am. Chem. Soc.* **94,** 7862 (1972); P. S. Skell, J. J. Havel, M. J. McGlinchey, *Accts. Chem. Res.* **6,** 97 (1973).

(b) P. J. Stang, *Accts. Chem. Res.* **11,** 107 (1978).

(c) C. Reiser, F. M. Lussier, C. C. Jensen and J. I. Steinfeld, *J. Am. Chem. Soc.* **101,** 350 (1979); C. Reiser and J. I Steinfeld, *J. Phys. Chem.* **84,** 680 (1980).

(d) A. H. Laufer, *J. Chem. Phys.* **73,** 49 (1980); *J. Chem. Phys.* **76,** 945 (1982); *Chem. Phys. Lett.* **94,** 240 (1983); *J. Photochem* **27**, 267 (1984); A. H. Laufer and Y. L. Yung, *J. Phys. Chem.* **87**, 181 (1983).

(e) P. H. Dasae, *J. Phys. Chem.* **86,** 4092 (1982), **18**, 607 (1983).

(f) J. L. Holmes and J. E. Szulejko, *Chem. Phys. Lett.* **107**, 301 (1984); **51**, 3941.

(g) E. Abramson, R. W. Field, D. Inne, K. K. Innes, and J. L. Kinsey, *J. Chem. Phys.* **80** 2298 (1984); Y. Chen, D. M. Jonas, J. L. Kinsey, and R. W. Field, *J. Chem. Phys.* **91** 3976 (1989).

10. M. Burnett, A. E. Stevens, C. S. Feigrle, and W. C. Lineberger, *Chem. Phys. Lett.* **100,** 124 (1983).

11. T. Carrington, Jr., L.M. Hubbard, H.F. Schaefer III, and W. H. Miller, *J. Chem. Phys.*, **80**, 4347 (1984).

12. For Transformations & action-angle variables see: H. Goldstein, in *Classical Mechanics*, (Addison-Wesley, Reading, MA, 1950), pp. 237 *et seq.*

13. G. Herzberger, *Molecular Spectroscopy and Molecular Structure*, (Prentice Hall, New York: 1939-1966).

14. For papers on malonaldehyde see:

(a) W. F. Rowe, R. W. Duerst and E. B. Wilson, *J. Am. Chem. Soc.* **98**, 4021 (1976); S. L. Baughcum, R. W. Duerst, W. F. Rowe, A. Smith

and E. B. Wilson, *J. Am. Chem. Soc.* **103**, 6296 (1981); Z. Smith, E. B. Wilson and R. W. Duerst, *Spectrochim. Acta. Part A* **39**, 1117 (1983); S. L. Baughcum, Z. Smith, E. B. Wilson and R. W. Duerst, *J. Am. Chem. Soc.* **106**, 2260 (1984); P. Turner, S. L. Baughcum, S. L. Coy and Z. Smith, *J. Am. Chem. Soc.* **106**, 2265 (1984).

(b) J. Bicerano, H. F. Schaefer and W. H. Miller, *J. Am. Chem. Soc.* **105**, 2250 (1983).

(c) M. J. Frisch, A. C. Scheiner and H. F. Schaefer, *J. Chem. Phys.* **82**, 4194 (1985).

15. N. Makri and W. H. Miller, *J. Chem. Phys.* **86**, 1451 (1987).

16. R. Jaquet and W. H. Miller, *J. Phys. Chem* **89**, 2139 (1985).

17. For Euler angles see: E. B. Wilson, Jr., J. C. Decius and P. C. Cross, **Molecular Vibrations** (McGraw-Hill, New York, 1955), pp. 273-279.

18. For papers using Feynman Path Integrals see:

(a) R. P. Feynman and A. R. Hibbs, *Quantum Mechanics and Path Integrals* (McGraw-Hill, New York, 1965).

(b) D. Chandler and P. Wolynes, *J. Chem. Phys.* **74**, 4078 (1981).

(c) W. H. Miller, S. D. Schwartz and J. W. Tromp, *J. Chem. Phys.* **79** 4889 (1983).

(d) A. O. Caldeira and A. J. Leggett, *Ann. Phys.* **149**, 374 (1983); S. Chakravarty and A. J. Leggett, *Phys. Rev. Lett.* **52**, 5 (1984).

(e) D. Thirumalai and B. J. Berne, *J. Chem. Phys.* **79**, 5029 (1983); D. Thirumalai, E. J. Bruskin and B. J. Berne, *J. Chem. Phys.* **79**, 5063 (1983); D. Thirumalai and B. J. Berne, *J. Chem. Phys.* **81**, 2512 (1984); A. Wallquist, D. Thirumalai and B. J. Berne, *J. Chem. Phys.* **85**, 1583 (1986).

(f) E. C. Behrmann, G. A. Jongeward and P. G. Wolynes, *J. Chem. Phys.* **79**, 6277 (1983); R. W. Hall and P. G. Wolynes, *J. Stat. Phys.* **43**, 935 (1986).

(g) J. D. Doll, *J. Chem. Phys.* **81**, 3536 (1984); D. L. Freeman, R. D. Coalson and J. D. Doll, *J. Stat. Phys.* **43**, 931 (1986).

(h) Y. Yamashita and W. H. Miller, *J. Chem. Phys.* **82**, 5475 (1985).

(i) H. Grabert and U. Weiss, *Phys. Rev. Lett.* **54** 1605 (1985).

(j) M. Sprik, M.L. Klein and D. Chandler, *J. Chem. Phys.* **83**, 3042 (1985); M. Sprik, R.W. Impey and M.L. Klein, *J. Chem. Phys.* **83**, 5802 (1985).

(k) A. T. Dorsey, M. P. A. Fisher and M. S. Wartak, *Phys. Rev. A* **33**, 1117 (1986).

(l) C. D. Jonah, C. Romeo and A. Rahman, *Chem. Phys. Lett.* **123**, 209 (1986).

(m) P. J. Rossky, J. Schnitker and R. A. Kuharski, *J. Stat. Phys.* **43**, 949 (1986).

19. For previous gaussian basis sets see: I. P. Hamilton and J. C. Light, *J. Chem. Phys.* **84**, 306 (1986).

20. For FC overlap calculations see:

(a) D. Gruner and P. Brumer, *Chem. Phys. Lett.* **138**, 310 (1987).

(b) M. Kupka and P. H. Cribb, *J. Chem. Phys.* **85**, 1303 (1986).

(c) F. T. Chau, *J. Mol. Spectrosc.* **103**, 66 (1984) and references therein.

21. R. Janoschek, E. G. Weidemann and G. Zundel, *J. Chem. Soc., Faraday Trans. 2* **69**, 505 (1973).

22. S. Carter and N. C. Handy, *Mol. Phys.* **47**, 1445 (1982); *Mol. Phys.* **57**, 175 (1986).

23. Concerning straight-line reaction paths:

(a) B. A. Ruf and W. H. Miller, *Faraday Trans. II* **84**, 1523 (1988).

(b) J. M. Bowman, K. T. Lee, H. Romanowski, and L. B. Harding, in *Resonances*, ed. D.G. Truhlar, ACS Symp. Series **263**, 43 (1984).

24. For diabatic vs adiabatic see: F. T. Smith, *Phys. Rev.* **179**, 111 (1969).

25. For angular momentum see: J. T. Hougen, P. R. Bunker, and J. W. C. Johns, *J. Mol. Sect.* **34**, 136 (1970).

26. For rotation matrix see: M. E. Rose, in *Elementary Theory of Angular Momentum*, Wiley, New York, 1957, p.65.

27. A. Warshel and R. M. Weiss, *J. Am. Chem. Soc.* **102** 6218 (1980); A. Warshel, *Biochemistry* **20** 3167 (1981); J. K. Hwang, G. King, S. Creighton, and A. Warshel, *J. Am. Chem. Soc.* **110** 5297 (1988).

28. P. K. Weiner and P. A. Kollman, *J. of Comp. Chem.* **2** 287 (1981); S. J. Weiner, P. A. Kollman, D. A. Case, U. Chandra Singh, C. Ghio, G. Alangona, S. Profeta, Jr., and P Weiner, *J. Am. Chem. Soc.* **106** 765 (1984); S. J. Weiner, P. A. Kollman, D. T. Nguyen, and D. A. Case, *J. of Comp. Chem.* **7** 230 (1986).

29. D. M. Ceperley and G. Jacucci, *Phys. Rev. Lett.* **58** 1648 (1987).

30. R. D. Coalson, *J. Chem. Phys.* **185** 926 (1986).

31. J. P. Valleau and S. G. Whittington, in *Modern Theoretical Chemistry,* ed. B. J. Bern, (Plenum, NY, 1977) vol 5 pp. 137-168.

LAWRENCE BERKELEY LABORATORY
TECHNICAL INFORMATION DEPARTMENT
1 CYCLOTRON ROAD
BERKELEY, CALIFORNIA 94720